

NASW-4435

11-91-CR

141.2

p.621

# PROJECT MINERVA

## A LOW COST MANNED MARS MISSION BASED ON INDIGENOUS PROPELLANT PRODUCTION



University of Washington  
 NASA/USRA Advanced Design Program  
 Department of Aeronautics and Astronautics  
 Seattle, Washington 98195



June 15, 1992

N93-18048

Unclass

G3/91 0141652

(NASA-CR-192020) PROJECT MINERVA:  
 A LOW COST MANNED MARS MISSION  
 BASED ON INDIGENOUS PROPELLANT  
 PRODUCTION Final Report  
 (Washington Univ.) 621 p

# **PROJECT MINERVA:**

## **A LOW COST MANNED MARS MISSION BASED ON INDIGENOUS PROPELLANT PRODUCTION**

### **FINAL REPORT**

**Space Systems Design, AA 420/421  
NASA/USRA Advanced Design Program**

#### **Prepared By**

David Beder  
Richard Bryan  
Tuyen Bui  
Kelly Caviezel  
Mark Cinnamon  
Todd Daggert  
Mike Folkers  
Mark Fornia  
Natasha Hanks  
Steve Hamilton  
Steven Hamling

Jim Jensen  
Bryan Johnson  
Martin Kalberer  
Mike Machula  
James Madison  
Kevin Mahn  
Joe Mason  
Leslie McCullough  
Pat McGuirk  
Genya Menkin  
Tim Oerting

Jim Phillips  
Clint Schneider  
Skylar Shaw  
Brian Thill  
John Tran  
Julian Varlay  
Beth Waddington  
Mark Walter  
Vince Westmark  
Lisa Wetherbee

#### **Instructor**

**Prof. Adam P. Bruckner**

#### **Teaching Assistant**

**Hobie E. Anderson**



**University of Washington  
Department of Aeronautics and Astronautics FS-10  
Seattle, Washington 98195**

**June 15, 1992**



# ABSTRACT

Project Minerva is a low-cost manned Mars mission designed to deliver a crew of four to the Martian surface using only two sets of two launches from the Kennedy Space Center. Key concepts which make this mission realizable are the use of near-term technologies and *in-situ* propellant production, following the scenario originally proposed by R. Zubrin. The first set of launches delivers two unmanned payloads into low Earth orbit (LEO): the first payload consists of an Earth Return Vehicle (ERV), a propellant production plant, and a set of robotic vehicles; the second payload consists of the trans-Mars injection (TMI) upper stage. In LEO, the two payloads are docked and the configuration is injected into a Mars transfer orbit. The landing on Mars is performed with the aid of multiple aerobraking maneuvers. On the Martian surface, the propellant production plant uses a Sabatier/electrolysis type process to combine nine tons of hydrogen with carbon dioxide from the Martian atmosphere to produce over a hundred tons of liquid oxygen and liquid methane, which are later used as the propellants for the rover expeditions and the manned return journey of the ERV.

Once the propellants for the return journey have been produced, approximately two years after the first set of launches, the manned portion of the mission leaves Earth. This set of two launches is similar to that of the unmanned vehicles. The Mars Transfer Vehicle (MTV) and the TMI stage are docked in LEO and injected into a Mars transfer orbit. The MTV contains the manned rover and the habitat which houses the astronauts *enroute* to Mars and, subsequently, on the Martian surface. During the 180-day trip to Mars artificial gravity is induced by tethering the MTV to the TMI upper stage and inducing rotation. Upon arrival the tether is cut and the MTV performs aerobraking maneuvers to land near the fully-fueled ERV, which is used by the crew a year later to return to Earth. The mission entails moderate travel times with relatively low-energy conjunction-class trajectories and allows ample time for

extended scientific exploration. The rover is designed with sufficient surface mobility for multiple remote-site excursions.

This set of missions can be repeated every two years in order to continue exploration at a variety of sites and gradually establish the infrastructure for a permanent base on Mars. In this scenario the second unmanned mission leaves Earth at about the same time as the first manned mission does, but lands at a different location on Mars, within rover range of the first site, and so on.

The Earth-to-LEO boost vehicle and TMI stage used for this mission are based on the Antares launch vehicle developed by the University of Washington's Advanced Design Program in 1991. The Antares is a modular, reusable, single-stage-to-orbit, H<sub>2</sub>/O<sub>2</sub>-propelled vehicle with a maximum payload capacity of 70 metric tons. Only a simple docking and latching process is necessary in LEO, as compared to the extensive in-orbit construction required in other proposed Mars exploration schemes.

This report presents in detail the necessary systems for the flights to and from Mars, as well as those needed for the stay on Mars. These systems include the transfer vehicle design, life support, guidance and communications, rovers and telepresence, power generation, and propellant manufacturing. Also included are the orbital mechanics, the scientific goals, and the estimated mission costs.

# PREFACE

Since 1985 the Department of Aeronautics and Astronautics at the University of Washington has participated in the NASA/USRA Advanced Design Program. From the beginning, student participation in this space-design activity has been integrated as much as possible with the faculty's NASA-funded research programs. The student response has been excellent and the synergism with the research program has been highly beneficial.

The course structure is aimed at exposing the students to a design situation which is "real world" as much as possible within the University framework. In addition, the course undertakes the responsibility of teaching the students those aspects of space engineering and science which are needed for a general capability in the field of space systems. Students are taught the fundamentals of re-entry physics, nuclear and solar power systems, space structures and thermal management, as well as selected topics on advanced propulsion systems and orbital mechanics. The design problems expose the students to situations in which they must understand the complete systems interdependence of structural, thermal, propulsive, and other components, and environmental constraints particular to space.

Our Senior-level, undergraduate course offering is titled "Space Systems Design", and consists of two, linked, 10-week academic quarters (Winter and Spring). The typical enrollment is 30-40 students. The first course (AA420) is initially structured as a formal lecture/discussion series which meets 5 hours per week. Formal lectures by the instructors and presentations by guest lecturers from industry and, when possible, from NASA, provide the students with the fundamental background they need to carry out their design studies. By the second or third week of the quarter, the students are divided into design teams whose responsibility is to address specific subsystems of the overall design. As the design progresses, more and more time is devoted to in-class discussions of the students' work. A teaching assistant supported by NASA/USRA funds works with the students and helps the

instructors with project management. The accomplishments of the first quarter's work are presented at the end of the quarter in the form of formal written progress reports, one by each of the design groups. In addition, as a further assessment of the students' skills and capabilities, weekly homework assignments are given, and mid-term and final examinations are administered.

The linked Spring Quarter offering (AA421) is intended to refine and advance the design developed during the Winter Quarter and to address key unresolved problem areas. The class continues to meet formally five hours a week in group discussion format. Early in the quarter a preliminary design review is conducted by the responsible faculty and aerospace engineers from local industry, e.g., Boeing and Rocket Research Co. At the end of the Spring Quarter the students submit a single final report on the overall design, as well as a summary report, and prepare for the NASA/USRA ADP Summer Conference. During this quarter only one or two homework assignments and one brief quiz are given. Most of the students' grade is based on their contributions to the final reports.

Although the students consider the work load for this course sequence to be very heavy, they are quick to agree that it provides them with an excellent introduction to the world of design. A general competitive atmosphere is maintained wherever possible, as an additional simulation of the real world. The feedback from the students also has proved effective in stimulating the instructors. The ongoing policy of integrating the research programs into the space design course has proven to be a fruitful way of providing both a sound background in space engineering disciplines and stimulating creative thinking to solve problems of importance to the exploration of space.

Under this program, since its inception, we have examined various problems relating to the critical needs of space prime power, propulsion, and transportation. Design topics have ranged from solar and nuclear prime power for space platforms and lunar bases, to innovative

space transportation systems for low cost delivery of payloads to low Earth orbit and interplanetary space. The choice of these topic areas for continuing design studies has been based on the historical emphasis on these areas in the space engineering research carried out by the instructors and their colleagues. This focus has also been based on the recognized need for innovative approaches in these key areas for successful expansion of the U.S. space program.

The design topic selected for 1992 is a case in point. The success of Antares, the modular launch system designed by the class in 1991, was such that we decided to examine its potential to support a major planetary mission, i.e., the manned exploration of Mars. Although numerous Mars mission studies have been carried out by NASA and industry, and universities participating in the Advanced Design Program, our approach differs substantially from most scenarios offered to date. We took our cue from the preliminary studies performed by Robert Zubrin, at Martin Marietta in Denver, on missions to Mars which would make use of *in situ* resources, namely the Martian atmosphere, to manufacture the propellant necessary for the return trip. This concept makes possible a "direct-to-Mars" scenario that circumvents any need to perform on-orbit assembly of the spacecraft that travel to and from Mars, thus reducing the overall mission costs by nearly an order of magnitude. Despite its rather daring nature, the freshness, elegance, and simplicity of this concept, and its potential for enormous cost savings make it the most feasible manned Mars scenario proposed to date. All other concepts suffer from extreme complexity and size, and would incur such astronomical costs that they virtually guarantee that they will not be initiated any time in the foreseeable future, if ever, particularly given the prevailing economic conditions in the U.S. and Russia.

Because our Antares launch vehicle concept is also based on the premise of simplicity and low cost, and because it is capable of heavy lift (70 metric tons to LEO) in its largest modular configuration, we felt that it would make a good match with the requirements of a direct-to-Mars mission concept. The class proceeded to develop this concept to a significantly greater detail than Zubrin' studies to date, in order to permit a more informed assessment of its

merits, and to better identify critical aspects and potential problems. In addition the students incorporated their own ideas and approaches to various aspects of the project. The results have been highly successful and have confirmed the viability of the Mars-direct approach. Our presentation at the NASA/USRA Summer Conference in Washington, DC, June 15-19, 1992, was well received by NASA, USRA, industry, and university representatives, and generated much discussion.

Adam P. Bruckner  
Professor of Aeronautics and Astronautics  
June 28, 1992

## ACKNOWLEDGEMENTS

The AA 420/421 class of 1992 completed this report with invaluable aid from many sources. Most importantly, thanks go to Prof. Adam Bruckner and Abraham Hertzberg for guidance and encouragement through the year. The knowledge and wisdom that they imparted will be with us throughout our careers. Also, we are thankful for the help from teaching assistant Hobie Anderson. We also wish to thank David Carlile, last year's teaching assistant, for his very helpful comments and suggestions.

Robert Zubrin was very influential in the initial design and concept of this manned Mars mission. His work laid the foundation for this project including integration of the concepts of in-situ propellant manufacturing, direct Mars architecture, tether for astronaut safety, independence on Space Station Freedom, and no in-orbit construction. We also thank R. Zubrin for his valuable time when he visited our class and listened to our ideas.

We are also grateful for the help we received from outside sources. These people sacrificed their valuable time to answer our questions. From the Boeing Company alone, there are numerous people to thank. These include Dana Andrews, Tim Vinapol, Gordon R. Woodcock, and John Anderson who shared their expertise in space transportation technology and other various subjects with us through lectures and individual consultations. Dana Andrews and Tim Vinapol are especially deserving because they sacrificed a full afternoon so that we could present our preliminary design for review. Thanks are also due to David Mercier for making available NASA's OPGUID trajectory analysis program.

Answers to many of our questions came from individuals representing other companies and universities. Chuck Limmerick at Pratt and Whitney supplied information on engine specifications. Ronald Greely at Arizona State University provided us information on Mars

landing sites. Michael E. Tauber and Demetrius A. Kourtides from NASA Ames sent us information on aerobrake thermal protection and answered general questions. Thanks to the Rocket Research Co. that offered help in the areas of rocket attitude control systems.

Furthermore, we would like to extend our gratitude and apologies to anyone who was inadvertently not acknowledged above. Due to the length and scope of Project Minerva, some individuals who helped us may have been omitted by accident.

Finally, thanks goes to NASA/USRA and Frank Swalley, out center mentor, for sponsoring this program and giving us the chance to develop this project. Thanks also goes to the Department of Aeronautics and Astronautics here at the University of Washington for additional funding and other help.

# TABLE OF CONTENTS

1.0 EXECUTIVE SUMMARY.....	1.1
2.0 ORBITAL ANALYSIS .....	2.1
3.0 DESIGN OF TRANSFER VEHICLES.....	3.1
4.0 AEROBRAKE.....	4.1
5.0 LIFE SCIENCES AND HABITAT DESIGN.....	5.1
6.0 GUIDANCE, COMMUNICATIONS, AND CONTROLS.....	6.1
7.0 POWER AND PROPELLANT PRODUCTION .....	7.1
8.0 ROVERS AND ROBOTICS.....	8.1
9.0 MARS SCIENCE.....	9.1
10.0 ECONOMICS.....	10.1
11.0 CONCLUSION .....	11.1
APPENDIX A: DERIVATION OF ORBITAL ELEMENTS.....	A.1
APPENDIX B: ENTRY PARACHUTES.....	B.1
APPENDIX C: LASER COMMUNICATION FEASIBILITY.....	C.1
APPENDIX D: MARS SURFACE POWER ALTERNATIVE.....	D.1
APPENDIX E: SUPPLEMENTAL OXYGEN PRODUCTION.....	E.1
APPENDIX F: IN-SITU PROPELLANT PRODUCTION ANALYSIS....	F.1
APPENDIX G: MARS CHARACTERISTICS.....	G.1

## **1.0 EXECUTIVE SUMMARY**

Kelly Caviezel  
Todd Daggert  
Mike Folkers  
Mark Fornia  
Steven Hamling  
Bryan Johnson  
Martin Kalberer  
Mike Machula  
Kevin Mahn  
Leslie McCullough  
Clint Schneider  
Vince Westmark

# TABLE OF CONTENTS

<b>1.1</b>	<b>INTRODUCTION</b> .....	1.1
<b>1.2</b>	<b>MISSION SCENARIO</b> .....	1.3
	1.2.1 ABORT CAPABILITIES.....	1.5
<b>1.3</b>	<b>ASTRODYNAMICS</b> .....	1.6
<b>1.4</b>	<b>DESIGN OF TRANSFER VEHICLES</b> .....	1.8
	1.4.1 UPPER STAGE/TMI BOOSTER VEHICLE.....	1.8
	1.4.2 UNMANNED MARS TRANSFER VEHICLE.....	1.9
	1.4.3 EARTH RE-ENTRY MODULE.....	1.10
	1.4.4 MARS DESCENT AND EARTH RETURN ENGINES.....	1.11
	1.4.5 MANNED TRANSFER VEHICLE.....	1.12
	1.4.6 HABITAT .....	1.13
<b>1.5</b>	<b>AEROBRAKE</b> .....	1.14
	1.5.1 HEAT SHIELDING.....	1.15
	1.5.2 STRUCTURE AND OPERATION .....	1.15
	1.5.3 AEROCAPTURE.....	1.16
<b>1.6</b>	<b>GUIDANCE, COMMUNICATIONS, AND CONTROLS</b> .....	1.17
	1.6.1 LANDING CAPABILITIES.....	1.18
	1.6.2 COMMUNICATION.....	1.18
<b>1.7</b>	<b>POWER SYSTEMS</b> .....	1.19
<b>1.8</b>	<b>IN-SITU PROPELLANT PRODUCTION</b> .....	1.20
<b>1.9</b>	<b>ROVERS AND ROBOTICS</b> .....	1.21
	1.9.1 UNMANNED ROVER .....	1.21
	1.9.2 MANNED ROVER.....	1.22
	1.9.3 HOPPER.....	1.23
	1.9.4 MINI ROVER.....	1.23
<b>1.10</b>	<b>MARS SCIENCE</b> .....	1.23
<b>1.11</b>	<b>ECONOMICS</b> .....	1.24
	<b>NOMENCLATURE</b> .....	1.26
	<b>REFERENCES</b> .....	1.28
	<b>FIGURES</b> .....	1.30



## 1.1 INTRODUCTION

For centuries humans have pondered the nature of Mars and developed many theories to support what was observed. Speculation on the presence and extent of life on Mars has long held the interest of both the scientific community and the general public. For the past 28 years Mars has been explored by unmanned space probes, beginning with the Mariner series in the late 1960's and followed in the mid 1970's by Viking I and Viking II. These missions have answered some of the questions surrounding Mars and have given rise to new ones. With the Mars Observer establishing the return to exploration of the red planet in 1993, Mars is currently receiving attention as a possible target for manned exploration in the early 21st century.

The National Space Council (NSC) has the responsibility of defining the future objectives of America's space program in what is known as the Space Exploration Initiative (SEI). NASA, the Department of Defense, and the Department of Energy are the primary participants that assist the NSC with forming the SEI, which includes a plan for the manned exploration of Mars. SEI's plans require in-orbit construction and multiple launches, and consequently would be extremely complex and costly. This is one reason why SEI did not receive any funding from Congress for fiscal year 1991, and why it continues to have difficulty in drawing support.<sup>1</sup> Therefore, an opportunity exists to develop a simple, low-cost alternative to SEI's present concept of placing humans on Mars for the purpose of effective exploration.

Such a mission has been suggested by R. Zubrin of Martin Marietta.<sup>2,3</sup> His so-called Mars-Direct Mission Architecture is based on the premises of using near-term technologies, going to Mars directly from Earth's surface on a conjunction class trajectory (thus circumventing in-space construction and dependence on Space Station Freedom), and manufacturing the propellant for the return journey on Mars from indigenous materials, i.e., the Martian atmosphere.

This year's Advanced Design Program at the University of Washington designed the Minerva manned mission to Mars, based on the Zubrin scenario and incorporating a number of new ideas. These range from the selection of the heavy lift vehicle and the design of the trans-Mars injection booster to the design of the manned habitat, the Mars rovers, and the Earth return vehicle.

The mission is undertaken in two main segments; in the first an unmanned spacecraft delivers a propellant production plant and the Earth Return Vehicle (ERV) to the surface of Mars. During the year and a half following the arrival of the unmanned spacecraft, the propellant production plant manufactures methane and oxygen by combining hydrogen brought from Earth with carbon dioxide from the Martian atmosphere, using a Sabatier-type chemical process complemented by water electrolysis. This process is very effective, converting only 6 tons of  $H_2$  into 78 tons of  $O_2$  and 22 tons of  $CH_4$ .

Once it has been confirmed that the necessary propellant for the return journey has been successfully produced and stored (about 2 years after the unmanned launch), the manned mission leaves Earth. To alleviate the problems of extended zero-gravity (~ 180 days) a 2.5 km tether is connected between the manned vehicle and its spent Trans Mars Injection (TMI) booster, and the two are spun at 1 RPM to produce artificial gravity. The capture of both the unmanned and manned vehicles at Mars is effected via aerobraking and a modest retro-rocket maneuver. Once on the surface, the crew of four astronauts uses  $CH_4$ - $O_2$  powered manned and unmanned rovers and a rocket propelled hopper to explore Mars.

One of the advantages of the Mars-direct scenario based on conjunction class trajectories is that the surface stay time on Mars is much longer than in the case of a high energy opposition class mission, i.e. ~ 1.5 years vs. ~35 days. Thus the astronauts will have ample time to carry out an in-depth exploration of a large area of the planet.

This summary report discusses the basic mission architecture and its major components, including the orbital analysis, the Unmanned Mars Transfer Vehicle (UMTV), the Manned Transfer Vehicle (MTV), Earth Return Vehicle (ERV), aerobrake design, life sciences, guidance, communications, power, propellant production, surface rovers, and Mars science. Also presented is an evaluation of the cost per mission over an assumed 8-year initiative. Although the scope of this report covers only the exploration of Mars, many of the same technologies and philosophies can apply to lunar and other planetary mission concepts.

## **1.2 MISSION SCENARIO**

The Mars mission model described here is arbitrarily based on an 8-year Mars exploration initiative, as shown in Fig. 1. The program consists of an unmanned mission to Mars followed two years later by simultaneous manned and unmanned missions. This launch procedure is then repeated every two years for a total of 8 years, ending with a manned mission to Mars in the eighth year. This model results in four manned and four unmanned missions to Mars.

Our proposed program will benefit by using a relatively small number of large, low-cost heavy lift launch vehicles (HLLV's). Although any HLLV capable of lifting at least 70,000 kg into LEO can be used, the single-stage-to-orbit (SSTO) vehicle Antares VII, which was developed during our 1991 design study,<sup>4</sup> has been chosen for the Minerva mission. The Antares system is a partially reusable, modular system based on a single unit vehicle. This unit uses a Dual Mixture Ratio Engine (DMRE), a new type of rocket engine studied by Pratt and Whitney specifically for SSTO applications.<sup>5</sup> The single Antares units can be clustered together to provide variable payloads to LEO, ranging from 10,000 kg to 70,000 kg, and beyond. Figure 2 shows the basic Antares I and the Antares VII vehicles with their standard payload fairings.

Project Minerva uses the Antares VII vehicle to place the Mars transfer vehicles (both manned and unmanned) and their TMI booster stages into orbit. No in-orbit assembly is required, other than the straightforward rendezvous, docking, and connection of the spacecraft and their TMI boosters.

All launches proceed from the Kennedy Space Center and insert their payloads into a 150 x 300 km elliptical orbit of 28.5° inclination. This orbit is then circularized to a 300 km parking orbit, where rendezvous and docking maneuvers occur. The program OPGUID, which was provided by NASA's Marshall Space Flight Center, was used to analyze all mission launches.

To boost each transfer vehicle to Mars, 105 metric tons\* of propellant are required. Since the Antares VII has a payload of 70 tons an upper stage is required to deliver the necessary propellant to LEO. This upper stage also doubles as a TMI booster (see Fig. 5). For the manned segment the spent TMI booster stage is used as a countermass for the rotating tether that supplies artificial gravity to the crew. The unmanned spacecraft simply discards the spent TMI booster once it is on its way to Mars.

In both the unmanned and manned missions the TMI booster is placed into LEO first. The propellant tanks of the Antares VII vehicle are partially filled in order to allow it to lift off with its fully fueled 250 ton upper/TMI stage. At an altitude of 109 km the upper stage separates and delivers itself to a 300 km circular parking orbit with the 105 tons of propellant needed for the TMI burn. After the upper/TMI stage has been successfully delivered to LEO the transfer vehicle is launched directly by an Antares VII operating as an SSTO vehicle. The two are joined using an Apollo-Soyuz type docking procedure and, after deployment of the aerobrake and a functionality test of all major systems, the journey to Mars is initiated.

---

\*Henceforth, "ton" will be understood to mean metric ton.

The unmanned segment of the mission has the primary purpose of producing propellant for the manned return trip, and delivering the ERV. It also has the secondary purpose of deploying an unmanned rover to scout around for areas of interest, deploy scientific instruments for a variety of measurements, and collect Martian samples for later analysis.

After about 1.4 years, all of the propellant for the return trip will have been manufactured and stored on Mars in the ERV and the minimum energy window for the manned mission will be available. The manned mission is launched in the same manner as the unmanned mission. Since the astronauts would be appreciably weakened by a six-month stay in zero-gravity, artificial gravity at 0.4 g is generated by tethering the MTV to its spent TMI booster and rotating the assembly at 1 RPM.

### **1.2.1 ABORT CAPABILITIES**

Abort capabilities are crucial for the manned mission. However, the direct to Mars mission architecture does not allow a return to Earth without the *in-situ* propellant manufactured using CO<sub>2</sub> from the Martian atmosphere.

If any system fails during or shortly after the TMI burn, the landing retro-rockets can be used to slow the MTV and place it in a highly elliptical, 300 km perigee orbit about Earth. Since the  $\Delta V$  capability of the retrorockets is small, the window of opportunity to abort after the TMI burn is only about two hours. A short burn at first apogee decreases the perigee altitude to within the Earth's atmosphere, where the already deployed aerobrake is used to lower the apogee to LEO. A further maneuver circularizes the orbit at 300 km, where the astronauts wait until the Space Shuttle can rendezvous for rescue at a later time.

## 1.3 ASTRODYNAMICS

There are many factors that influence the type of transfer trajectory from LEO to low Mars orbit (LMO) and vice-versa. Some examples are the type of propulsion system used (chemical, nuclear, or electric), life support mass for the manned vehicle, sensitivity to radiation, tolerable solar flux, and desired stay time on the surface of Mars. Minimizing the required energy is an important factor in defining the capability of any mission. Energy savings ultimately result in a savings of propellant and an increase in payload capacity.

The first design consideration is opposition versus conjunction class missions. Although the quickest round trip time to Mars would be an opposition class mission, there are many drawbacks to that type of trajectory. An opposition class mission is defined as a high energy trajectory in which the departure position of Earth and arrival position at Mars are on generally the same side of the sun. Because of the high energy involved, a very large mass of propellant is required. This class of mission would take approximately 1.6 years, with only 0.1 year on the Martian surface. In addition, it would require an extended period of time closer to the sun than Earth's orbit on the return journey.<sup>2</sup> The increased particle radiation levels at this distance from the sun would be hazardous to the astronauts and would require additional shielding. The solar heat load to the vehicle would also be very high. This type of mission also requires a high-energy aerocapture at Mars, submitting the astronauts to between 8 and 10 g of acceleration. It is for these reasons that a conjunction class mission was selected for Project Minerva.

Conjunction class missions are close to minimum energy transfers, in which the departure position of Earth and the arrival position of Mars are approximately on opposite sides of the sun. The total mission time using a conjunction class trajectory is approximately 2.6 years.<sup>2</sup> The risks involved are longer radiation exposure and an extended period of zero gravity for the astronauts. Solar radiation exposure will be limited, since the mission will

remain outside the Earth's orbit at all times. In addition, the vehicle will rotate about a tether to provide the astronauts with artificial gravity.

The following windows, excess velocities, and energy values for manned and unmanned segments have been specified utilizing Jet Propulsion Laboratory data.<sup>6</sup> Two types of missions will be flown, an unmanned flight followed by a manned flight. The first unmanned mission will depart from Earth in 2001 and the first manned mission will depart in 2003, as shown in Figs. 3 and 4. The launch windows have been identified by the minimum departure energy limits. The departure energy,  $C_3$ , is equal to the square of the hyperbolic excess velocity. The first manned and unmanned flight windows are assumed to be limited by a maximum  $C_3$  value of  $10 \text{ km}^2/\text{s}^2$ . For a near-minimum energy conjunction class mission, the launch window for the unmanned mission opens March 4, 2001 and closes April 2, 2001. For a minimum energy transfer, the unmanned departure date would occur March 19, 2001, with arrival at Mars on September 10, 2001. The arrival window at Mars is from August 18, 2001 to October 17, 2001. The maximum hyperbolic excess velocity for the given launch window is 6.3 km/s at Martian arrival and the corresponding maximum entrance velocity in the Martian atmosphere at 100 km altitude is 7.95 km/s.

The manned mission, as shown in Fig. 4, has a minimum departure  $C_3$  of  $8.81 \text{ km}^2/\text{s}^2$ . The launch window for Earth departure, limited by a maximum  $C_3$  value of  $10 \text{ km}^2/\text{s}^2$ , is from May 22, 2003 to June 22, 2003. The minimum  $C_3$  departure date from Earth is June 7, 2003 with a Mars arrival date of December 25, 2003. The Mars arrival window is from November 17, 2003 to January 27, 2004. The maximum arrival hyperbolic excess velocity for the given launch window is 3.6 km/s.<sup>6</sup>

The mission dates and Earth to Mars trajectory have been selected by performing trade studies between the energy of the transfer orbit and the stay time on Mars. If minimum energies for arrival at Mars and departure to Earth are used, the manned vehicle will arrive at

Mars on December 25, 2003 and the return trip will begin on June 28, 2005. This results in a total surface time of 1.44 years (526 days), which should be ample to complete a considerable amount of scientific experimentation and exploration. (The low energy windows for the conjunction class missions discussed above allow a range of 1.35 to 1.55 years (493 to 566 days) of surface stay time).

The window for Mars departure with a maximum  $C_3$  of  $14 \text{ km}^2/\text{s}^2$  is June 17, 2005 to July 9, 2005. For the return vehicle, the departure date from Mars for a minimum departure energy is June 28, 2005, with an Earth arrival date of January 6, 2006. The Earth arrival window is from December 28, 2005 to January 15, 2006.<sup>7</sup> The maximum Earth arrival hyperbolic excess velocity for the given launch window is 3.6 km/s. The capture at Earth will be similar to that used in the Apollo program, i.e., a ballistic reentry. The entrance velocity will be  $11.6 \text{ km/s}^2$  at an altitude of 100 km.<sup>7</sup>

## **1.4 DESIGN OF TRANSFER VEHICLES**

### **1.4.1 UPPER STAGE/TMI BOOSTER VEHICLE**

In addition to performing the burn to LEO, the upper stage also has the role of performing as the TMI booster (see Fig. 5). It carries 105 tons of propellant for the TMI burn. The upper stage also requires a propulsive system with a high thrust and high specific impulse. To allow for redundancy and eliminate the possibility of a single point failure, at least two engines need to be used. Pratt and Whitney's RL10-A4 and the Space Shuttle Main Engine (SSME) were considered, but Japan's Mitsubishi LE-7 engine<sup>8</sup> was found to have the characteristics most desirable for this mission.

This engine is similar to the SSME but smaller, and is used as a first stage engine in the Japanese H-2 launch vehicle. The LE-7 operates on a staged combustion cycle and has a

vacuum thrust of 1180 kN and vacuum specific impulse of 449 sec.<sup>8</sup> It burns liquid oxygen and liquid hydrogen at a ratio of 6:1. The LE-7 has already been designed, built, and tested, and is scheduled for first flight in 1993, after which it will become available in the U.S.

The upper stage/TMI booster has a diameter of 8.2 m and a length of 29.4 m. The payload fairing length of the Antares VII is increased by 5 m to accommodate this configuration. A docking mechanism is attached to the top of the TMI stage via a stub adapter.

An orbital maneuvering system (OMS) is used for the orbital circularization and rendezvous maneuvers. The OMS and reaction control systems are similar to those used on the Space Shuttle.

#### **1.4.2 UNMANNED MARS TRANSFER VEHICLE**

The mission requires that two types of vehicles be placed safely on the surface of Mars. The first vehicle sent is the unmanned Mars transfer vehicle (UMTV), shown in Fig. 6. The UMTV has a diameter of 9.1 m and a height of 32.0 m. At the base (in stowed position) the aerobrake is folded up against the vehicle with an effective diameter of 11.1 m. The vehicle consists of the ERV stage atop the UMTV descent stage. The ERV contains a habitat in which the astronauts live during the return trip to Earth. Centered in the middle of the ERV habitat is the Earth Re-entry Module (ERM). The astronauts and their payload re-enter the Earth's atmosphere in the ERM, while the ERV detaches and continues on its hyperbolic trajectory back out to deep space. Below the habitat are two hemispherical propellant tanks which will carry 96 tons of methane and oxygen that the propellant production unit will make on the Martian surface. The ERV sits atop the UMTV and has a height of 20 m, including its 5.5 m long nose cone, and a diameter of 9.1 m. The ERV is attached to the UMTV by studs and pyrotechnic separation nuts so that the two vehicles can be separated just prior to launch of the ERV.

The payload bay comprises the main section of the UMTV, and houses the unmanned rover, science equipment, and propellant production unit. The latter is shielded from the ERV's exhaust when it leaves Mars by means of Shuttle-like tiles. Protecting the unit will enable it to be used in subsequent missions, should the need arise. The UMTV also carries eight tons of hydrogen, six for propellant production and two for descent maneuvers. The oxygen required for landing is contained in the ERV LOX tank and is piped to the two descent engines in the UMTV. Using this tank for both descent and take-off reduces the vehicle mass. Table 1 lists the mass breakdown of major unmanned system components.

Table 1 Mass breakdown of unmanned transfer vehicle.

SYSTEM COMPONENT	Mass (ton)
Earth Return Vehicle	18.0
Structure of Payload Bay and Engine Supports	10.0
Propellant for Landing (LH <sub>2</sub> & LOX)	10.0
Hydrogen Feed Stock	6.0
Propellant Tanks	3.0
Aerobrake	9.0
Power Supply	7.6
Propellant Manufacturing Unit	2.0
Retro-Rocket System for Martian Descent	0.7
Piping and Wiring	1.0
Reaction Control System	0.5
Unmanned Rover	1.0
Science Equipment	0.5
<b>TOTAL</b>	<b>69.3</b>

### 1.4.3 EARTH RE-ENTRY MODULE

Re-entering the entire ERV into the Earth's atmosphere at the end of the mission would incur unacceptable mass penalties. This consequence led to the concept of using a smaller

Earth re-entry module (ERM) just large enough for the astronauts and any returning Martian samples. The ERM is similar to the command module of the Apollo lunar missions, however, it is based on a Boeing design capable of returning four astronauts.<sup>9</sup> Prior to re-entry at Earth it separates from the ERV. Two small solid rockets located on the ERV provide sufficient  $\Delta V$  to the ERV so that its trajectory does not overlap that of the ERM. After re-entering with the use of an ablator heat shield and deployable parachutes, the ERM splashes down for a water recovery. The ERV remains in a hyperbolic trajectory, continuing back out into deep space. (It is not desirable to have the ERV re-enter and break up in the atmosphere because of the danger of scattering plutonium from its dynamic isotope power system).

The ERM re-entry velocity is 11.6 km/sec and is comparable to that of the Apollo missions. It has a ballistic coefficient of 280 kg/m<sup>2</sup>, L/D of 0.5, and an angle of attack of 25 degrees. This type of design was chosen due to its cross range capability, simple structure, and reliable recovery method (water landing). The shield is made of a brazed stainless steel honeycomb and filled with an ablative type carbon-carbon composite.

#### **1.4.4 MARS DESCENT AND EARTH RETURN ENGINES**

The UMTV, as well as the MTV, use retrorockets for final descent after atmospheric entry at Mars. The engines required to successfully complete this part of the mission must be highly reliable. This requirement is satisfied by the Pratt and Whitney RL10A-4 engine, due to its simple cycle and conservative design. As for the reliability of the engine, "the RL10 has accumulated over 20 hours of operation in space; 174 engines have produced 282 in-space firings without a single engine failure, and the engine has demonstrated the highest reliability of any operational liquid rocket engine."<sup>10</sup> The two RL10A-4 engines used for the descent stage use LOX/LH<sub>2</sub> as propellant. These engines have a specific impulse of 449 sec, a thrust of 185 kN, and a mass of 167.8 kg each. In addition, the ERV uses four RL10A-4's modified to

burn LOX/LCH<sub>4</sub> propellant, which incurs a reduction in specific impulse to 376 sec and an increase in engine mass to 363 kg.<sup>10</sup>

#### 1.4.5 MANNED TRANSFER VEHICLE

The Manned Transfer Vehicle (Fig. 7) is similar to the UMTV, except that instead of an ERV there is the habitat which houses the astronauts *enroute* to Mars and on the Martian surface. In the MTV payload bay are carried the manned rover, more science equipment, and three more tons of hydrogen for additional propellant production on Mars. The manned vehicle has a height of 15.6 m and a diameter of 9.1 m (not including the aerobrake, which is similar to that of the UMTV). Table 2 shows the mass breakdown of the major system components.

Table 2 Mass breakdown of manned transfer vehicle.

SYSTEM COMPONENT	Mass (ton)
Habitat	28.0
Structure of payload bay and engine supports	5.0
Propellant for landing	10.0
Propellant Tanks	3.5
Aerobrake	9.0
Power on Mars	2.0
Manned Rover	3.0
Science Equipment	1.5
Reaction Control System	0.5
Retro-Rocket System	0.7
Piping and Wiring	1.0
Tether	2.0
Hydrogen	3.0
<b>TOTAL</b>	<b>69.2</b>

Artificial gravity is provided during the manned voyage from Earth to Mars by tethering the MTV to the expended TMI booster in a "dumbbell" configuration, as shown in Fig. 8,

using a 2.5 km tether made from Spectra 1000. The entire system is designed to rotate at one RPM which produces 0.4 g, approximately the same as the gravity on Mars. Without this artificial gravity, the crew would require significant recovery time upon arrival to Mars.

The habitat module and TMI booster are rigidly connected during the TMI burn. Immediately after this burn, the MTV separates from the spent TMI stage, rotates 180°, and attaches to the tether mechanism on the TMI stage. Subsequently, the tether is deployed using a tension control device to prevent tether snap oscillations. The reorientation of the MTV before deployment keeps the apparent artificial gravity force vector in the same direction as during engine firing and aerobraking. Prior to entry into Mars' orbit, the tether and spent TMI booster are detached. A tether system is not used on the ERV for the return journey to Earth, since the crew will have plenty of time to recover from the effects of ~180 days of zero gravity once they are back on Earth.

#### **1.4.6 HABITAT**

The MTV habitat is designed to shelter four astronauts on the two-year mission. This crew size was selected to provide the minimum psychological stress to individual crew members, while keeping life support requirements manageable and realizable. The MTV habitat provides the four astronauts with a safe, “shirt-sleeve” environment in which to live and work. In addition, all systems are closed and self-supporting (see Fig. 9). To these ends, it uses chemical regeneration systems instead of biological systems. Chemical systems have been proven reliable in the past and are well understood, whereas biological systems, although very promising, are not yet scaled for such long term missions.<sup>11</sup>

To protect the crew from harmful radiation and space debris, the MTV has galactic cosmic radiation and meteor shielding. Solar flare and radiation belt protection comes from a special water jacket that surrounds the airlock and can be filled when needed. Another consideration which influences the design of the MTV is the effect of zero gravity. Without

artificial gravity the crew would require significant recovery time upon arrival at Mars. This concern led to the design of the tether system, described earlier, to provide artificial gravity at 0.4 g.

The habitat level on the MTV has a floor area of 51 m<sup>2</sup> and consists of eight rooms, as shown in Fig. 10. The MTV has one 3.51 m<sup>2</sup> stateroom for each member of the crew. The staterooms have a fold-out bed, desk and chair, storage space for personal items and clothing, and a small window. The bathroom is equal in size to a stateroom and houses the shower, toilet, and laundry equipment. The science room (11.4 m<sup>2</sup>) is the main control center for the MTV. In addition, it contains the analysis lab used to perform experiments on Martian samples. The airlock is where the astronauts will seek safety during solar particle events (SPE), in which case a water jacket around the airlock is filled, as noted above.

Once on Mars, the crew will use the airlock to enter the rover or payload bay (see Fig. 7). The airlock is the same size as a stateroom (3.51 m<sup>2</sup>) and contains a three-day food supply for the crew during a SPE. The health room (11.4 m<sup>2</sup>) will enable the astronauts to exercise, conduct biological and space-flight experiments, and use medical equipment and supplies. The commons area (7.68 m<sup>2</sup>) is in the center of the MTV habitat level and contains the cooking facilities, the ship's library, and the table and chairs.

## **1.5 AEROBRAKE**

The aerobrake is an integral part of both the manned and unmanned missions. The aerobrake geometry selected is a blunt body with low lift to drag (L/D) ratio. It serves to slow the incoming craft at Mars and ensure capture, and to provide thermal protection of the craft within its wake zone. The aerobrake is folded up like an umbrella around the TMI stage during launch from Earth (see Fig. 11). It is opened and locked firmly into place in LEO, before the journey to Mars is initiated.

The deployed aerobrake (Fig. 12) has a symmetric modified conical shape with a cone half-angle of  $60^\circ$ . The middle section is a spherical shape with a radius of curvature of 9.1 m. This aerobrake has a coefficient of drag of 1.8 and a lift-to-drag ratio of approximately 0.5.

The cross-sectional diameter of the aerobrake is 22.5 m (with 6.7 m extended outward from the vehicle), providing a total cross-sectional area of  $398 \text{ m}^2$ . Protecting the entire vehicle by having it within the aerobrake's  $25^\circ$  wake angle would have required a much larger, extremely heavy aerobrake. Instead, protection outside the wake zone is provided by thermal tile shielding on the vehicle, as shown in Fig. 12.

### **1.5.1 HEAT SHIELDING**

For the unmanned mission a heating rate of approximately  $35.2 \text{ W/cm}^2$  will exist at the stagnation point. The manned mission will have a heating rate of approximately  $15.7 \text{ W/cm}^2$ . To withstand these heating rates both missions will use AETB-8 (Alumina Enhanced Thermal Barrier)<sup>12</sup> which can withstand heat fluxes up to  $53.4 \text{ W/cm}^2$ . This material has a density of approximately  $128 \text{ kg/m}^3$  and will result in a heat shielding mass of 1800 kg. The upper part of the vehicle not shielded by the aerobrake is protected by Shuttle tiles, as noted earlier.

### **1.5.2 STRUCTURE AND OPERATION**

The aerobrake is stored against the side of the spacecraft during Earth launch in a flower petal format. The aerobrake consists of eight identical "petals" that are folded around the transfer vehicle (see Fig. 11). Each petal has four main support struts, four radial ribs, and two sets of circumferential members to provide rigidity. In LEO the aerobrake is deployed by opening up the petals by means of the main support struts, fastening the petals together, and locking the support struts into place. The aerobrake doors for the retro-rocket engines, located at the bottom of the spacecraft, are then tested to ensure all systems are operating properly. A manual override system for the aerobrake doors is provided on the manned spacecraft in the

event of mechanical failure. The aerobrake petals are discarded when the retro-rockets are fired at Mars and fall away from the vehicle. The main support struts are then lowered to provide landing legs for the vehicle.

The structural components of the aerobrake are made of Graphite/Epoxy (fiber volume of 55%) which has a density of  $1490 \text{ kg/m}^3$ . This composite has a very low coefficient of thermal expansion ( $-0.36 \times 10^{-6} \text{ K}^{-1}$ ) which is necessary because the aerobrake experiences high heating rates. The aerobrake structure was designed to withstand  $8.3 \text{ g}$  deceleration. For minimal displacements, diameters of  $20 \text{ cm}$  for the main tubular support struts and  $10 \text{ cm}$  for the other structural elements are needed to provide adequate rigidity. A thin graphite/epoxy sheet attached to an aluminum honeycomb core covers the structural members of the aerobrake; to this is attached the heat shielding material. The overall mass of the aerobrake, including structure, heat shielding, and thermal tiles on the vehicle body, is approximately  $9000 \text{ kg}$ .

### **1.5.3 AEROCAPTURE**

Upon completing the transfer orbit to Mars, both the manned and unmanned missions will make a first close pass within the Martian atmosphere (at approximately  $50 \text{ km}$  and  $45 \text{ km}$ , respectively) to ensure aerocapture into a highly elliptical  $24.6$  hour, one Martian day orbit (MDO). The altitude for this first pass is determined by the hyperbolic excess velocity. The manned mission, with a lower hyperbolic excess velocity, needs to pass through less atmosphere than the higher energy unmanned mission. The corridor height, which is similarly defined by hyperbolic excess velocity, defines the acceptable margin of error in periapsis altitude for a given mission pass. The manned mission has a corridor height of approximately  $55 \text{ km}$ , whereas the unmanned mission has a  $25 \text{ km}$  corridor.<sup>13</sup>

After this initial aerobrake at a close altitude a small adjustment burn is made at apoapsis to raise the periapsis to  $250 \text{ km}$ . This one MDO matches the rotation period of the planet and has an apoapsis radius of  $37,180 \text{ km}$  (see Fig. 13). The MDO is not a necessity, but a

precautionary measure to ensure that all equipment is functioning properly prior to descent and that the landing site is confirmed to be clear of dust storms and large boulders. It is unlikely that the aerobrake would suffer any atmospheric dust-related damage, even during the close first pass. Dust storm effects are believed to occur only at altitudes below 40 km, which is below the first pass altitude for both missions.<sup>14</sup>

Descent for both missions is initiated by a small impulsive retro-burn at apoapsis to reduce the periapsis altitude from 250 km to an altitude within the atmosphere again. Although both the manned and unmanned spacecraft could then descend directly to the Martian surface, they are placed into a second elliptical orbit in order to launch a small communications satellite into a Mars synchronous circular orbit at 20,406 km radius. This orbit allows communication between the habitat and the rover while on Mars. Insertion of the satellite into this orbit is accomplished by a small booster. After the satellite is deployed the spacecraft makes a final periapsis pass and descends at an angle of attack of  $10^\circ$  below the local horizontal.

## **1.6 GUIDANCE, COMMUNICATIONS, AND CONTROLS**

The tasks of communication, navigation, guidance and control of a mission such as this encompass a wide range of requirements, constraints, objectives, and solutions, some of which are unique to this mission. One such requirement is the need for artificial gravity during the outbound leg of the manned mission. The solution, as already stated, is to tether the manned Mars transfer vehicle (MTV) to the spent TMI booster, and slowly spin the vehicles about the center of mass. Although this poses some difficulties, especially for the onboard navigation and control, it requires no new technologies. In fact, most of our objectives are achieved with existing off-the-shelf systems.

### **1.6.1 LANDING CAPABILITIES**

The manned MTV must land relatively close to the previous unmanned landing site, where the fully fueled ERV is waiting. The MTV will be carrying a rover with a 500 km radius of operation or a one way range of 1000 km that, if necessary, can transport the astronauts to the Earth return vehicle (ERV). A "homing" beacon at the unmanned site will help guide the MTV to the landing site. Control during entry is provided by attitude thrusters that adjust the angle of attack of the vehicle.

### **1.6.2 COMMUNICATION**

Guidance and navigation of both the outbound and return trips will be made possible with the use of the Deep Space Network (DSN)<sup>15</sup> and onboard guidance control systems that will work in conjunction with the DSN. The onboard system includes navigation devices such as Sun and star sensors, rate-integrating gyros for attitude determination, and computer systems that continually check and compare the trajectory of the vehicle against the desired trajectory.

The DSN will also form the backbone of our communication scheme. A high gain antenna will be in constant contact with the DSN, allowing communication and data transmission to occur at all times.

The small communication satellite, deployed at Mars during the aerobraking maneuver, will allow the habitat to communicate with the manned and unmanned rovers during excursions. It will also be used as an emergency communication link between the habitat and Earth during the periodic 12.5 hour black-outs that occur when the habitat is not in a direct line of sight with Earth.

## 1.7 POWER SYSTEMS

The MTV and ERV power needs are supplied by Dynamic Isotope Power Systems (DIPS). Each DIPS system consists of a spherical plutonium dioxide ( $^{238}\text{PuO}_2$ ) heat source surrounded by a tungsten gamma ray shield. The gamma ray shield is, in turn, surrounded by a lithium hydride neutron shield. Two Stirling engines are connected to the spherical ( $4\pi$ ) heat source/radiation shield assembly by heat pipes. Waste heat is taken from the Stirling engines by a pumped loop heat exchange system which is connected to the spacecraft's heat pipe radiators, located on the outer cylindrical wall.

Table 3 DIPS characteristics.

	MTV	UMTV
Number of DIPS	1	3
Output Power per DIPS	15 kWe	20 kWe
Thermal Power (BOL)	54 kWt	108 kWt
Thermal Power (EOL)	50 kWt	100 kWt
Total Output Power	15 kWe	60 kWe
Total Thermal Power (BOL)	54 kWt	216 kWt
Total Thermal Power (EOL)	50 kWt	200 kWt
Operating Lifetime	10 years	10 years
Stirling Engines	2	6
Stirling Engine Efficiency	30%	30%
<b>Mass per DIPS(kg)</b>		
Shield and Heat Source Mass	1250	1550
Stirling Engines	240	320
Radiator Mass	300	400
Structural Mass	210	280
<b>Total</b>	<b>2000</b>	<b>2550</b>
<b>Total Power System Mass</b>	<b>2000</b>	<b>7650</b>

(BOL) - Beginning of Life

(EOL) - End Of Life

Heat is generated by the plutonium dioxide through radioactive decay. The harmful decay products are weak gamma rays and neutrons. The gamma rays are blocked by the thin layer of tungsten and the neutrons are blocked by the substantially thicker lithium hydride shield. Each DIPS is designed so that the crew will receive no more than 10 rems per year from the PuO<sub>2</sub> decay.<sup>16</sup>

Each DIPS has two Stirling engines for redundancy. Normally, the two Stirlings will run at 50% power, but in the event that one fails, the remaining Stirling engine can run at 100% power and supply the vehicle with the power it needs. Table 3 shows the characteristics of the 15 and 20 kW<sub>e</sub> DIPS for the manned and unmanned spacecraft, respectively.

## **1.8 IN-SITU PROPELLANT PRODUCTION**

In-situ propellant production is used to produce the propellant needed for the ERV because of its huge mass savings. Taking hydrogen to Mars on the unmanned spacecraft allows all propellant for the return trip to be produced before the astronauts leave Earth. The ERV uses methane/LOX engines because of the ease in producing methane by combining hydrogen with the Martian atmosphere, which is mostly carbon dioxide (CO<sub>2</sub>). The unmanned spacecraft carries the propellant production unit to make methane and oxygen at Mars. Table 4 shows the major characteristics of the propellant production system.

Methane and oxygen are produced by utilizing already proven technologies: an enhanced Sabatier type reaction and electrolysis (see Fig 14).<sup>17</sup> The Sabatier process produces methane by the reaction  $\text{CO}_2 + 4\text{H}_2 \Rightarrow \text{CH}_4 + 2\text{H}_2\text{O}$ . The electrolysis process produces oxygen by:  $2\text{H}_2\text{O} \Rightarrow 2\text{H}_2 + \text{O}_2$ . The methane and oxygen are produced and then liquefied and pumped into storage tanks on the ERV.

The propellant manufacturing unit is singly redundant. Two identical chemical plants will run at 50% capacity, but in the event that one fails, the remaining one will run at 100%, producing the propellant in the allotted time (before the manned mission leaves Earth).

Table 4 Propellant production characteristics.

Total Propellant Produced	100 tons
Fuel (Methane)	22 tons
Oxidizer (Oxygen)	78 tons
ERV Mixture Ratio (mass ratio)	3.5:1
Production Time	550 days
Power Required	60 kWe
Initial H <sub>2</sub> Feed stock (from Earth)	6 tons
Propellant Plant Mass	1.5 tons

All the propellant can be produced from a feed stock of 5.5 tons of H<sub>2</sub>. Six tons are taken from Earth to account for boil-off during the Mars transfer. The manned mission will take three more tons of hydrogen for the production of propellant for the manned rover, which also runs on methane and oxygen.

## 1.9 ROVERS AND ROBOTICS

On any mission aimed at the exploration of Mars, it is desirable to collect samples and conduct experiments at a wide variety of sites. To do this, Project Minerva has a group of four rovers designed to facilitate a detailed exploration of the Martian surface.

### 1.9.1 UNMANNED ROVER

The unmanned rover (Fig. 15) has a mass of 750 kg and is powered by a methane/oxygen internal combustion engine. Its dimensions are 3.5 m long, 2.5 m wide, and

1.5 m high, with a maximum ground clearance of 65 cm. The payload bed can be tilted fore and aft to facilitate loading and unloading of cargo. The rover has a maximum radius of exploration of 200 km. Before the manned spacecraft arrives, the rover will deploy seismic detectors and survey the Martian terrain. The unmanned rover will also have the task of transferring the extra hydrogen brought by the manned vehicle to the propellant manufacturing unit of the unmanned vehicle. This extra hydrogen is for manned and unmanned rover use during the 1.44 year stay time on Mars. Afterwards, the unmanned rover will primarily act as a “mother ship” for the hopper and minirover. It will be able to be teleoperated from both the manned rover and habitat.

## **1.9.2 MANNED ROVER**

The manned rover (Fig. 16) is the prime instrument used in the exploration of the Martian surface. This rover is capable of taking core samples to a depth of 10 m, delivering scientific experiments, collecting samples, and performing limited sample analysis. Powered by a 35 kW methane/oxygen internal combustion engine, the rover has the capability of traversing 1000 km with a maximum radius of exploration of 500 km. The manned rover has a ground clearance of 1 m.

With a dry mass of only 2250 kg, the manned rover provides a versatile tool for the exploration of Mars. The shirt-sleeve environment of the rover can accommodate two astronauts for up to two weeks and has an emergency back-up capability of supporting all four astronauts for up to a week. An airlock located at the rear of the rover allows easy access to the MTV habitat, through the ceiling airlock door, and to the surface of Mars through the back airlock door. The manned rover stores its life support end products for processing and distillation at the habitat.

### **1.9.3 HOPPER**

The hopper (Fig. 17) travels to inaccessible regions of Mars via ballistic trajectories and soft landings. The hopper has a dry mass of 250 kg and is powered by an 8000 N methane/oxygen, pressure-fed rocket engine. It has a nominal round trip range of 15 km. The hopper can accommodate the mini rover or a single bucket seat on its payload bed. This will allow the minirover or an astronaut to journey where the manned rover cannot. The dimensions of the hopper are 2.1 m long, 1.6 m wide, and 1.25 m high.

### **1.9.4 MINI ROVER**

The mini rover, which has a three-section articulated design, has a mass of 50 kg, and is powered by rechargeable nickel hydride batteries, which give it a range of about 2 km, depending on the terrain. The dimensions are 1.5 m long, 1 m wide, and 0.8 m high. It has 6 conical shaped wheels, allowing a high level of mobility. It can be used to scout around the outside of the habitat, to piggyback aboard the unmanned rover for remote scouting, or as the primary payload of the hopper for reaching normally inaccessible areas of Mars.

## **1.10 MARS SCIENCE**

While the overall mission rationale is to explore Mars, potential landing sites had to be determined and a scientific payload package put together. In late 1992, Mars Observer will begin its mission to further explore Mars robotically. Minerva will seek to increase the knowledge of Mars, as well as to provide manned exploration of the "Red Planet."

The ideal landing site was determined by the number of scientific questions that could be answered, the safety of landing, and the establishment of a site near the equator to facilitate

an easier orbital insertion. The four sites considered were the Lunae Planum, the Mangala Vallis, the Chryse Planitia, and the Argyre Planitia regions (see Fig. 18).

The primary site is located on the southern edge of the Lunae Planum, so that the rovers can reach the Juventae Chasma and the Ophir Chasma, which are within the Vallis Marineris. Figure 19 shows the Lunae Planum ideal landing site. The area also offers possible river basins and cratered areas.<sup>18</sup> Goals relating to site selection are the determination of elemental composition, tectonic activity (past or present), geologic/morphologic studies, and exobiological analysis. The existence of carbonates would give evidence of past life and that liquid water once existed on Mars.

The scientific package includes field equipment, exobiology and geoscience measuring instruments of various types, and sample collection containers for both field use and for possible Earth return.<sup>19</sup> Also included are astronomical instruments to be used during the space flight to Mars.

## **1.11 ECONOMICS**

The mission model for the Minerva project is based on an assumed eight-year Mars exploration initiative. The eight year initiative begins with an unmanned mission to Mars in 2001, followed two years later by a manned and an additional unmanned mission. This launch procedure is then repeated every two years for eight years, resulting in a total of four unmanned and four manned missions to Mars (see Fig. 1). This model is assumed to end after eight years for cost analysis purposes but could continue as long as desired.

The vehicle costs have been broken down into three categories: Research and Development (R&D), Production Costs, and Operations and Support (O&S). The vehicle costs are the costs necessary to produce the number of launch vehicles required. A cost was

estimated for each of these categories on a per year basis, based on previous missions. The R&D costs were assumed to last for 28 years and the O&S costs were assumed to last for 18 years, while the production costs were calculated on a per vehicle basis. The total for the vehicle costs amounts to \$11.7 billion.

The unmanned mission costs were calculated by dividing the mission into different components and estimating the cost based on previous space systems. The unmanned mission also contains its own R&D and O&S costs. These costs are also assumed to last for 28 and 18 years respectively. A cost was then estimated for each of these categories and the amount was summed. The total for the unmanned mission vehicle costs amounts to \$23.3 billion.

The manned mission costs were estimated based on the same method as the unmanned mission, allowing for differences in components. These costs were also assumed to last for 28 and 18 years, respectively. The total for the manned mission amounts to \$21.5 billion.

Table 5 Total mission cost in billions of dollars.

	Vehicle	Unmanned	Manned	Total
Mission 1	2.9	6.9	5.4	\$15.3
Mission 2	2.9	5.4	4.4	\$13.2
Mission 3	2.9	5.4	4.4	\$13.2
Mission 4	2.9	5.4	4.4	\$13.2
<b>Total</b>				<b>\$55</b>

By summing these costs we can come up with a total mission cost. The total cost for our eight year Mars Exploration Initiative is \$55 billion (see Table 5). This cost is considerably lower than other manned Mars missions suggested by NSC.<sup>20</sup>

# NOMENCLATURE

Antares I	Single Antares launch vehicle
Antares VII	Seven unit Antares launch vehicle configuration
C3	Departure energy (equal to the square of the hyperbolic excess velocity)
CO	Carbon monoxide
DIPS	Dynamic isotope power system
DMRE	Dual mixture ratio engine
DSN	Deep space network
EOL	End of life
ERM	Earth re-entry module
ERV	Earth return vehicle
EVA	Extra vehicular activity
g	Acceleration on Earth ( $9.8 \text{ m/s}^2$ )
HGA	High gain antenna
HLLV	Heavy Lift Launch Vehicle
$I_{sp}$	Specific Impulse
IMU	Inertial measuring unit
KSC	Kennedy Space Center
LEO	Low Earth Orbit
LGA	Low gain antenna
LMO	Low Mars Orbit
LOX	Liquid oxygen
MDO	Martian day orbit
MOR	Mars Orbit Rendezvous
MSO	Mars synchronous orbit
MTV	Mars Transfer Vehicle

NASA	National Aeronautics and Space Administration
NSC	National Space Council
PuO <sub>2</sub>	Plutonium Oxide
RIG	Rate integrating gyro
SEI	Space Exploration Initiative
SOP	Supplemental oxygen production
SSTO	Single Stage to Orbit
TMI	Trans - Mars Injection
UMTV	Unmanned Mars Transfer Vehicle
DV	Velocity increment for departure at Earth
$V_{\infty,D}$	Departure hyperbolic excess velocity
$V_{\infty,A}$	Arrival hyperbolic excess velocity

## REFERENCES

1. "NASA's Role in Moon and Mars Missions Narrows," Aerospace America, Vol. 30, April 1992, p. 1.
2. Zubrin, R., Baker, D., and Gwynne, O., "Mars Direct: A Simple, Robust, and Cost Effective Architecture for the Space Exploration Initiative," AIAA Paper No. 91-0326, 1991.
3. Zubrin, R., "In-Situ Propellant Production: The Key Technology Required for the Realization of a Coherent and Cost-Effective Space Exploration Initiative," Paper No. IAF 91-668, 42nd Congress of the International Astronautical Federation, Montreal, Canada, October 7-11, 1991,.
4. Project Antares: A Low Cost Modular Launch Vehicle for the Future, Final Report, Space Systems Design, AA420/421 NASA/USRA Advanced Design Program, Department of Aeronautics and Astronautics University of Washington, Seattle, WA, June 1991.
5. Limerick, C.D., "Dual Mixture Ratio H<sub>2</sub>/O<sub>2</sub> Engine for Single Stage to Orbit Application," Journal of Propulsion and Power, Vol. 7, No. 1, 1991, pp. 65-67.
6. Sergeevsky, A., Snyder, G., and Cunniff, R., Earth to Mars Ballistic Mission Opportunities, 1990-2005, Jet Propulsion Laboratory Publication 82-43, Pasadena, CA, 1983, pp. 109-111, 133-135.
7. Sergeevsky A., and Cunniff R., Mars to Earth Ballistic Mission Opportunities, 1990-2005, Jet Propulsion Laboratory Publication 82-43, Pasadena, CA, 1983, pp. 103-105.
8. Wilson, A., ed., Interavia Space Directory, 1990-1991, Jane's Information Group, United Kingdom, 1990.
9. Andrews, D., Boeing Space and Defense Group, Seattle, WA, Personal Communication, April, 1992.
10. Brown, J.R. and Limerick, C.D., Expander Cycle Engine Applicability to Advanced Space Missions, 1989 JANNAF Propulsion Meeting, May 23-25, Cleveland, Ohio.
11. Mendell, W., "A Personal History of the Human Exploration Initiative with Commentary on the Pivotal Role for Life Support Research," NASA N91-13855, p 103.
12. Kourtides, D.A., Chiu, S.A., Iverson, D.J., and Lowe, D.M., "Thermal Response of Rigid and Flexible Insulations and Reflective Coatings in an Aero-convective Heating Environment", NASA TM 103925, March 1992.
13. Woodcock, G R., Space Transfer Concepts Analysis for Exploration Missions, Boeing Defense and Space Group, Advanced Civil Space Systems, Huntsville, Alabama, March 1991, p.193.
14. Sherwood, B., and Woodcock, G.R., "Engineering Aerobrakes for Exploration Missions," Acta Astronautica, Vol. 21, No. 6/7, 1990, p. 399.

15. Polocz, S., "Mars Observer Mission and Systems Overview," Journal of Spacecraft and Rockets, Vol. 28, No. 5, 1991, pp 491-497.
16. Eichholz, G.G., Radioisotope Engineering, Marcel Dekker Inc., New York, NY, 1972, pp 244, 387-389.
17. Chemical and Process Technology Encyclopedia, McGraw-Hill Book Company, New York, 1974, p. 603.
18. Nedell, S.S., Squyres, S.W., and Andersen, D.W., Origin and Evolution of the Layered Deposits in the Valles Marineris, Mars, Academic Press, Inc., 1987.
19. Budney, C.J., Snyder, G.C., Ionasescu, R., and Wallace, R.A., eds., "SEI Science Payloads: Description and Delivery Requirements," Report No. JPL D-7955, Rev. A, Jet Propulsion Laboratory, Pasadena, CA, May 17, 1992.
20. Asker, J. R., "NASA Offers Five Alternatives for Landing on Mars by 2018," Aviation Week and Space Technology, Vol. 131, November 27, 1989, pp. 30-31.

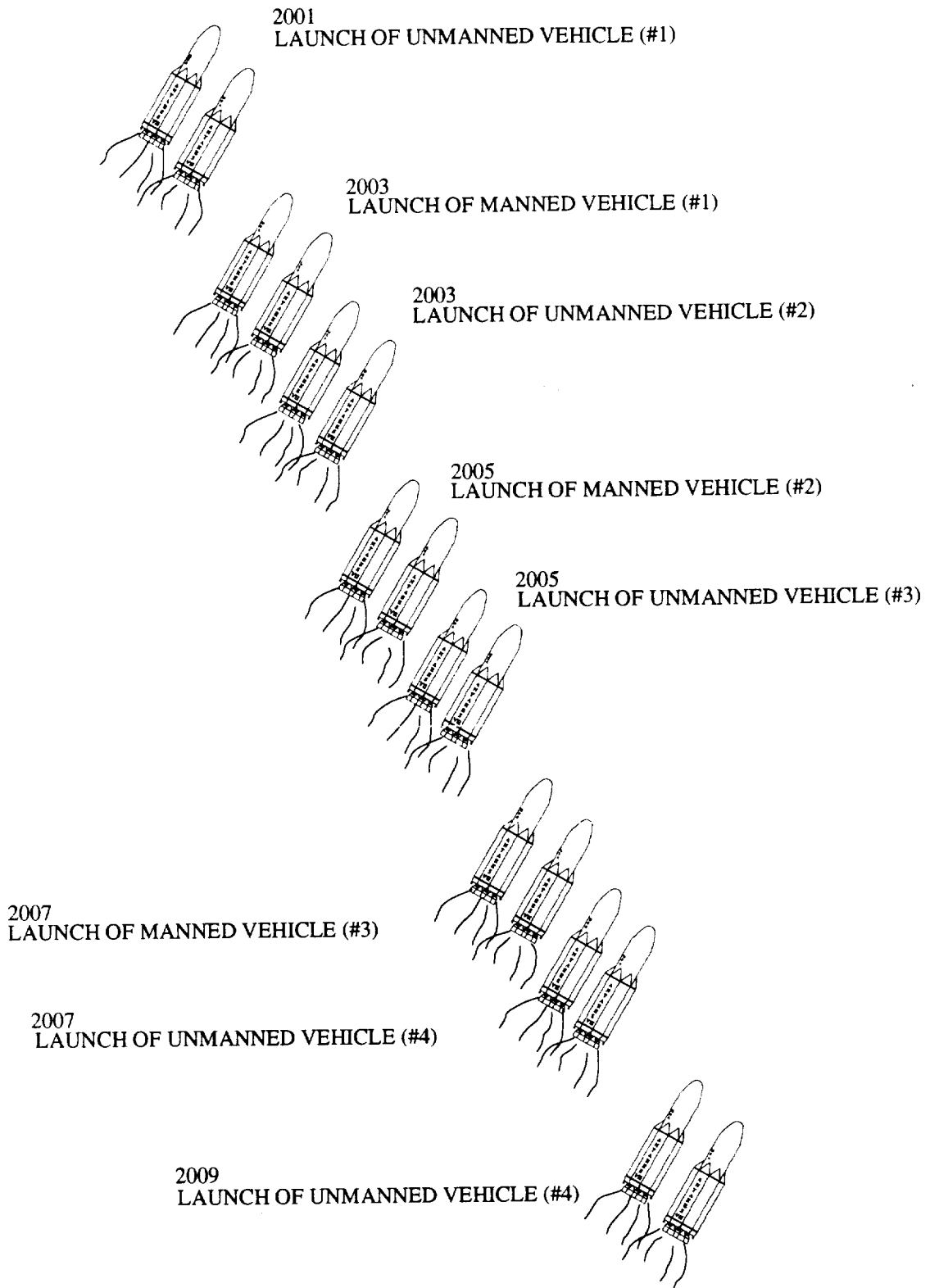


Fig. 1 Eight year mission model.

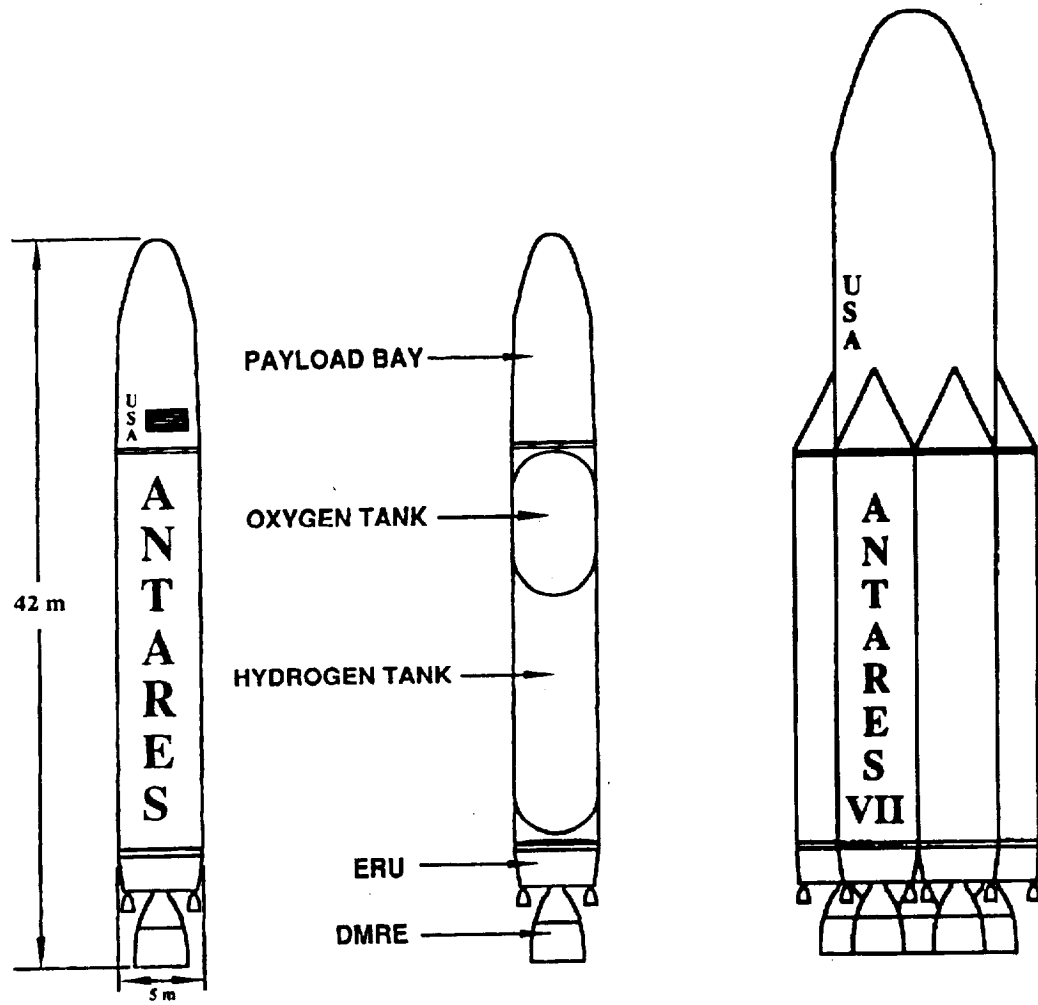


Fig. 2 Antares vehicle configurations.

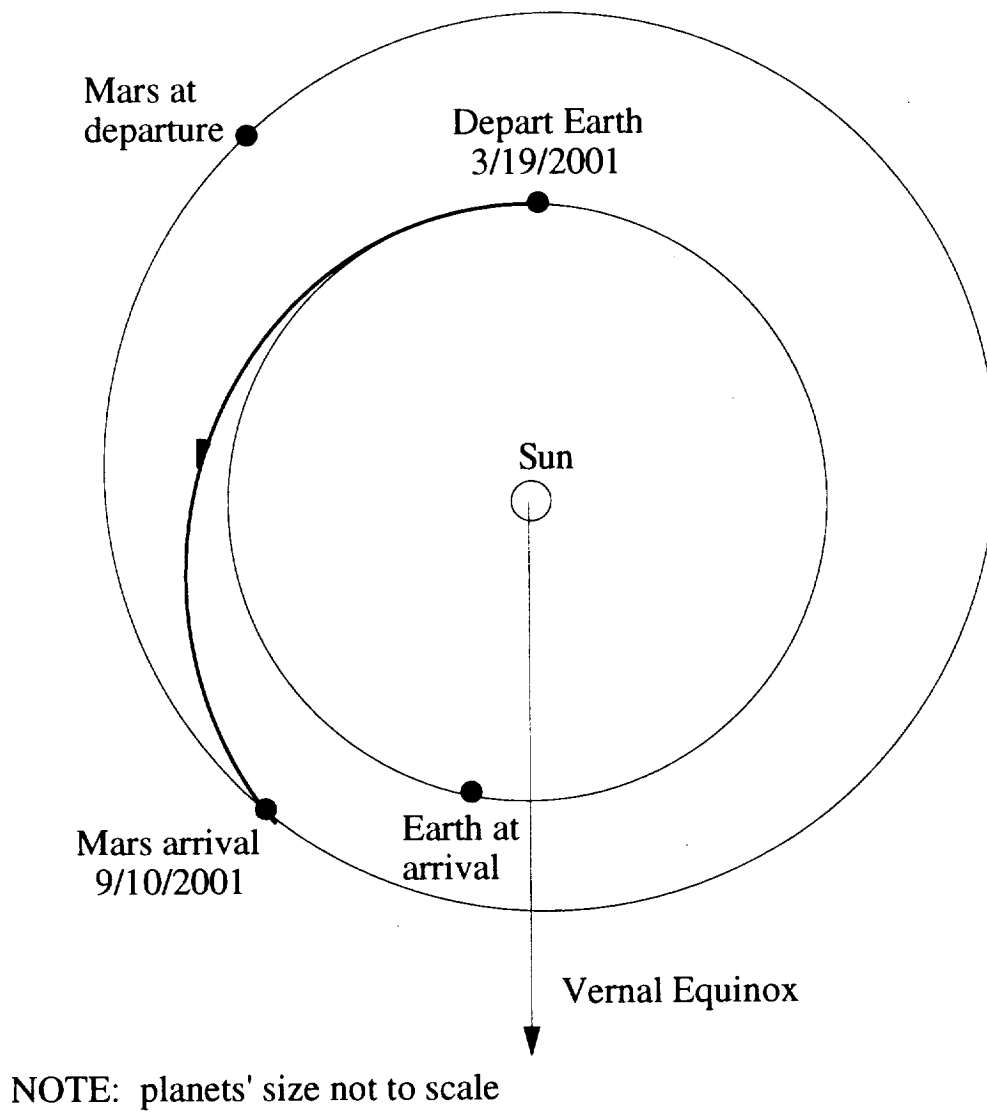


Fig. 3 Outbound unmanned transfer trajectory.

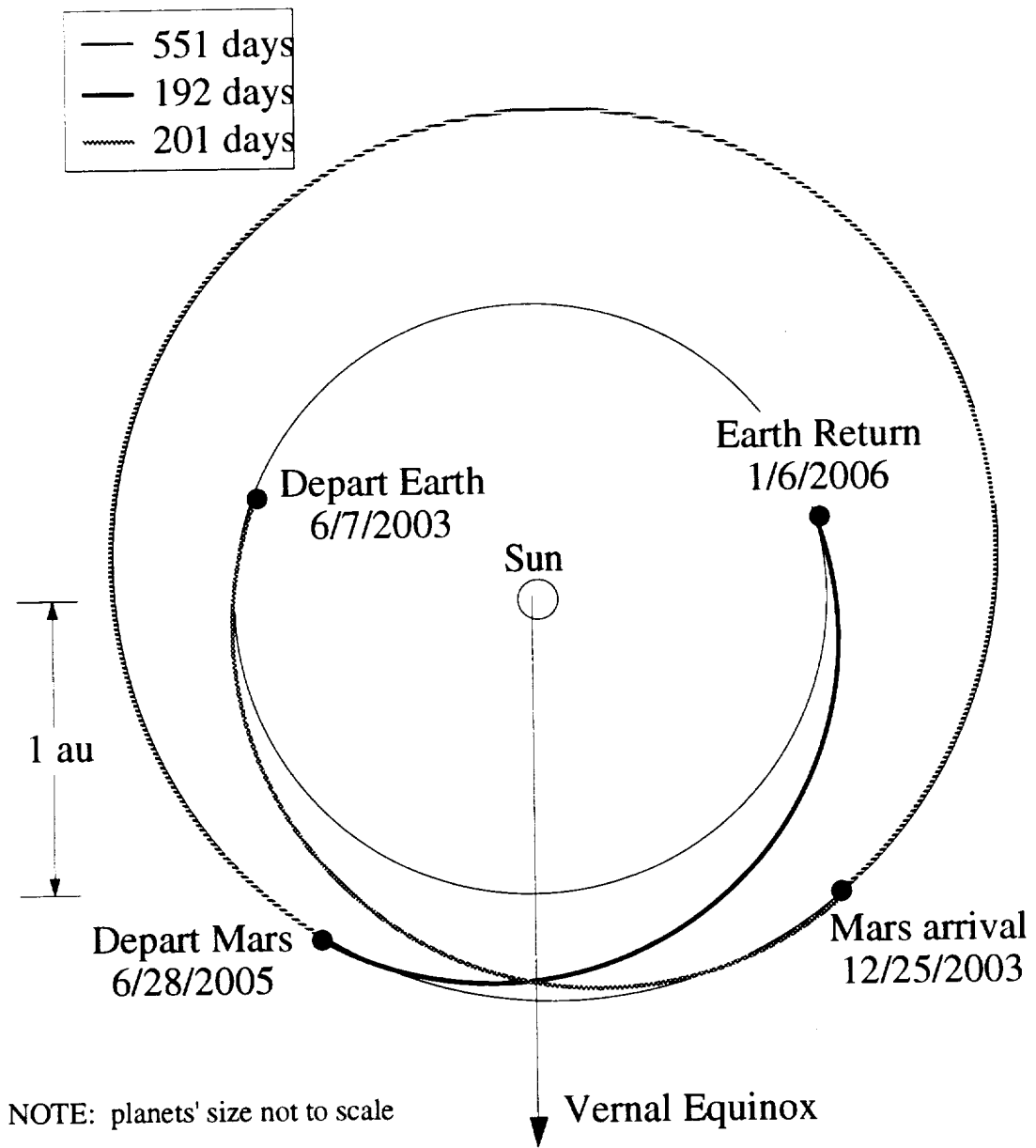


Fig. 4 Manned mission transfer trajectories.

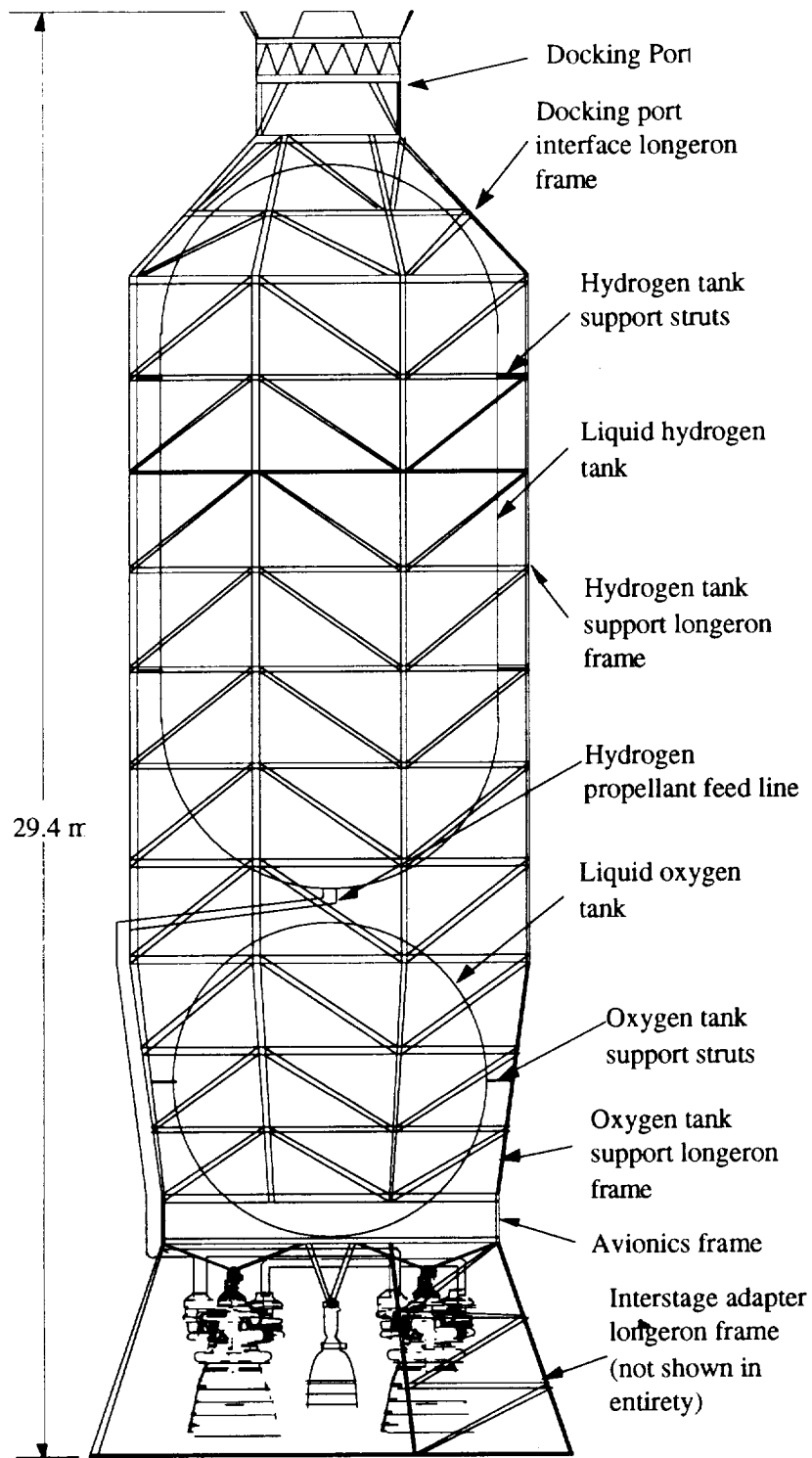


Fig. 5 Schematic of upper stage/TMI booster.

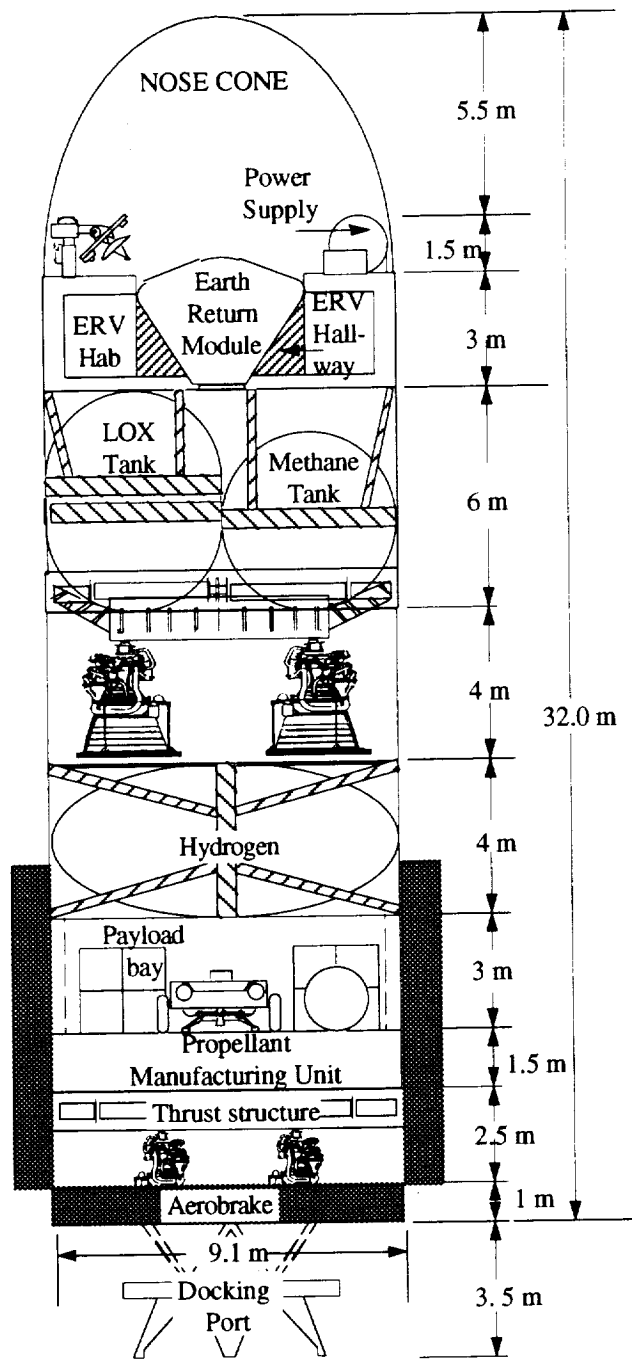


Fig. 6 Unmanned Mars transfer vehicle (UMTV).

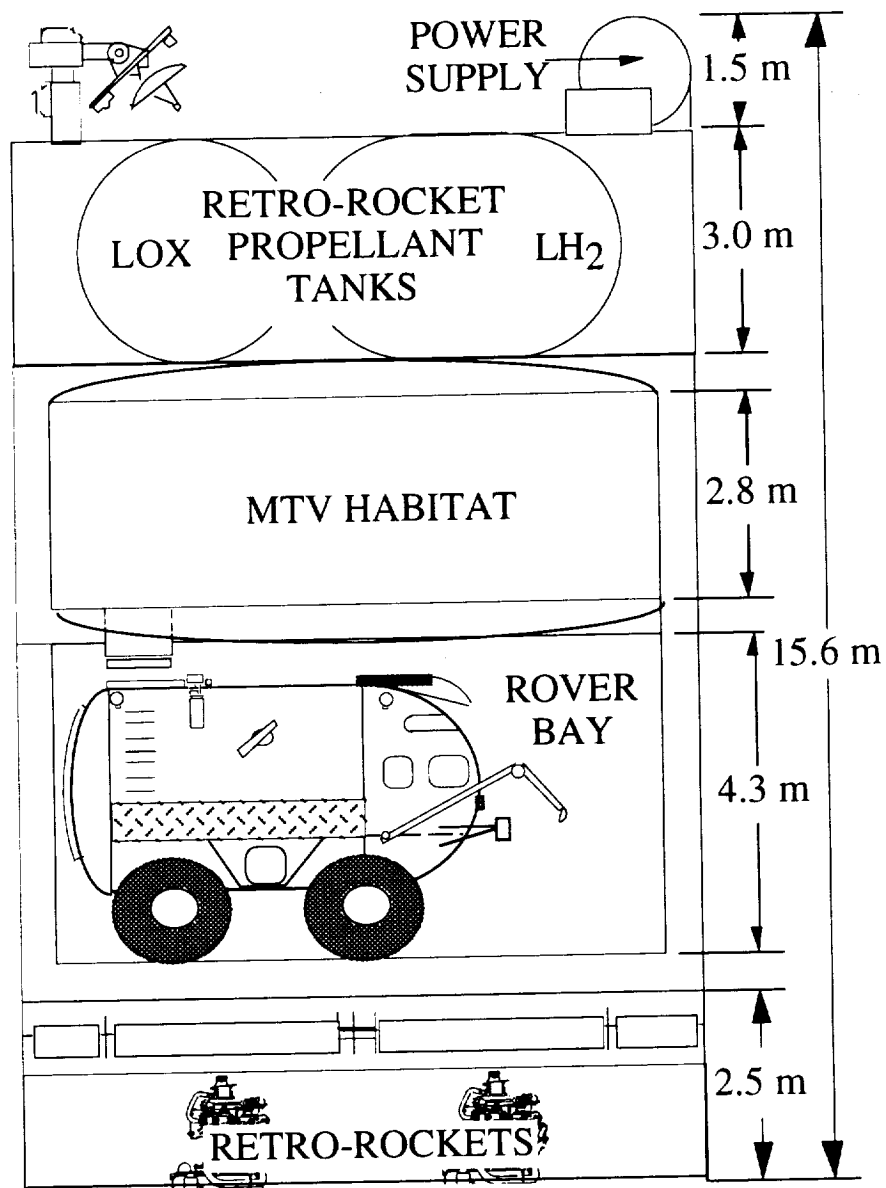


Fig. 7 Cutaway view of manned transfer vehicle.

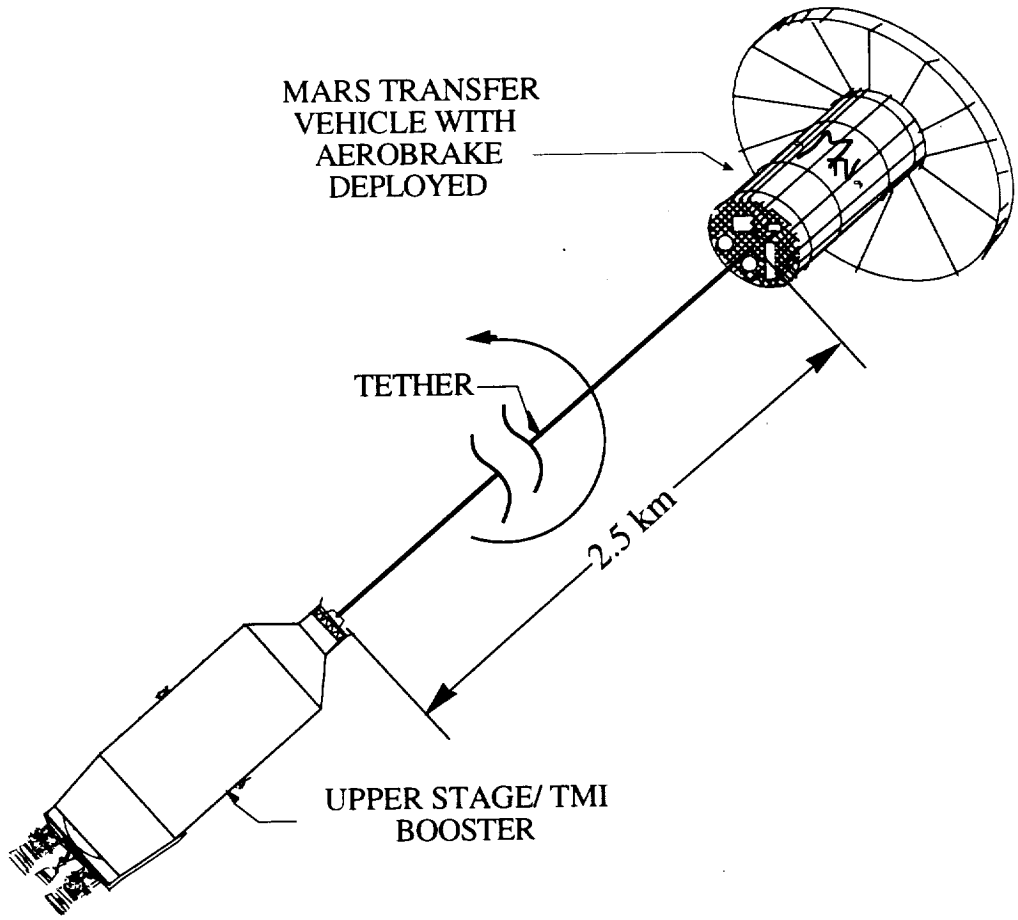


Fig. 8 Deployed tether.

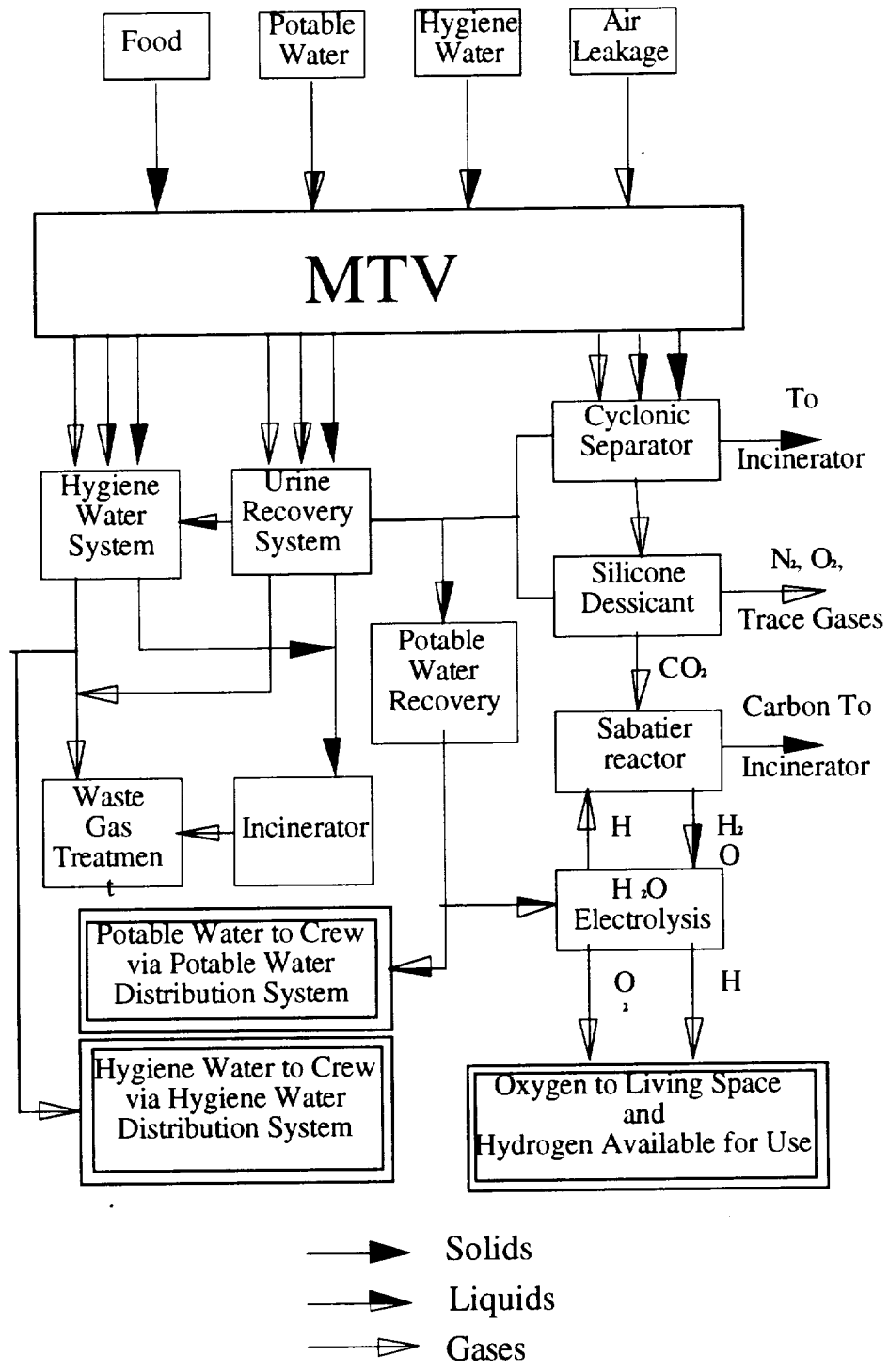


Fig. 9 Chemical regeneration system schematic.

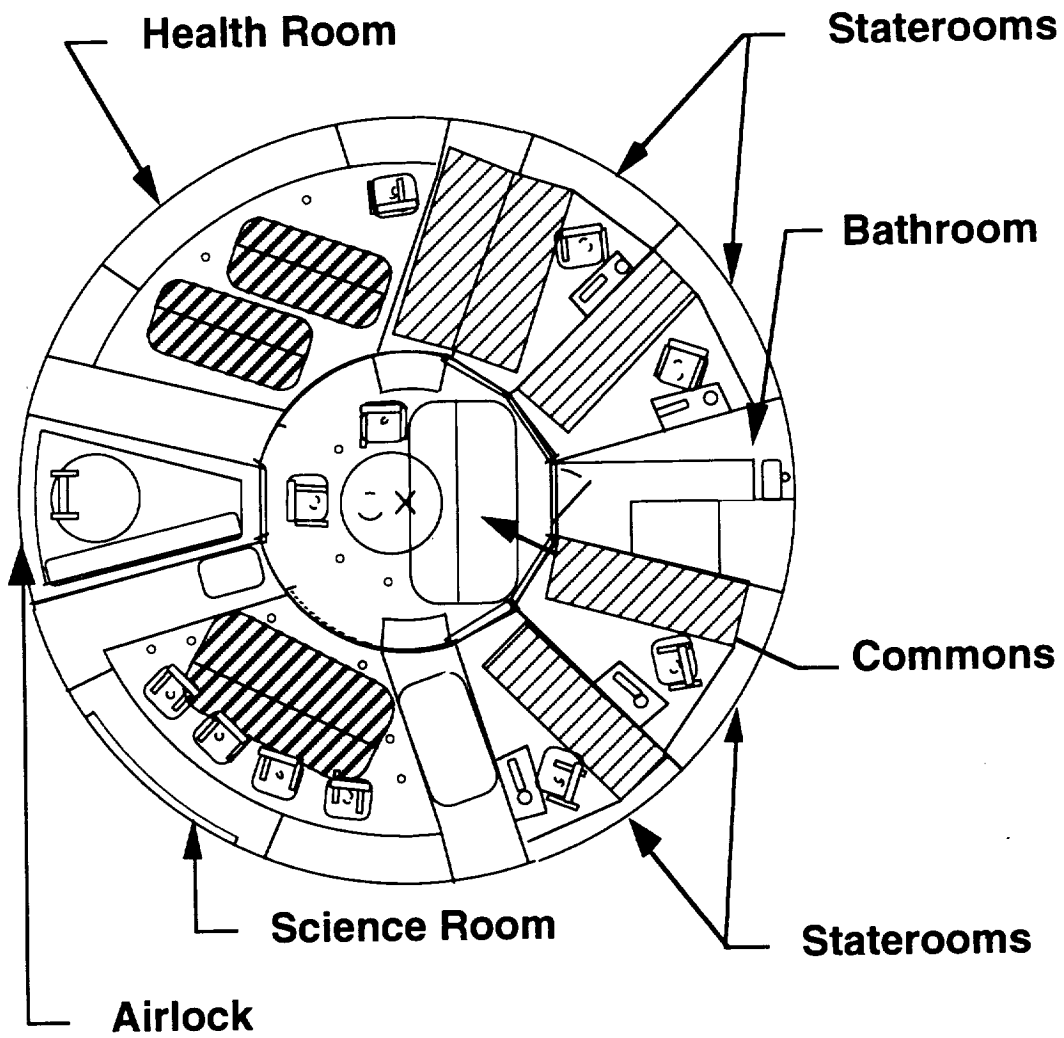


Fig. 10 Habitat floor plan.

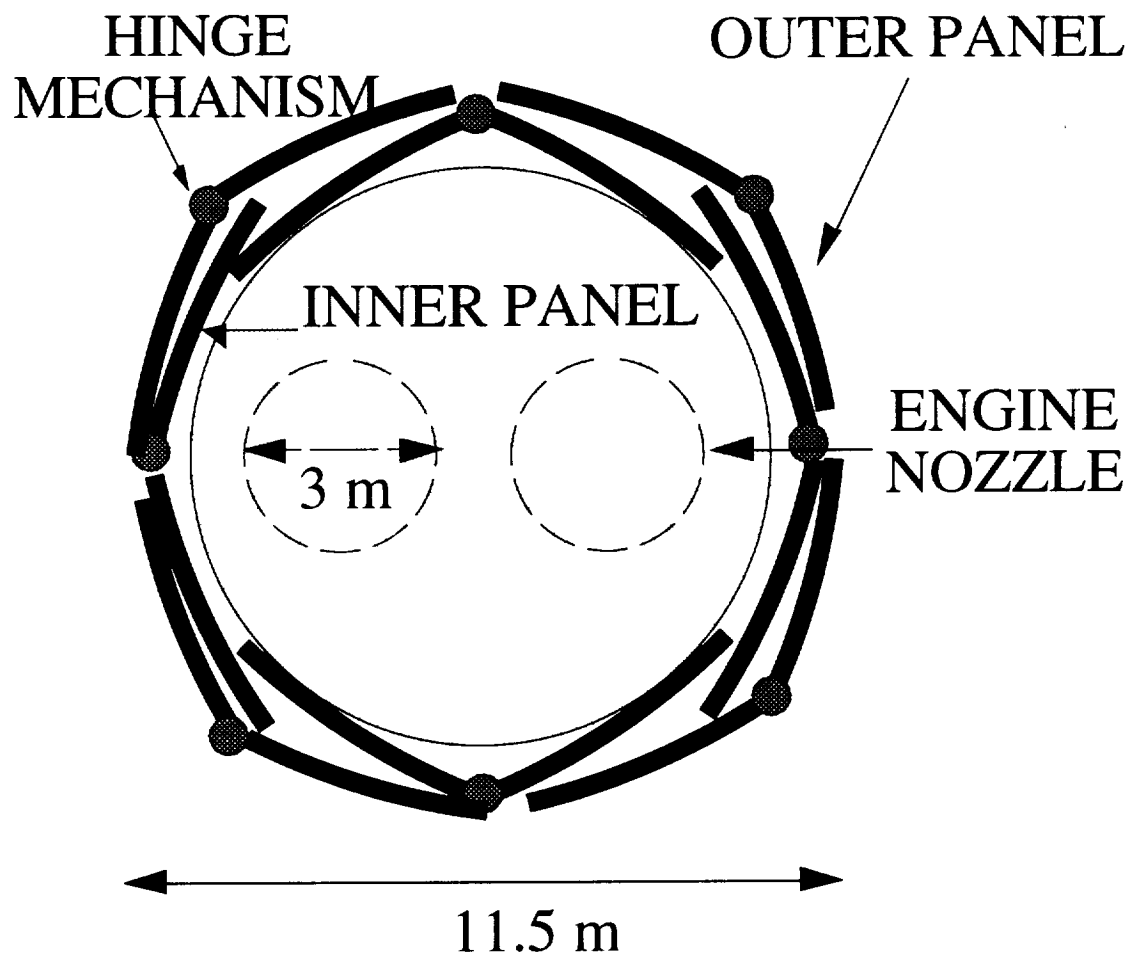


Fig. 11 Top view of aerobrake launch configuration.

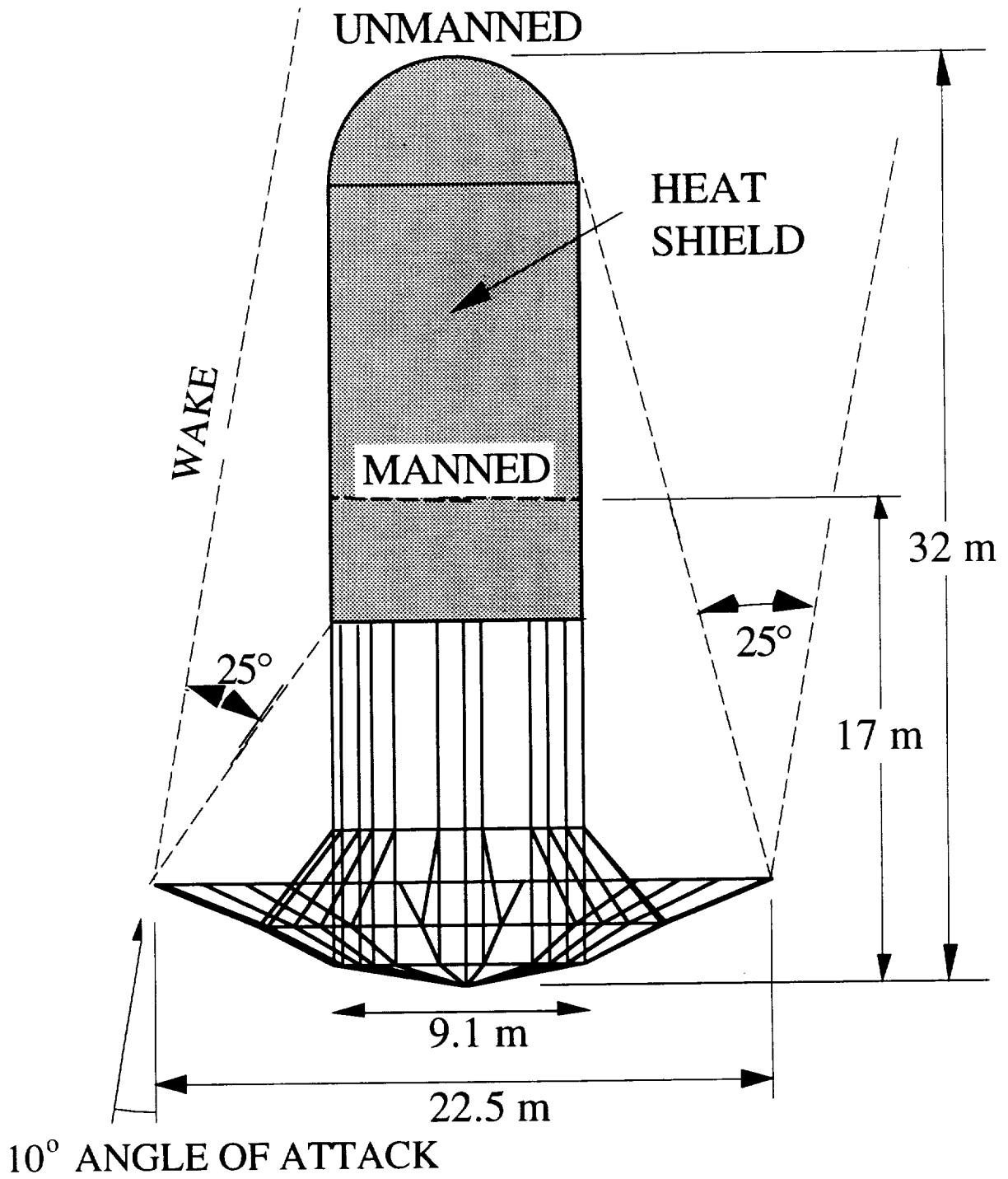


Fig. 12 Deployed aerobrake and transfer vehicle.

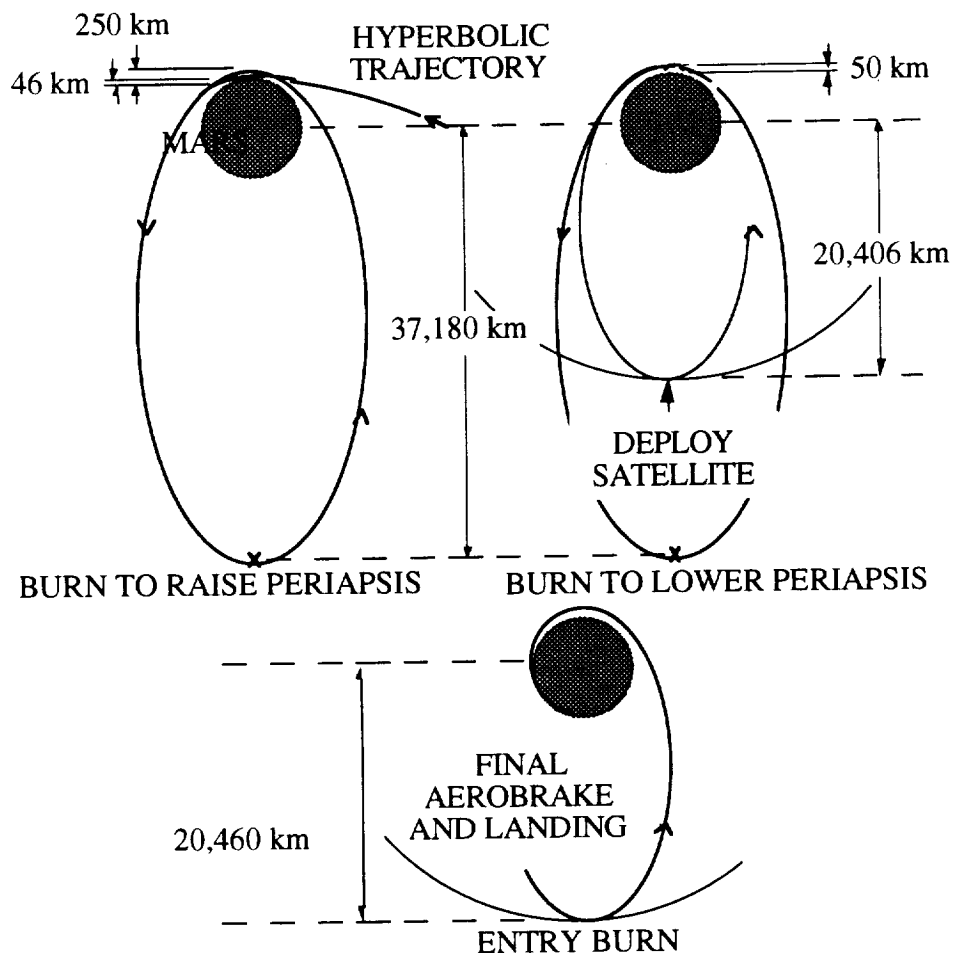


Fig. 13 Aerocapture and descent at Mars.

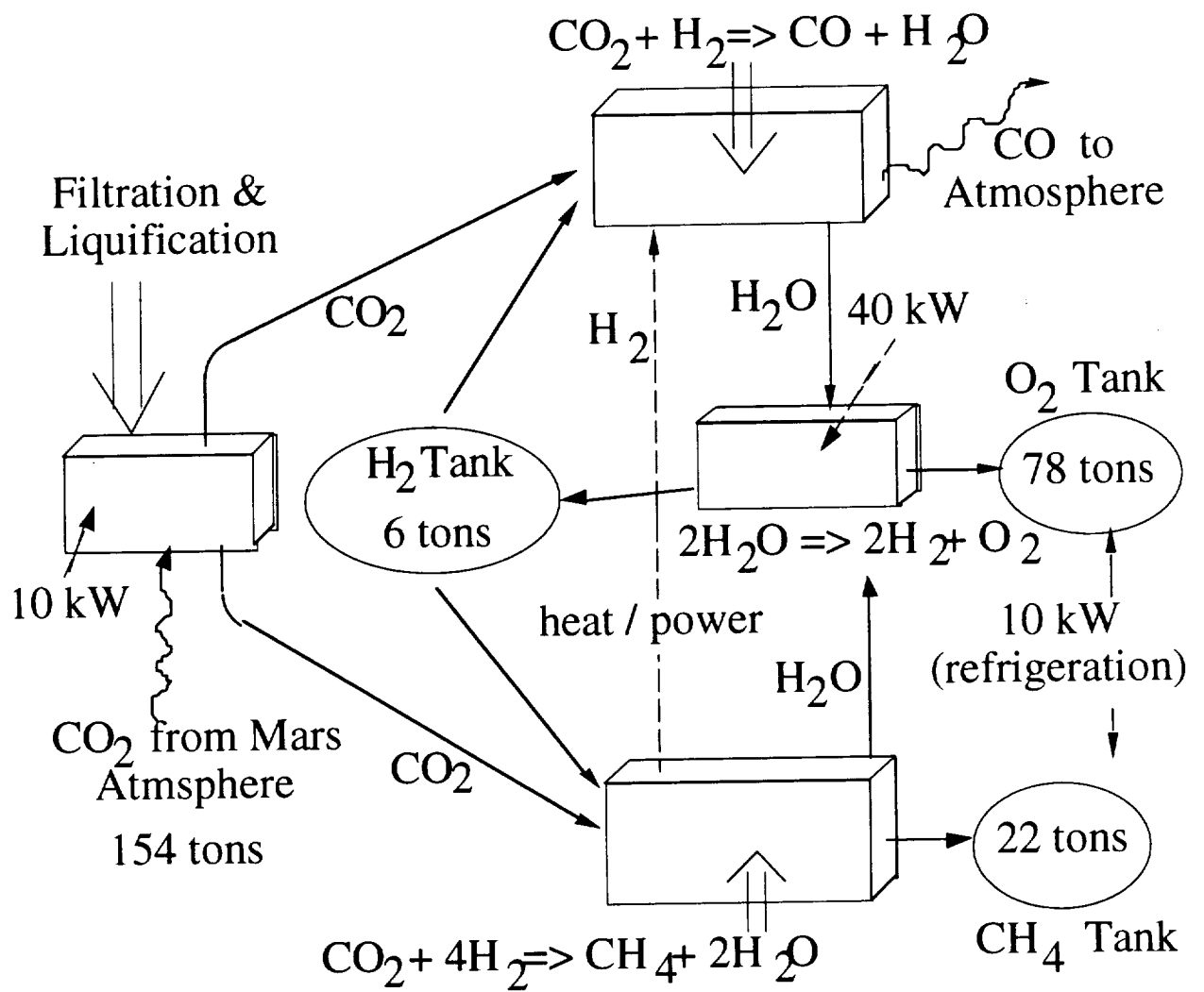
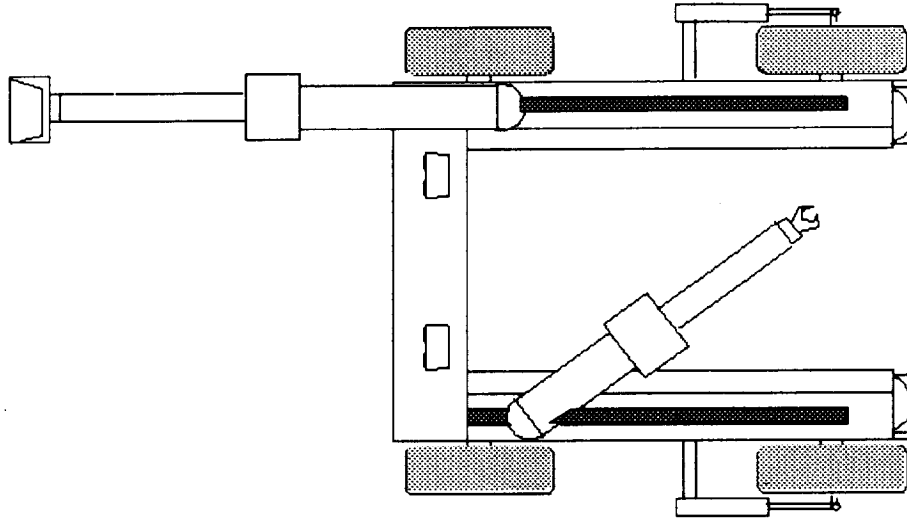


Fig. 14 Schematic of propellant production process.



Range: 400 km  
Mass: 1000 kg  
Ground Clearance: 0.65 m

Internal Combustion Engine  
Fuel Methane/Oxygen  
Speed: 8 km/hr

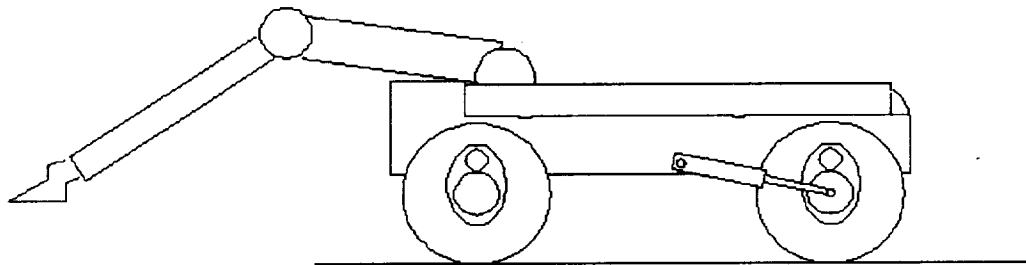
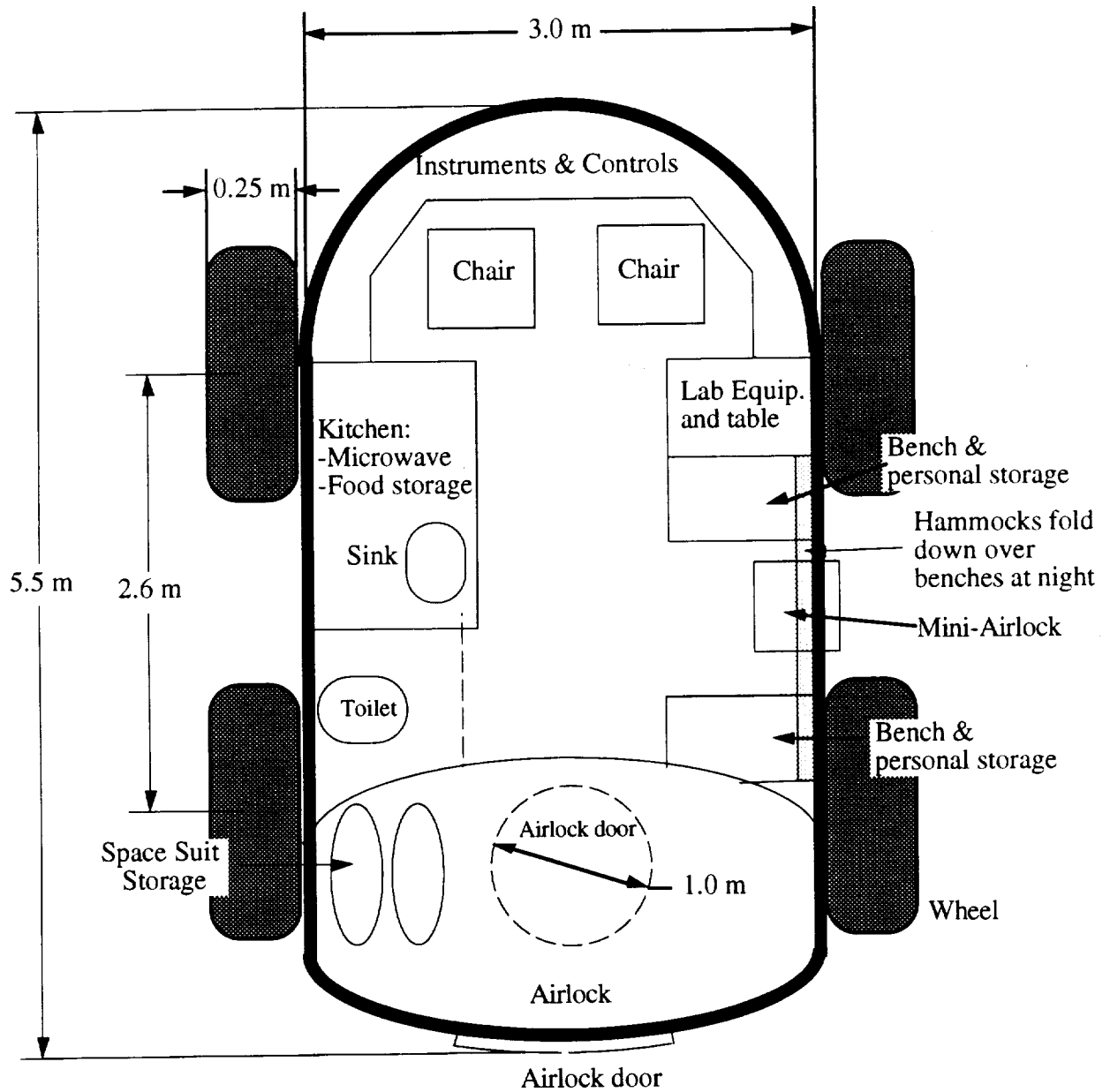


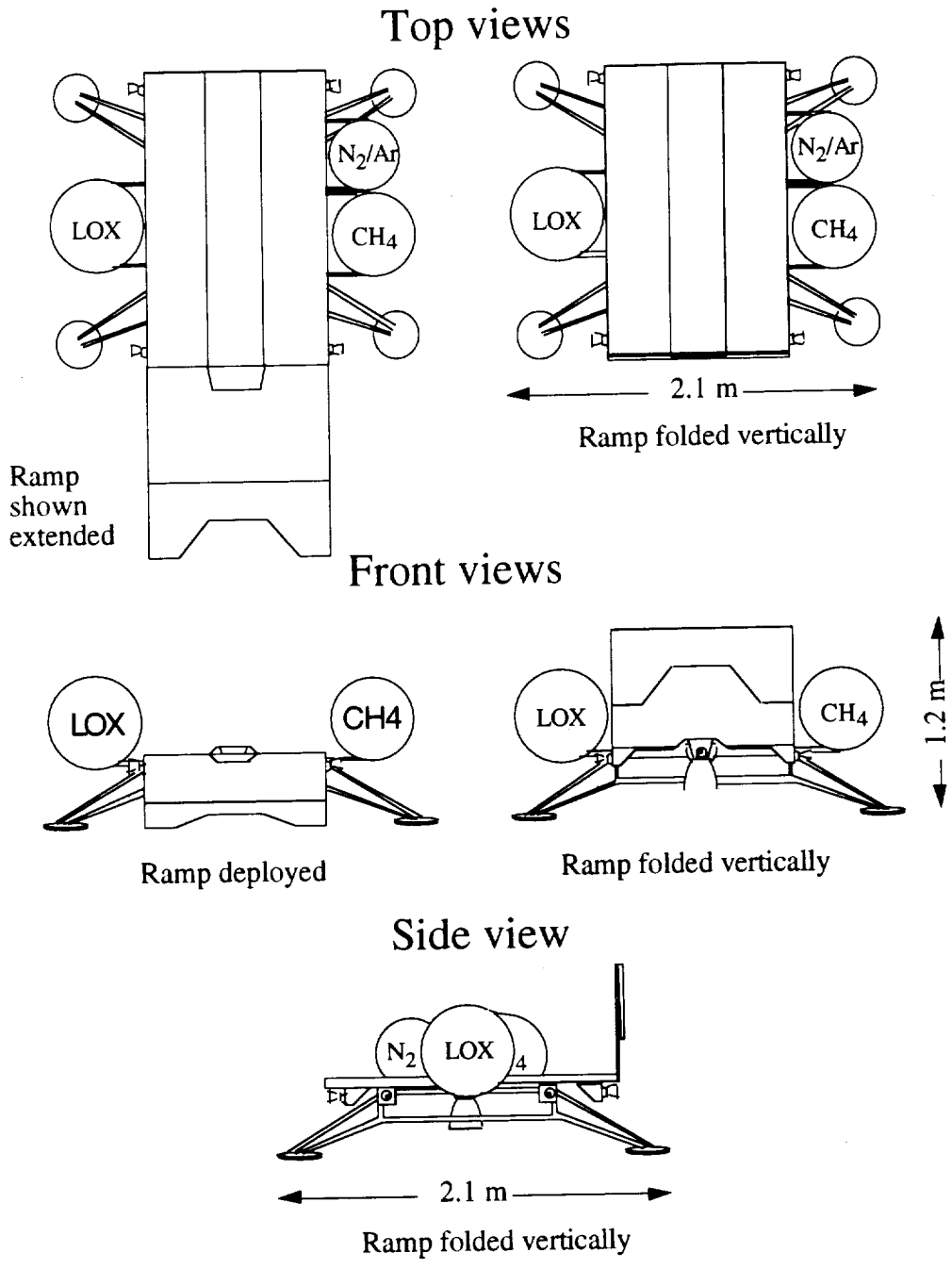
Fig. 15. Unmanned rover with robotic arms.



Range: 1000 km  
 Mass: 2250 kg  
 Ground Clearance: 0.5-1.0 m

Internal Combustion Engine  
 Fuel: Methane/Oxygen  
 Speed: 15 km/hr

Fig. 16 Manned Mars roving vehicle plan view.



Range: 11km  
 Mass: 250 kg

**Methane/Oxygen Engine**  
 Specific Impulse: 370 sec  
 Thrust: 8000 N

Fig. 17 Methane/LOX hopper.

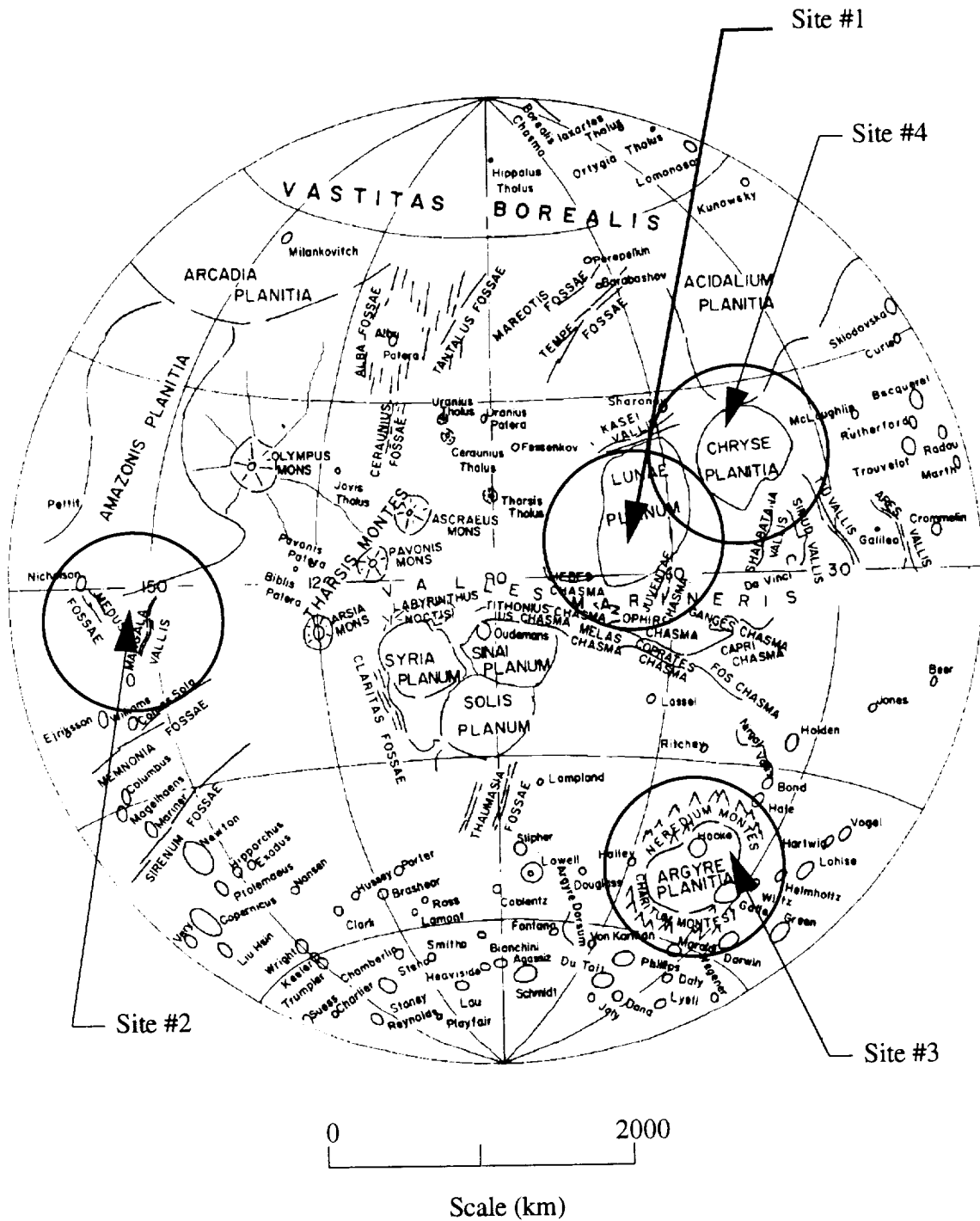


Fig. 18 Possible landing sites on Mars.

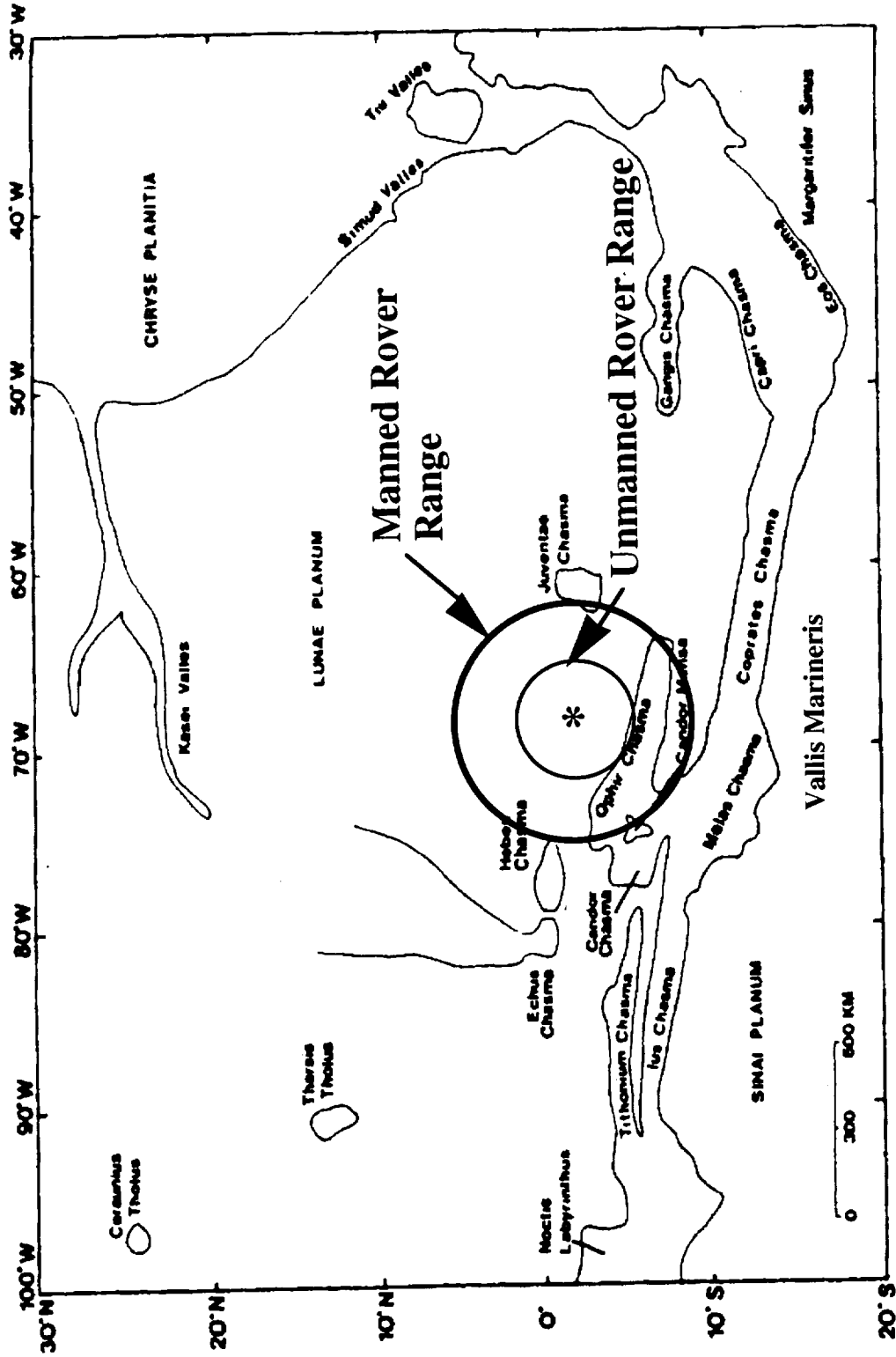


Fig. 19 Lunae Planum. Landing site is denoted by asterisk.

## **2.0 ORBITAL ANALYSIS**

Natasha Hanks  
Bryan Johnson  
Brian Thill

# TABLE OF CONTENTS

<b>2.1 INTRODUCTION</b> .....	2.1
<b>2.2 MISSION WINDOWS</b> .....	2.2
<b>2.3 MISSION OVERVIEW</b> .....	2.4
2.3.1 EARTH LAUNCH.....	2.4
2.3.2 EARTH ESCAPE.....	2.4
2.3.3 EARTH-MARS HELIOCENTRIC TRANSFER.....	2.6
2.3.4 MARS ARRIVAL.....	2.12
2.3.5 MARS SURFACE STAY.....	2.13
2.3.6 MARS ESCAPE.....	2.13
2.3.7 MARS-EARTH HELIOCENTRIC TRANSFER.....	2.14
2.3.8 EARTH CAPTURE.....	2.14
<b>2.4 MISSION CONSTRAINTS</b> .....	2.14
<b>2.5 TRAJECTORY ALTERNATIVE</b> .....	2.16
<b>2.6 CONCLUSIONS</b> .....	2.16
<b>NOMENCLATURE</b> .....	2.18
<b>REFERENCES</b> .....	2.20
<b>FIGURES</b> .....	2.21

## 2.1 INTRODUCTION

(Natasha Hanks)

Following the Mars Direct scenario outlined in Section 1 [1], a manned vehicle and an unmanned vehicle will depart from Earth every two years. Mission windows for the first unmanned mission in 2001 and the first manned mission in 2003 have been specified utilizing the Jet Propulsion Laboratory's plots of departure energy, hyperbolic excess velocity and time of flight [2]. Given departure and arrival dates, these plots, referred to as "pork chop" plots because of their appearance, define trajectory variables for the outbound and inbound orbits. The trajectory data obtained is based on elliptical, non-coplanar, "real" orbits. The options for the outbound transfer trajectory are opposition and conjunction class missions.

Although the quickest round trip time to Mars would be an opposition class mission, there are many drawbacks to that type of trajectory. An opposition class mission is defined as a high energy trajectory in which the departure position of Earth and arrival position of Mars are generally on the same side of the sun. Because of the large  $\Delta V$  required, a greater mass of propellant is required. This class of mission would take approximately 1.4 years round trip, with only 0.1 year on the Martian surface.[1] In addition, it would require an extended period of time in the inner solar system on the return journey, closer to the sun than the Earth's orbit. The particle radiation levels at this solar proximity would result in increased risks to the astronauts and the heat load to the vehicle would be significantly higher. In addition, the high-energy aerocaptures at Mars and Earth would submit the astronauts to as high as 8 to 10 g. It can be seen, therefore, that a number of limiting and dangerous factors exist for opposition class missions.[2]

For this project, a conjunction class mission has been chosen for both the unmanned and manned flights to and from Mars. Conjunction class missions are close to minimum energy orbits in which the departure position of the vehicle at Earth and the arrival position at Mars are approximately on opposite sides of the sun. The total mission time for a conjunction

class trajectory is on the order of 2.7 years with 1.4 years on the surface [1]. The risks involved are longer radiation exposure and an extended period of zero gravity for the astronauts. To limit the radiation exposure, the mission chosen will remain outside the Earth's orbit at all times. In addition, the vehicle will rotate about a tether to provide the astronauts with artificial gravity.

## 2.2 **MISSION WINDOWS**

(Natasha Hanks, Bryan Johnson, Brian Thill)

The first unmanned mission will depart in 2001 and the first manned mission will depart in 2003. The launch windows have been identified from the minimum energy limits represented in the "pork chop" plots [3,4]. These plots are called this because of their remarkable resemblance to the item of the same name. These plots are designed for non-coplanar, elliptical, "real" orbits. Use of these plots limit the accuracy of the hyperbolic excess speed at arrival to two decimal places. The departure energy,  $C_3$ , is equal to the square of the hyperbolic excess velocity and both flight windows are arbitrarily defined by a maximum  $C_3$  value of  $10 \text{ km}^2/\text{s}^2$  (see Fig. 2.1).

Windows of departure and arrival dates for the unmanned mission are based on the range of departure energy ( $C_3$ ) from the "pork chop" plots [3]. For a minimum energy transfer, the unmanned departure date will occur March 19, 2001, with arrival at Mars on September 10, 2001 for a flight time of 6 months. This is equivalent to a Hohmann Transfer, with  $C_3$  equal to  $8.634 \text{ km}^2/\text{s}^2$ . For a near minimum energy conjunction class mission, the launch window for the unmanned mission opens March 4, 2001 and closes April 2, 2001. The arrival window at Mars for this flight is from August 18, 2001 to October 17, 2001 as portrayed in Fig. 2.2. The flight trajectory is represented in Fig. 2.3 where the planets' locations were obtained from an orbital program (Voyager, version 1.2). An alternative method of plotting orbital trajectories is presented in Appendix A.

The minimum energy outbound trajectory for the unmanned mission has a Martian arrival hyperbolic excess speed of 3.6 km/s. The maximum hyperbolic excess velocity for the given launch window will be 6.3 km/s at Martian arrival. For design considerations, including Martian aerocapture, the maximum value will be used, in order to be conservative.

For the manned mission, the minimum departure energy,  $C_3$ , is equal to  $8.810 \text{ km}^2/\text{s}^2$ . The corresponding departure date from Earth is June 7, 2003 with a Mars arrival date of December 25, 2003 (Christmas Day). The launch window for Earth departure is from May 22, 2003 to June 22, 2003 and the Mars arrival window is from November 17, 2003 to January 27, 2004 [3] as shown in Fig. 2.4 and Fig. 2.5.

The minimum energy outbound trajectory for the manned mission has an arrival hyperbolic excess speed of 2.7 km/s. The maximum arrival hyperbolic excess velocity for the given launch window is 3.6 km/s for the manned mission. Again, for design considerations, including Martian aerocapture, the maximum value will be used.

For the return vehicle, the departure date from Mars for a minimum departure energy  $C_3$  of  $13.56 \text{ km}^2/\text{s}^2$  is June 28, 2005 and the Earth arrival date is January 6, 2006. The window for Mars departure, with an upper limit  $C_3$  of  $14 \text{ km}^2/\text{s}^2$ , is from June 17, 2005 to July 9, 2005. The Earth arrival window is from December 28, 2005 to January 15, 2006 [4], as shown in Fig. 2.6 and Fig. 2.7.

The minimum energy inbound trajectory for the manned mission has an Earth arrival hyperbolic excess speed of 2.9 km/s. The maximum Earth arrival hyperbolic excess velocity for the given launch window is 3.6 km/s. Again, for design considerations the maximum value will be used.

It should be noted that in the “pork chop” plots [3] the mission window for the minimum Earth arrival hyperbolic excess speed is different from the window for the minimum

departure energy from Mars. Since these dates differ, the launch window selected for this project is defined by the minimum departure energy,  $C_3$ , instead of the minimum arrival hyperbolic excess speed. Departure energy,  $C_3$ , has been given priority over hyperbolic excess speed in defining windows for this mission because defining the window by minimum arrival hyperbolic excess speed would require a significantly higher departure energy in most cases.

## **2.3 MISSION OVERVIEW**

### **2.3.1 EARTH LAUNCH**

(Natasha Hanks, Bryan Johnson, Brian Thill)

The first set of launches for both the unmanned and manned segments, will use an Antares VII [5] as a sub-orbital first stage booster to deliver an upper stage into a circular parking orbit. This upper stage will provide the propellant and propulsive system for the trans-Mars injection (TMI) burn. The second set of launches will involve an Antares VII launch from Earth to deliver a Mars Transfer Vehicle (MTV) that will rendezvous and dock with the upper stage/TMI booster in the same 300 km circular orbit. From this orbit the TMI burn will take place, sending the MTV into a hyperbolic escape trajectory. All Antares VII boosters will be launched from the Kennedy Space Center and result in a 150 km by 300 km elliptical orbit at a  $28.5^\circ$  inclination to the Earth's equator. Due to rate of orbital decay and time between Antares VII launches, this elliptical orbit will be circularized at 300 km. Details are provided in Section 3.0.

### **2.3.2 EARTH ESCAPE**

(Natasha Hanks, Bryan Johnson, Brian Thill)

From the 300 km circular orbit, a single propulsive burn will insert the vehicle into a hyperbolic Earth escape trajectory, as shown in Fig. 2.8. The burn can be modeled as impulsive because the chemical rocket expends its propellant over a relatively short time. The

$\Delta V$  for departure is determined using the maximum departure energy,  $C_3$ . For the given launch window,  $\Delta V$  is 3.649 km/s as calculated below.

Using the mechanical energy equation [6]:

$$\begin{aligned} V_I &= \sqrt{V_{\infty,D}^2 + 2\mu_E / r_I} \\ r_I &= h_I + r_E \\ V_{\infty,D} &= \sqrt{C_3} \end{aligned} \quad (2.1)$$

where:  $\mu_E$  = gravitational parameter of Earth =  $3.986 \times 10^5 \text{ km}^3/\text{s}^2$  [3]  
 $r_I$  = injection radius = 6678 km  
 $h_I$  = injection altitude = 300 km  
 $r_E$  = radius of Earth = 6378 km [3]  
 $V_{\infty,D}$  = departure hyperbolic excess velocity  
 $V_I$  = injection velocity

The following velocities are calculated for a  $C_3$  of  $10 \text{ km}^2/\text{s}^2$ :

$$\begin{aligned} V_{\infty,D} &= 3.162 \text{ km / s} \\ V_I &= 11.374 \text{ km/s} \end{aligned}$$

Using the equation for the velocity of an object in a circular orbit [5]:

$$V_{CS} = \sqrt{\frac{\mu_E}{r_{CS}}} \quad (2.2)$$

where:  $r_{CS}$  = radius of circular orbit = 300 km +  $r_E$   
 $V_{CS}$  = spacecraft velocity in circular orbit

It is found that the velocity of the spacecraft in LEO is:

$$V_{CS} = 7.726 \text{ km/s}$$

The propulsive burn,  $\Delta V_I$ , made at low Earth orbit (LEO) is calculated as follows:

$$\begin{aligned} \Delta V_I &= V_I - V_{CS} \\ \Delta V_I &= 3.649 \text{ km/s} \end{aligned} \quad (2.3)$$

### 2.3.3 EARTH-MARS HELIOCENTRIC TRANSFER (Natasha Hanks, Brian Thill)

The pork chop plots have eliminated the need to directly calculate the intricacies of the heliocentric transfer orbits. However, for purposes of mission planning it is important to understand the details of this phase of the mission. It is especially important to understand the definition of the design variables available to the astrodynamics group, and how they affect the parameters of the mission. Therefore, an increasingly complex investigation of the orbital trajectories, and the trends that they follow is necessary to make informed design decisions. For the purpose of recognizing and charting these trends, the following analysis has been developed.

The initial analysis is not complex: all planetary orbits are assumed to be both circular and coplanar. The model begins with the propellant mass ( $m_p$ ) expended in a single impulsive burn from LEO. Values have been given in terms of propellant masses rather than the more traditional  $\Delta V$ 's since the mass values are more intuitive and more easily applied to the design problem. Knowing the initial mass of the vehicle in LEO, 187,000 kg (see Section 3), the specific impulse (449 sec), and Earth's surface gravity ( $9.81 \text{ m/s}^2$ ), the rocket equation can be used to determine the  $\Delta V$  for the initial propellant mass:

$$\Delta V = g_E \cdot I_{sp} \cdot \ln\left(\frac{m_o}{m_o - m_p}\right) \quad (2.4)$$

$m_o$  = initial spacecraft mass

$m_p$  = propellant mass

$I_{sp}$  = specific impulse

$g_E$  = gravity at Earth's surface =  $9.81 \times 10^{-3} \text{ km/s}^2$

$\Delta V$  = velocity increment for a given burn

The initial velocity at the time of propellant burn is equal to the circular velocity of the 300 km low Earth orbit, 7.726 km/sec, as noted earlier.

The radius of the Earth's sphere of influence,  $r_{SE}$ , is given by [7]:

$$r_{SE} = R_E \left( \frac{\mu_E}{\mu_S} \right)^{\frac{2}{5}} \quad (2.5)$$

$R_E$  = Mean radius of Earth's orbit about the sun

$$= 1.495 \times 10^8 \text{ km}$$

$\mu_S$  = Gravitational parameter of the sun

$$= 1.327 \times 10^{11} \text{ km}^3 / \text{s}^2 \quad [3]$$

Thus,  $r_{SE} = 9.24 \times 10^5 \text{ km}$ .

The vehicle's velocity,  $V_{SE}$ , at the sphere of influence is then obtained from conservation of mechanical energy:

$$\frac{(V_{CS} + \Delta V)^2}{2} - \frac{\mu_E}{r_p} = \frac{V_{SE}^2}{2} - \frac{\mu_E}{r_{SE}}$$

Thus,

$$V_{SE} = \sqrt{(V_{CS} + \Delta V)^2 + 2\mu_E \left( \frac{1}{r_{SE}} - \frac{1}{r_{CS}} \right)} \quad (2.6)$$

After escaping the Earth's sphere of influence, the hyperbolic excess velocity of the vehicle, relative to Earth, is added vectorially to the orbital speed of the Earth, relative to the sun, to obtain the transfer orbit velocity near Earth,  $V_{TE}$ . Figure 2.9 is a graphical explanation of the vector addition. The flight path angle,  $\phi_1$ , is defined as the angle between the Earth's tangential velocity vector and the vehicle's departure velocity vector. This angle is determined by the departure asymptote at the sphere of influence and is an independent variable for the mission designer. Small variations of the flight path angle will have a great effect on several parameters which will be discussed later. Knowing the flight path angle and the velocity at Earth's sphere of influence, the velocity at the Martian sphere of influence can be determined

using the Law of Cosines, the conservation of mechanical energy about the sun, and the conservation of angular momentum about the sun.

First of all, the circular speeds of Earth,  $V_{CSE}$ , and Mars,  $V_{CSM}$ , about the sun can be found from:

$$\begin{aligned} V_{CSE} &= \sqrt{\frac{\mu_S}{R_E}} = 29.974 \text{ km / s} \\ V_{CSM} &= \sqrt{\frac{\mu_S}{R_M}} = 24.142 \text{ km / s} \end{aligned} \quad (2.7)$$

where  $R_E$  = Radius of Earth's orbit =  $1.495 \times 10^8$  km

$R_M$  = Radius of Martian orbit =  $2.278 \times 10^8$  km

Then the transfer orbit velocity at Earth,  $V_{TE}$ , can be found by the Law of Cosines (see Fig. 2.8). the flight path angle at Earth,  $\phi_1$ :

$$\begin{aligned} V_{SE}^2 &= V_{TE}^2 + V_{CSE}^2 - 2V_{TE} V_{CSE} \cos \phi_1 \\ V_{TE} &= (V_{SE} \cos(\phi_1)) \pm \sqrt{(V_{SE} \cos \phi_1)^2 - (V_{CSE}^2 - V_{SE}^2)} \end{aligned} \quad (2.8)$$

Now, knowing that the mechanical energy of this heliocentric transfer orbit is conserved, the velocity at Mars,  $V_{TM}$ , relative to the sun may be found as follows:

$$\begin{aligned} \frac{V_{TM}^2}{2} - \frac{\mu_S}{R_M} &= \frac{V_{TE}^2}{2} - \frac{\mu_S}{R_E} \\ V_{TM} &= \sqrt{V_{TE}^2 + 2\mu_S \left( \frac{1}{R_M} - \frac{1}{R_E} \right)} \end{aligned} \quad (2.9)$$

Again using the Law of Cosines the inbound velocity,  $V_{SM}$ , at the Martian sphere of influence can be determined.

$$V_{SM} = \sqrt{V_{TM}^2 + V_{CSM}^2 - 2V_{CSM} V_{TM} \cos \phi_2} \quad (2.10)$$

The flight path angle at Mars,  $\phi_2$ , can be found from the fact that the angular momentum,  $h$ , must also be conserved.

$$h = R_E V_{TE} \cos \phi_1 = R_M V_{TM} \cos \phi_2$$

$$\phi_2 = \cos^{-1} \left[ \frac{V_{TE}}{V_{TM}} \cdot \frac{R_E}{R_M} \cos \phi_1 \right] \quad (2.11)$$

Equation 2.10 and 2.11 are combined to find the velocity at the Martian sphere of influence as a function of the Earth transfer orbit velocity, and the Earth flight path angle:

$$V_{SM} = \sqrt{V_{TM}^2 + V_{CSM}^2 - 2V_{CSM} V_{TE} \left( \frac{R_E}{R_M} \right) \cos \phi_1}$$

$$V_{SM} = \sqrt{V_{TE}^2 + \mu_S \left( \frac{3}{R_M} - \frac{2}{R_E} \right) - 2V_{CSM} V_{TE} \left( \frac{R_E}{R_M} \right) \cos \phi_1} \quad (2.12)$$

Using Eq. 2.5, the radius of the Martian sphere of influence,  $r_{SM}$ , can be found:

$$r_{SM} = R_M \left( \frac{\mu_M}{\mu_S} \right)^{\frac{2}{5}}$$

where  $\mu_M =$  gravitational parameter of Mars

$$4.2828 \times 10^4 \text{ km}^3 / \text{s}^2 \quad (2.13)$$

$$\text{Thus, } r_{SM} = 5.766 \times 10^5 \text{ km}$$

Finally, the velocity of the vehicle as it enters the Martian atmosphere can be determined knowing that mechanical energy is conserved. For the purpose of aerobraking, the Martian atmosphere is assumed to extend to a 100 km altitude.

$$\frac{V_E^2}{2} - \frac{\mu_M}{r_{\text{atm},M}} = \frac{V_{SM}^2}{2} - \frac{\mu_M}{r_{SM}}$$

$$V_E = \sqrt{V_{SM}^2 + 2\mu_M \left( \frac{1}{r_{\text{atm},M}} - \frac{1}{r_{SM}} \right)} \quad (2.14)$$

$$r_{\text{atm},M} = \text{Radius of Martian atmosphere} = (100 + r_M) \text{ km}$$

$r_M$  - Radius of Martian surface = 3397.5 km

$V_E$  = Vehicle's velocity at entry into the Martian atmosphere

Now a relationship between the mass of the propellant burned at Earth and the Martian atmospheric entrance velocity can be plotted. The flight path angle at Earth,  $\phi_1$ , can be varied independently as well. A plot of the resulting trend can be seen in Fig. 2.10. Notice that the incoming velocity at Mars increases with the mass of propellant burned at Earth. Also, increasing the flight path angle reduces the Martian atmospheric entrance velocity for a given amount of propellant burn at Earth. Although the heliocentric velocity at Mars is greater, the relative velocity to Mars, or the vehicle velocity at the Martian Sphere of Influence, is smaller. This could become important for sizing the aerobrake, and deciding what ranges of Martian atmospheric entrance velocities to expect for aerobraking.

The time of flight for the heliocentric transfer trajectory is important for sizing of the life support requirements, and for calculating the useful time on the surface of Mars. Limiting the time of flight reduces passengers' exposure to solar radiation and zero gravity conditions. Also, minimizing the time of flight will add to the useful time on the Martian surface and contribute to the productivity of the mission.

Neglecting the travel time from the planet's surface to the point of hyperbolic escape at both the Earth-centered and the Mars-centered coordinate systems, the transfer orbit time of flight can be approximated as the heliocentric time of flight between Earth and Mars. For convenience, three general orbital elements of the heliocentric transfer orbit are first calculated before calculating the time of flight. These are the semi-major axis length,  $a$ , the magnitude of the angular momentum vector,  $h$ , and the orbital eccentricity,  $e$ . The semi-major axis length can be calculated from the mechanical energy equation, the angular momentum from the definition of the angular momentum, and the orbital eccentricity from Reference [6].

$$\frac{V_{TE}^2}{2} - \frac{\mu_S}{r_{TE}} = -\frac{\mu_S}{2a}$$

$$a = \frac{1}{\frac{2}{R_E} - \frac{V_{TE}^2}{\mu_S}} \quad (2.15)$$

$$\vec{h} = \vec{r} \times \vec{V}$$

$$|h| = R_E V_{TE} \cos(\phi_1) \quad (2.16)$$

$$e = \sqrt{1 - \frac{h^2}{\mu_S a}} \quad (2.17)$$

In order to calculate the heliocentric time of flight, the true anomaly of the vehicle at both Earth and Mars must be known. Because this model has circular planetary orbits about the sun, Earth's starting true anomaly,  $v_E$ , can be defined as zero when departure occurs. The Martian true anomaly,  $v_M$ , at arrival can be computed [6] from the orbital elements previously determined.

$$v_M = \cos^{-1} \left( \frac{1}{e} \left( \frac{h^2}{\mu_S R_M} - 1 \right) \right) \quad (2.18)$$

Next, the true anomalies are converted to eccentric anomalies,  $E$ , via the equations given below [6]:

$$E_E = \cos^{-1} \left( e + \frac{R_E}{a} \cos v_E \right)$$

$$E_E = \cos^{-1} \left( e + \frac{R_E}{a} \right) \quad (2.19)$$

$$E_M = \cos^{-1} \left( e + \frac{R_M}{a} \cos v_M \right)$$

$$E_M = \cos^{-1} \left( e + \frac{1}{a \cdot e} \left( \frac{h^2}{\mu_S} - R_M \right) \right) \quad (2.20)$$

$E_E$  = eccentric anomaly at Earth

$E_M$  = eccentric anomaly at Mars

Finally, the time of the outbound flight,  $TOF_1$ , along the elliptic heliocentric orbital trajectory can be determined using the following relation:

$$TOF_1 = \sqrt{\frac{a^3}{\mu_s}} [(E_M - e \cdot \sin E_M) - (E_E - e \cdot \sin E_E)] \quad (2.21)$$

Plotting the propellant mass burned at Earth versus the time of flight, while again varying the initial flight path angle, yields the relationship shown in Fig. 2.11. It can be seen from this plot that small increases in the propellant burned at Earth yield dramatic improvements in time of flight up to a certain point on the curve. Because of this relationship, it is desirable that the time of flight be on the order of 200 days where the benefits of added propellant result in small decreases of flight time so as to become unjustified. Also note that increasing the flight path angle does produce shorter missions with less propellant expended in the shorter time of flight (higher energy) region of the curve. As previously discussed, an increase in flight path angle for a given Earth propellant burn may shorten or lengthen the time of flight to Mars, but it will always reduce the velocity with which the vehicle enters the Martian atmosphere.

#### **2.3.4 MARS ARRIVAL** (Natasha Hanks, Bryan Johnson, Brian Thill)

When the vehicle enters the Martian sphere of influence it will be in a hyperbolic trajectory relative to Mars. During the hyperbolic flight, the vehicle will initially enter the Martian atmosphere at a height of 100 km above the surface, as assumed earlier. The vehicle will aerobrake in the Martian atmosphere at an initial close approach distance of approximately 50 km and exit the atmosphere with a velocity sufficient for a highly elliptical orbit around Mars. In the elliptical orbit, the vehicle will conduct aerobraking maneuvers and propulsive

burns to reduce the size of this orbit. Eventually the orbit will be circular and will begin to decay. This is discussed in Section 4.0.

The initial entrance speed,  $V_E$ , into the Martian atmosphere is determined from the mechanical energy Eq. 2.1:

$$V_E = \sqrt{V_{\infty,A}^2 + 2 \frac{\mu_M}{r_{atm,M}}} \quad (2.22)$$

$V_{\infty,A}$  = arrival hyperbolic excess velocity at Mars

For the unmanned segment, with a maximum hyperbolic arrival speed,  $V_{\infty,A} = 6.3$  km/s, the atmospheric entrance velocity is  $V_E = 7.95$  km/s. The manned segment will have a  $V_{\infty,A} = 3.6$  km/s and  $V_E = 6.04$  km/s.

### **2.3.5 MARS SURFACE STAY** (Natasha Hanks, Bryan Johnson, Brian Thill)

The mission dates and Earth to Mars trajectory have been selected to maximize the stay on Mars. If the minimum energies for arrival at Mars and departure to Earth are observed, the vehicle would arrive at Mars on December 25, 2003 and depart on June 28, 2005 [2,3]. This grants a total surface time of 1.44 years (526 days). This should be ample time to carry out a considerable amount of exploration and experimentation. The low energy windows for a conjunction class mission allow approximately 1.35 to 1.55 years (493 to 566 days) as a range of surface stay time.

### **2.3.6 MARS ESCAPE** (Natasha Hanks, Bryan Johnson, Brian Thill)

The vehicle will launch from the Martian surface and will be directly inserted into an Earth transfer orbit. The vehicle will be inserted into a hyperbolic Mars escape trajectory similar in appearance to Fig. 2.8.

### **2.3.7 MARS-EARTH HELIOCENTRIC TRANSFER** (Natasha Hanks, Bryan Johnson, Brian Thill)

This analysis is performed in a similar manner to Section 2.3.3. Similar design variables can be used to reduce the inbound time of flight, and improve the length of time on the Martian surface. These variables include the propellant mass expended in low Mars orbit, and the heliocentric flight path angle at Mars.

### **2.3.8 EARTH CAPTURE** (Natasha Hanks, Bryan Johnson, Brian Thill)

The capture at Earth will be similar to the Apollo program in that it will be a ballistic reentry. The maximum hyperbolic approach velocity for the given window is 3.6 km/s. From Eq. 2.22 and using an arbitrary altitude at entry of 100 km, the entrance velocity will be 11.6 km/s.

## **2.4 MISSION CONSTRAINTS** (Natasha Hanks, Bryan Johnson, Brian Thill)

Mass considerations are the limiting factor when computing the energy and velocity required to make a conjunction class transfer trajectory. Currently, the total propellant mass available will be 105,000 kg for the outbound Earth to Mars mission and 96,000 kg for the inbound Mars to Earth trip, as discussed in Section 3.

It is also desirable to maximize the surface time on Mars so that as much scientific data as possible may be collected. In order to do this, the relative phase angles of the planets and the times of flight on the inbound and outbound trajectories must be considered. The analysis here has been done using the circular and coplanar model discussed previously. Defining the time of Earth departure as "time zero," the true anomalies of Earth and Mars at any time,  $t$ , the mission time in Earth years, can be found as follows:

$$v_E = 2\pi t \quad (2.23)$$

$$v_M = \cos^{-1}\left(\frac{1}{e}\left(\frac{h^2}{\mu_S R_M} - 1\right)\right) + 2\pi\left(\frac{R_M}{R_E}\right)^{\frac{3}{2}}(t - \text{TOF}_1) \quad (2.24)$$

$\text{TOF}_1$  = Outbound time of flight in years

Note that when  $t=0$ ,  $v_E$  is zero. Also, it can be shown that the true anomaly of Mars at arrival ( $t=\text{TOF}_1$ ) is equal to the true anomaly that was expressed earlier in Eq. 2.17. The ratio of Mars to Earth's orbital radius is used to scale the mission time to Martian years.

What also must be known is the inbound time of flight,  $\text{TOF}_2$ , and the true anomaly,  $\Delta v$ , that is swept out during this trajectory. The inbound time of flight has been chosen as about 180 days for the same reason as the outbound time of flight (see Fig. 2.11). The true anomaly that is swept out cannot be solved for algebraically, but can be found using numerical methods on the time of flight, Eq. 2.15 to 2.21 above. The surface time,  $\tau_S$  can be calculated, given that Earth's true anomaly at the end of the mission must equal the sum of the true anomaly of Mars (at Mars departure) and the true anomaly swept out by the heliocentric transfer orbit. Note that all times must be expressed in Earth years.

Now the relationship between the mission duration on the Martian surface and other parameters can be examined. For example, Fig. 2.12 shows the relationship between outbound time of flight and time spent on the Martian surface. As one might expect, getting to Mars faster yields a longer time on Mars. Similarly, the propellant can be related to the mission surface time. The results of this are shown in Fig. 2.13. Again, the benefits of a finite flight path angle,  $\phi_1$ , at Earth are evident, since the time spent on the Martian surface increases with  $\phi_1$ . The time of flight for the heliocentric transfer trajectory is important for sizing the life support requirements, and for calculating the useful time on the surface of Mars. Limiting the time of flight reduces passengers' exposure to solar radiation and zero gravity conditions.

Also, minimizing the time of flight will add to the useful time on the Martian surface and contribute to the productivity of the mission.

## **2.5 TRAJECTORY ALTERNATIVE**

(Natasha Hanks, Bryan Johnson, Brian Thill)

With any manned mission it is necessary to examine the possibility of a mission critical failure occurring at any time during the mission. Therefore, one issue to explore is possible abort modes both in transit to Mars and at Mars. One abort mode for the trip to Mars that was examined was a heliocentric transfer orbit whose orbital period is an integer number of Earth years. With this type of trajectory the vehicle would be guaranteed to intersect the Earth's orbit without having to carry along fuel for a major trajectory change. The least energetic possibility was a heliocentric transfer orbit with a two year period which was determined to be too costly in propellant mass (see Fig. 2.11 around  $TOF_1=126$  days).

However, an abort mode at Earth departure was investigated. If improper injection were to occur during the TMI burn, then a retro-burn would be made to insert the vehicle into a highly elliptical orbit about Earth. At apoapsis of this elliptical orbit, an apogee burn will be made to decrease the periapsis altitude to within the Earth's atmosphere. The aerobrake will then be used for orbital circularization. From this orbit a space shuttle rendezvous would take place. Details are provided in Section 6.

## **2.6 CONCLUSIONS**

(Natasha Hanks, Bryan Johnson, Brian Thill)

Minimizing the required departure energy is an important factor in defining the capability of each mission. Energy savings ultimately results in a savings of propellant and an increase in payload capacity. However, a slight increase in the energy of the transfer trajectory (C<sub>3</sub>) yields a significant decrease in travel time and a large increase in useful time on the Martian surface. The ideal case is to discover an optimum balance between payload capability

and stay time on Mars. Ultimately, the final objective is to have as much time on Mars as possible, and a conjunction class mission best satisfies this mission's goals.

The astrodynamics of the mission are not independent of other areas of the mission design. Instead it is coupled with all aspects of the mission. Some examples are life support mass for the manned vehicle, and  $H_2$  boil-off for the unmanned vehicle. Where the propellant mass expended at Earth decreases with a longer time of flight, the mass of life support expendables increases. Therefore, looking at the propellant usage alone may not give a true impression of the mass trends involved. In order to examine these effects, the mass of life support expendables is combined with the propellant mass relations discussed previously. The mass of the expendables that must be taken on the manned vehicle is a function of the sum of the outbound time of flight and the time on the surface of Mars. This relationship is shown in Fig. 2.14 as obtained from information provided in Section 5.0. Then in Fig. 2.15, the propellant mass expended at Earth is added. By looking at more than one source of mass as a function of mission duration on the Martian surface, it can be seen that the mass penalty for a longer stay on the surface is actually much worse than what propellant mass alone (Fig. 2.13) would indicate.

# NOMENCLATURE

a	Semi major axis length
Antares VII	Seven unit Antares launch vehicle configuration
$C_3$	Departure energy (equal to the square of the hyperbolic excess velocity)
e	Orbital eccentricity
$E_E$	Eccentric anomaly at Earth
$E_M$	Eccentric anomaly at Mars
$g_E$	Gravitational acceleration at Earth's surface = $9.81 \times 10^{-3} \text{ km/s}^2$
h	Magnitude of the angular momentum vector
$h_I$	Injection altitude
$h_T$	Transfer orbit angular momentum
$I_{sp}$	Specific Impulse
LEO	Low Earth Orbit
LMO	Low Mars Orbit
MTV	Mars Transfer Vehicle
m	Vehicle mass
$m_o$	Initial vehicle mass
$m_p$	Propellant mass
$\phi_1$	Flight path angle of the heliocentric transfer orbit at Earth at departure
$\phi_2$	Flight path angle of the heliocentric transfer orbit at Mars at arrival
$r_{cs}$	Radius of circular Earth orbit = $300 \text{ km} + R_E$
$R_E$	Mean radius of Earth's orbit about the sun = $1.495 \times 10^8 \text{ km}$
$R_M$	Mean radius of Martian orbit about the sun = $2.278 \times 10^8 \text{ km}$
$r_I$	Injection radius = $R_E + H_I = 6678 \text{ km}$
$r_E$	Radius of Earth = $6378.14 \text{ km}$ [3]
$r_M$	Radius of Mars = $3397.5 \text{ km}$ [3]
$r_{SE}$	Radius of the Earth's sphere of influence

$r_{SM}$	Radius of the Martian sphere of influence
$r_{TE}$	Radius of Mars orbit around the Sun at arrival
$r_{atm.M}$	Radius of Martian atmosphere = (100 + 3397.5) km
$t$	Mission time in Earth years
$t_S$	Surface time on Mars in Earth years
TMI	Trans-Mars Injection
$TOF_1$	Outbound time of flight in years
$TOF_2$	Inbound time of flight in years
$\mu_E$	Gravitational parameter of Earth = $3.986 \times 10^5 \text{ km}^3/\text{s}^2$ [3]
$\mu_M$	Gravitational parameter of Mars = $4.2828 \times 10^4 \text{ km}^3/\text{s}^2$ [3]
$\mu_S$	Gravitational parameter of the Sun = $1.327 \times 10^{11} \text{ km}^3/\text{s}^2$ [3]
$V_I$	Injection velocity
$\Delta V_1$	Velocity increment for departure at Earth
$\Delta V_2$	Velocity increment for departure at Mars
$V_{\infty,D}$	Departure hyperbolic excess velocity on Earth
$V_{\infty,A}$	Arrival hyperbolic excess velocity at Mars
$V_E$	Vehicle's velocity at entry into the atmosphere
$V_{CS}$	Spacecraft velocity in circular orbit around Earth
$V_{SE}$	Vehicle's velocity at the sphere of influence of the Earth
$V_{SM}$	Vehicle's velocity at the Martian sphere of influence
$V_{CSE}$	Circular heliocentric orbital speed of Earth = 29.794 km/s
$V_{CSM}$	Circular heliocentric orbital speed of Mars = 24.142 km/s
$V_{TE}$	Transfer orbit velocity at Earth
$V_{TM}$	Transfer orbit velocity at Mars
$v_M$	The Martian true anomaly at arrival
$v_E$	Earth's starting true anomaly
$\Delta v$	True anomaly that is swept out during an inbound orbital trajectory

## REFERENCES

1. Drake, B., Joosten, K., Lineberry, E., and Weaver, D., "Orbital Mechanics Tutorial Presentation to the Synthesis Group," Lunar and Mars Exploration/ Mission Development Office, National Aeronautics and Space Administration, September 4, 1990.
2. Zubrin, R., Baker, D., and Gwynne, O., "Mars Direct: A Simple, Robust, and Cost Effective Architecture for the Space Exploration Initiative," AIAA Paper No. 91-0326, American Institute of Aeronautics and Astronautics, Inc., Washington, D.C., 1991.
3. Sergeevsky A., Snyder G., and Cunniff R., Earth to Mars Ballistic Mission Opportunities, 1990-2005, Jet Propulsion Laboratory Publication 82-43, Pasadena, CA, 1983, pp. 109-111, 133-135.
4. Sergeevsky A., and Cunniff R., Mars to Earth Ballistic Mission Opportunities, 1990-2005, Jet Propulsion Laboratory Publication 82-43, Pasadena, CA, 1983, pp. 103-105.
5. Project Antares: A Low Cost Modular Launch Vehicle for the Future, Final Report, Space Systems Design, AA420/421 University of Washington Department of Aeronautics and Astronautics, Seattle, WA, June 1991.
6. Bate R., Mueller D., and White J., Fundamentals of Astrodynamics, Dover Publications Inc., New York, N.Y., 1971.
7. Battin, R. H., An Introduction to the Mathematics and Methods of Astrodynamics, American Institute of Aeronautics and Astronautics, Inc., New York, N.Y., 1987, pp. 395-396.

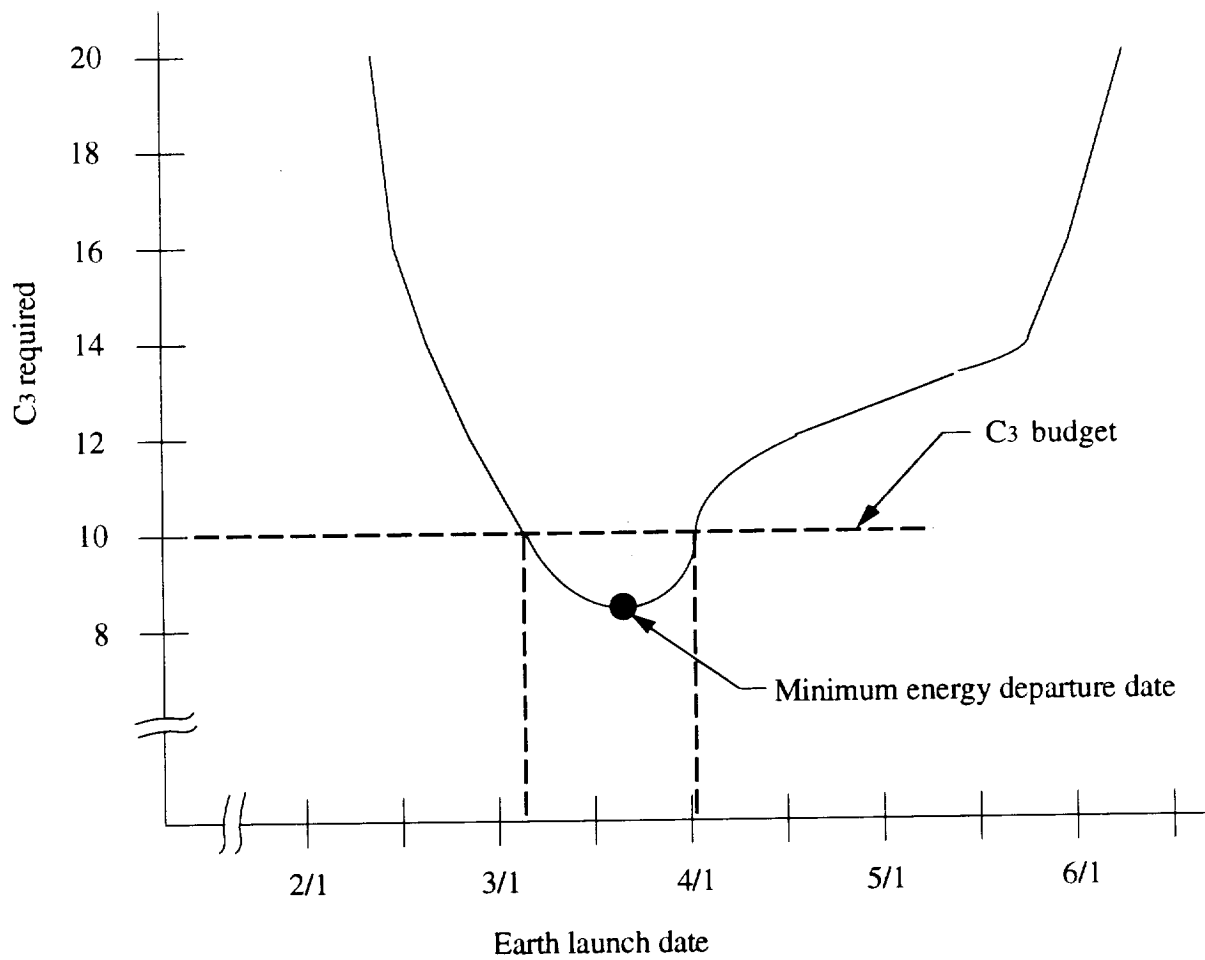


Fig. 2.1 Earth departure C3 variation with launch date for 2001 [3]

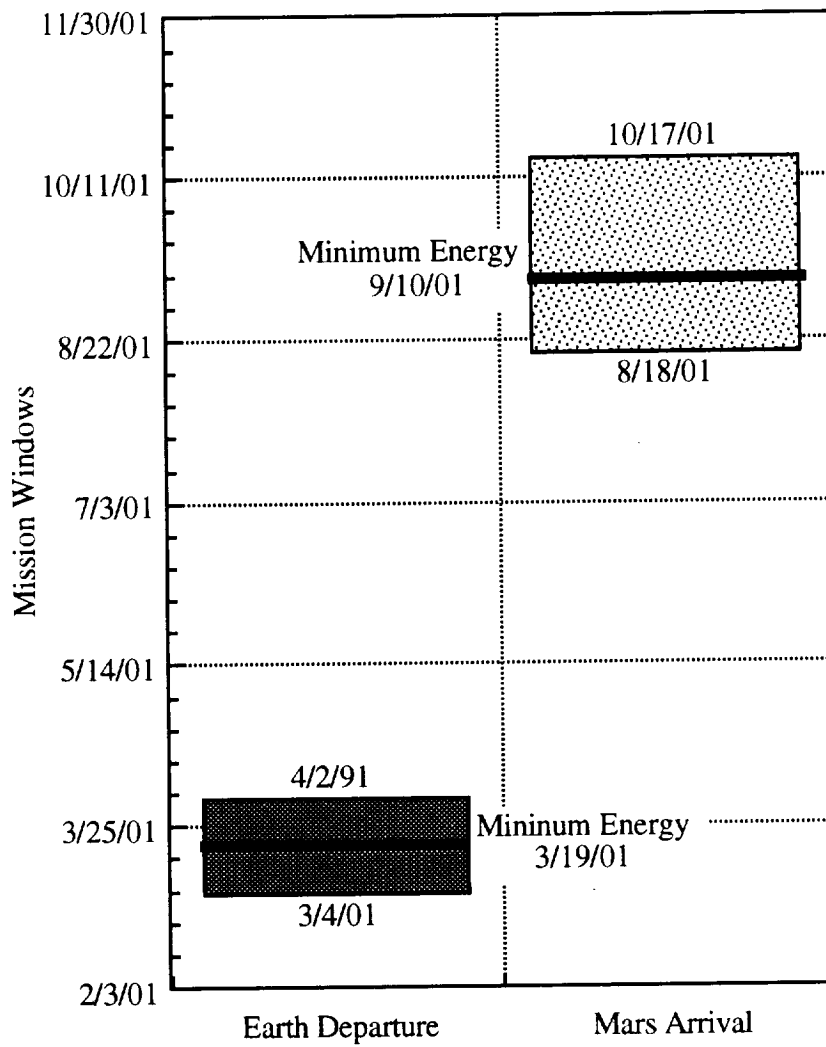


Fig. 2.2 Mission windows for outbound unmanned segment.

NOTE: sun's and planets' sizes not to scale

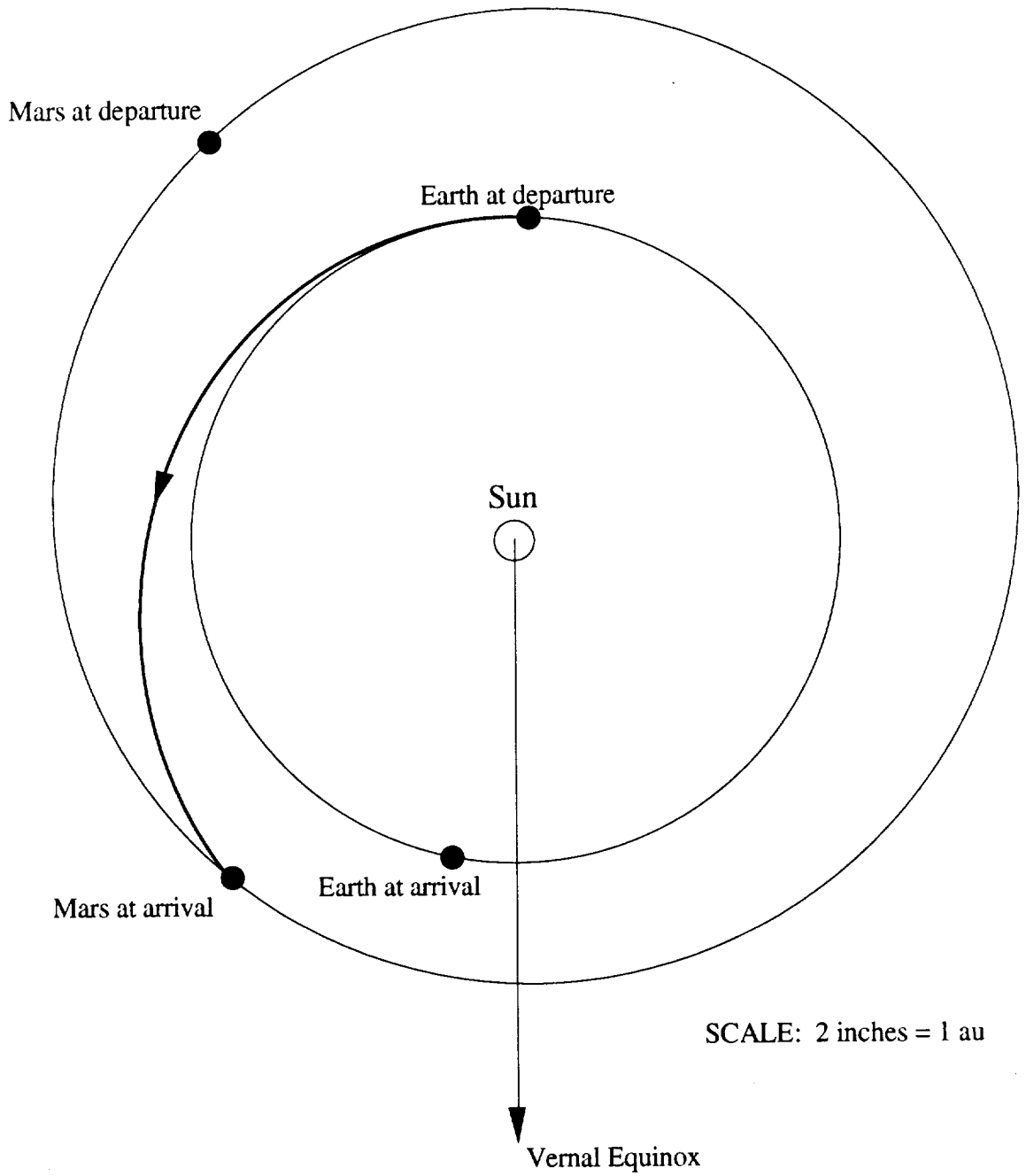


Fig. 2.3 Outbound unmanned mission conjunction class transfer trajectory for the year 2001.

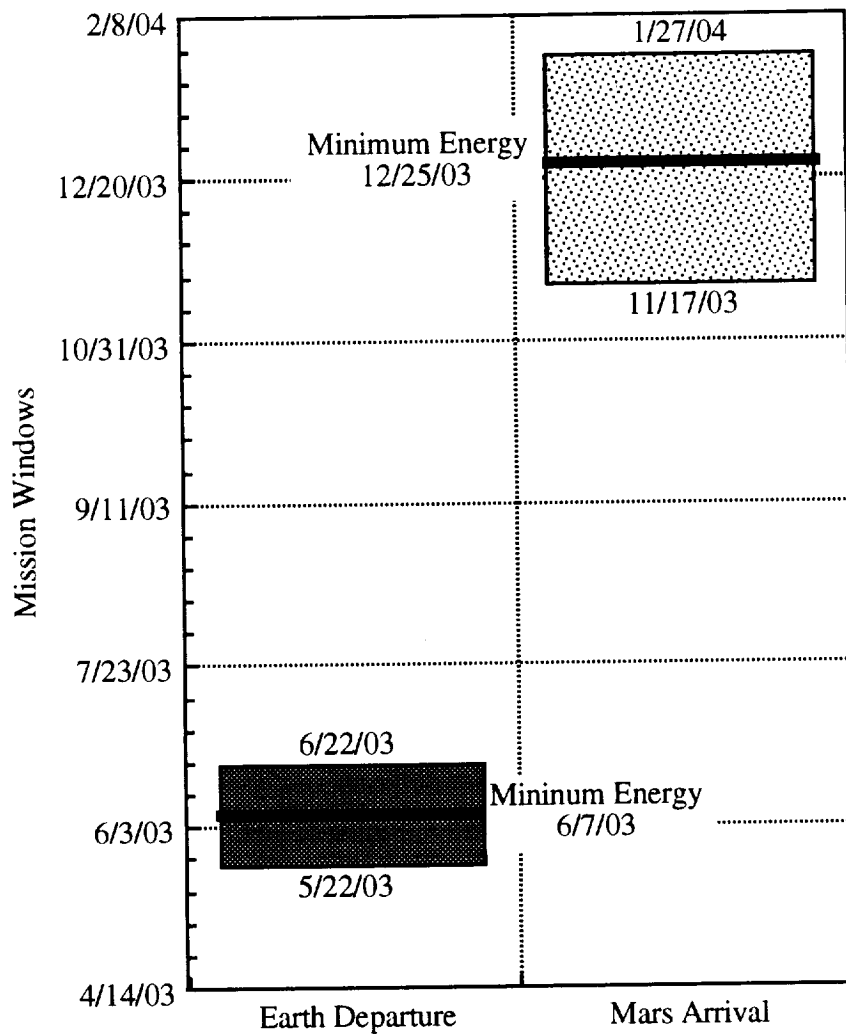


Fig. 2.4 Mission windows for outbound leg of manned flight.

NOTE: sun's and planets' sizes not to scale

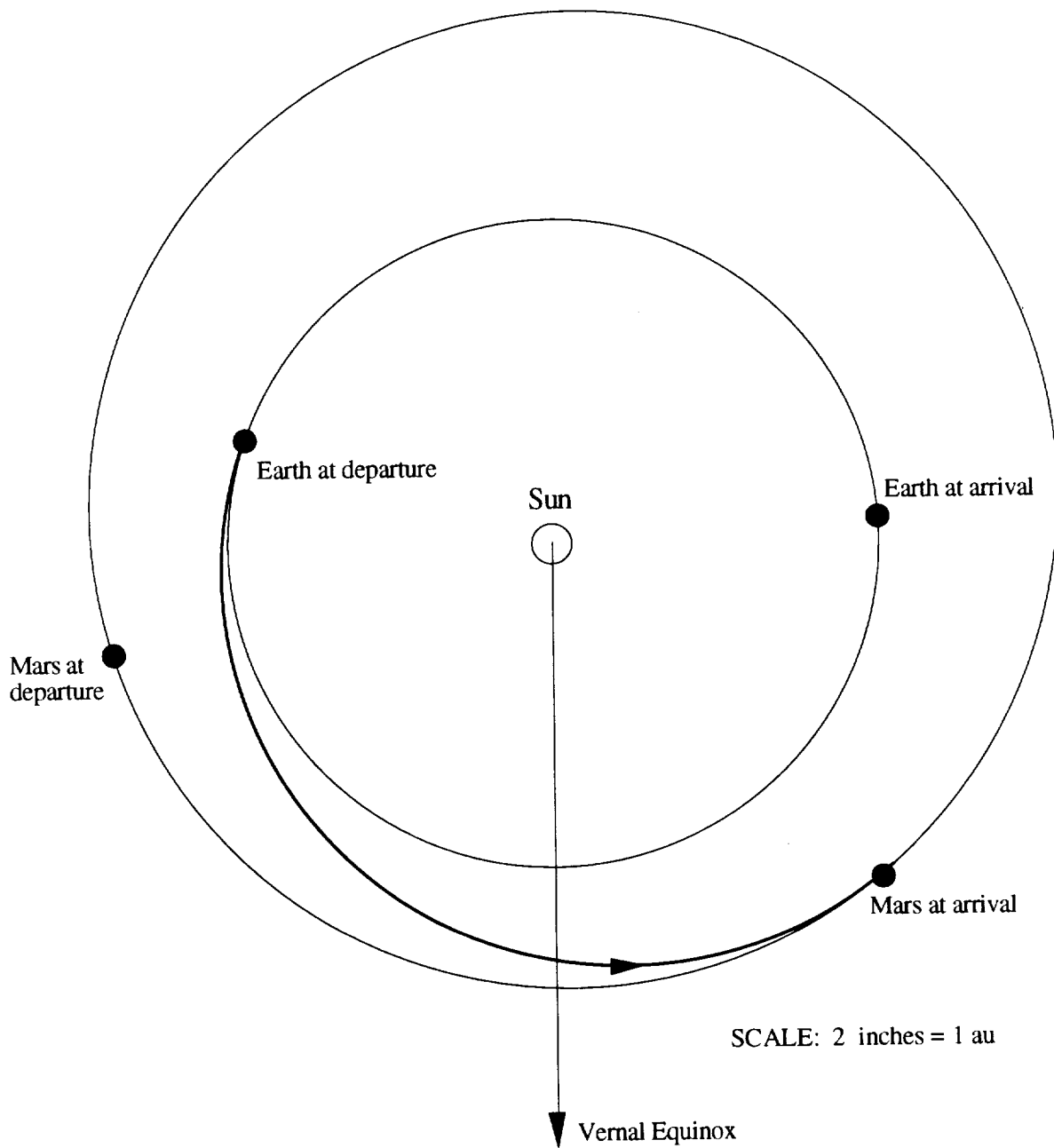


Fig. 2.5 Outbound manned mission conjunction class transfer trajectory for the year 2003.

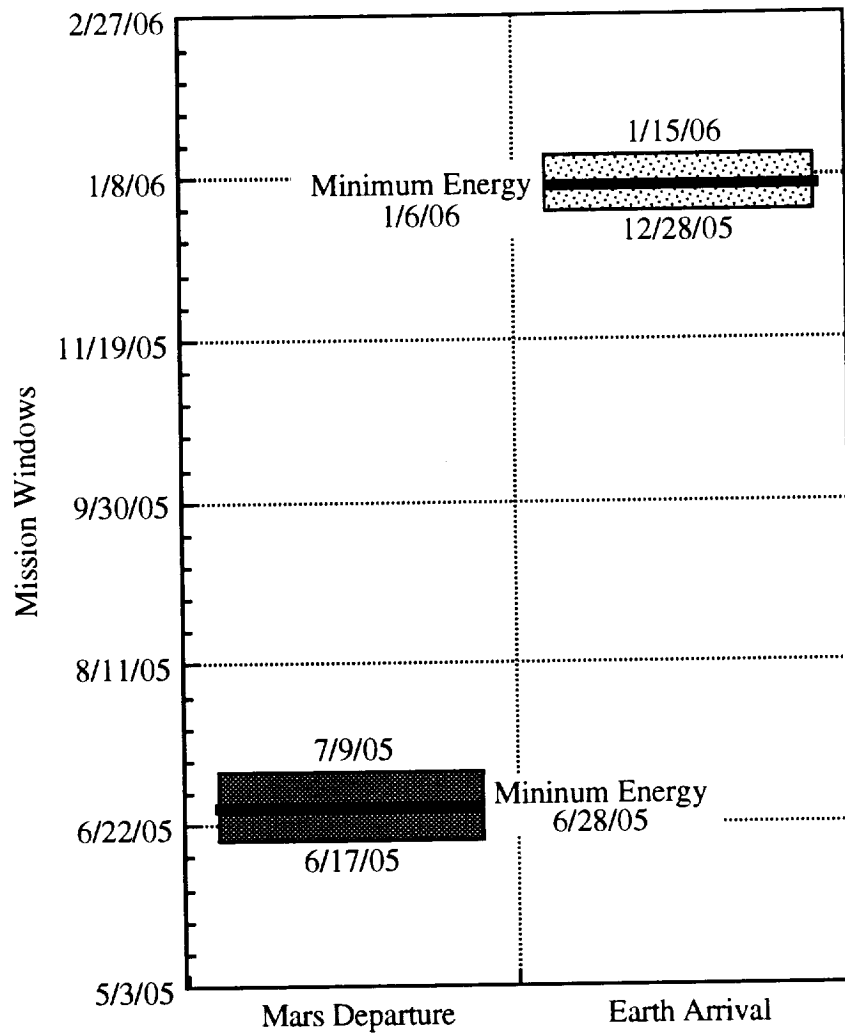


Fig. 2.6 Mission windows for inbound leg of manned flight.

NOTE: sun's and planets' sizes not to scale

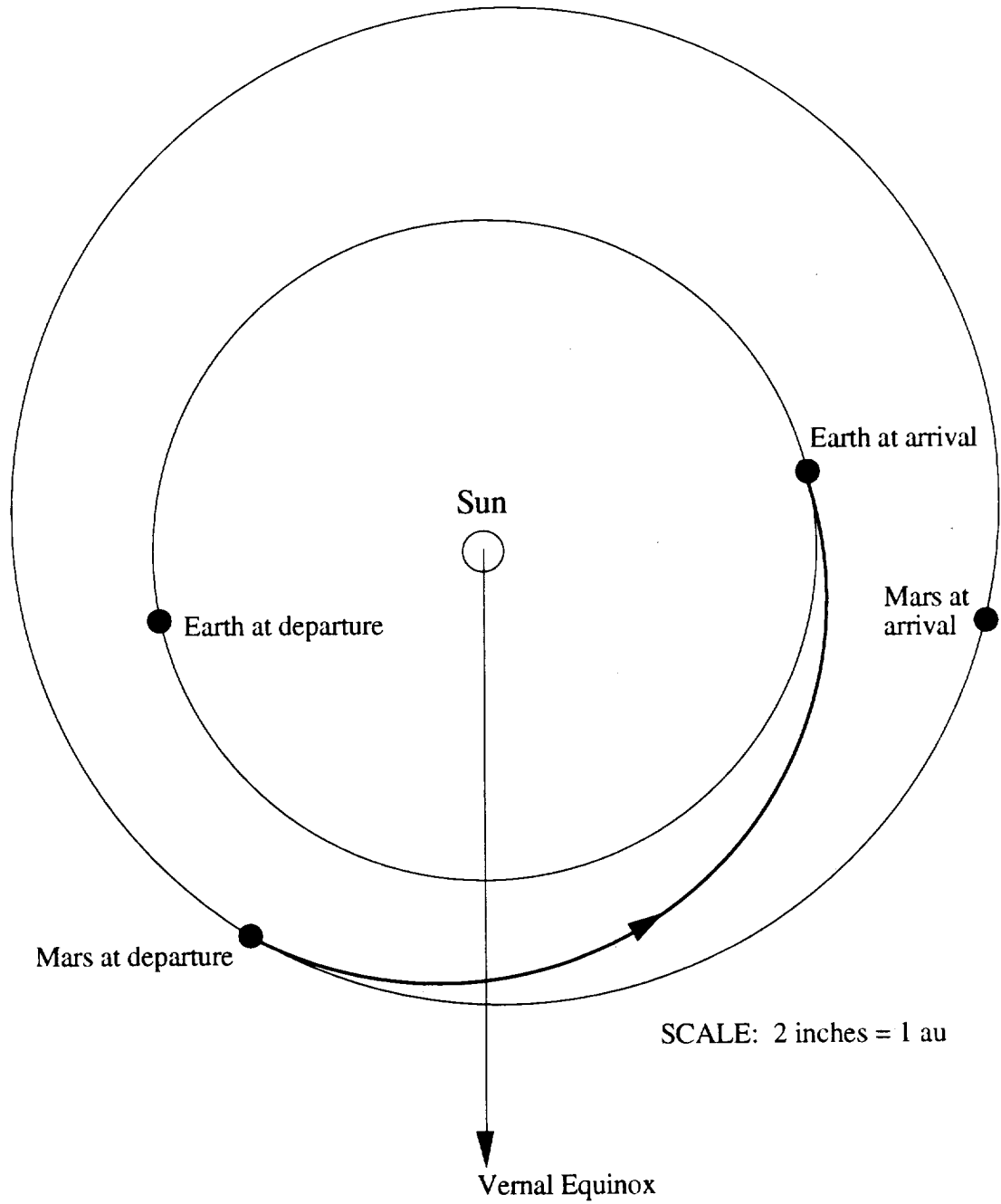


Fig. 2.7 Inbound manned mission conjunction class transfer trajectory for the year 2005.

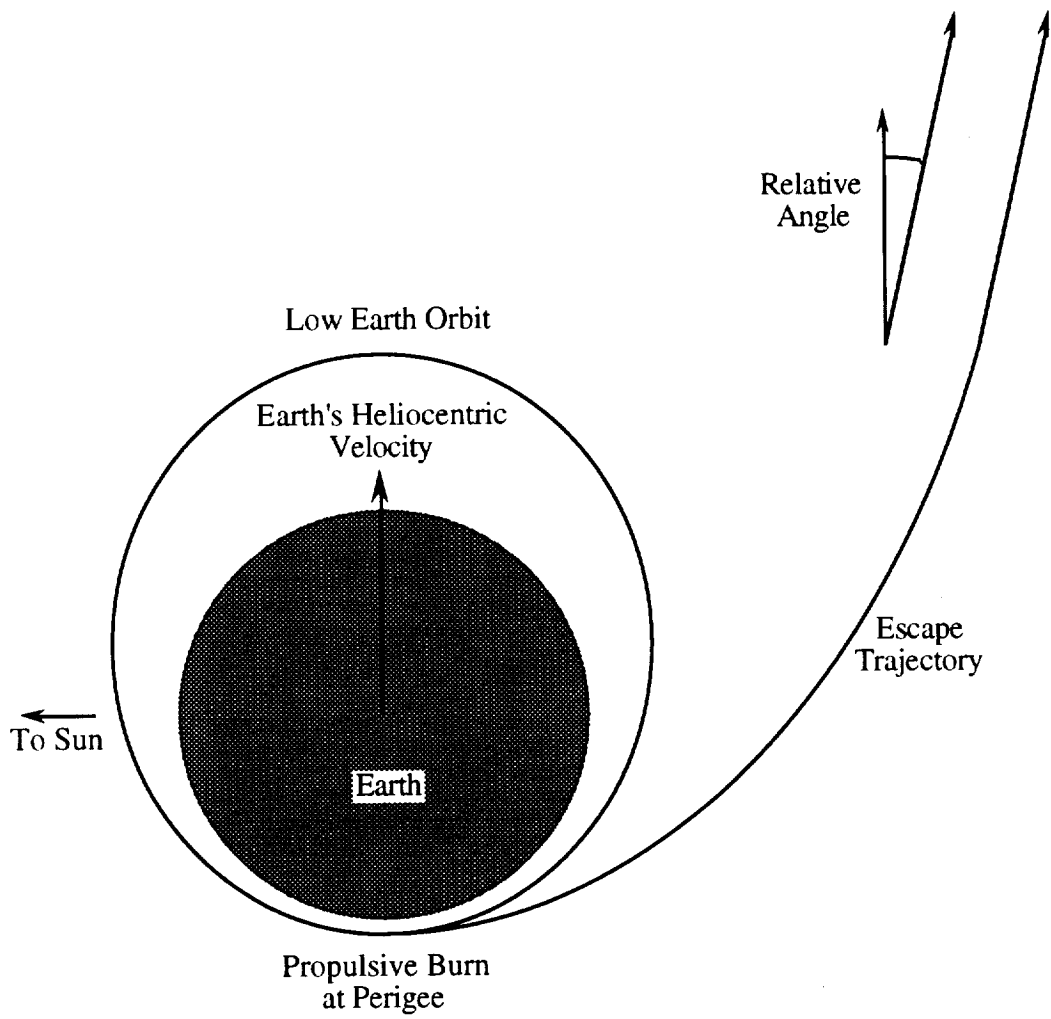


Fig. 2.8 Schematic of Earth escape trajectory (not to scale).

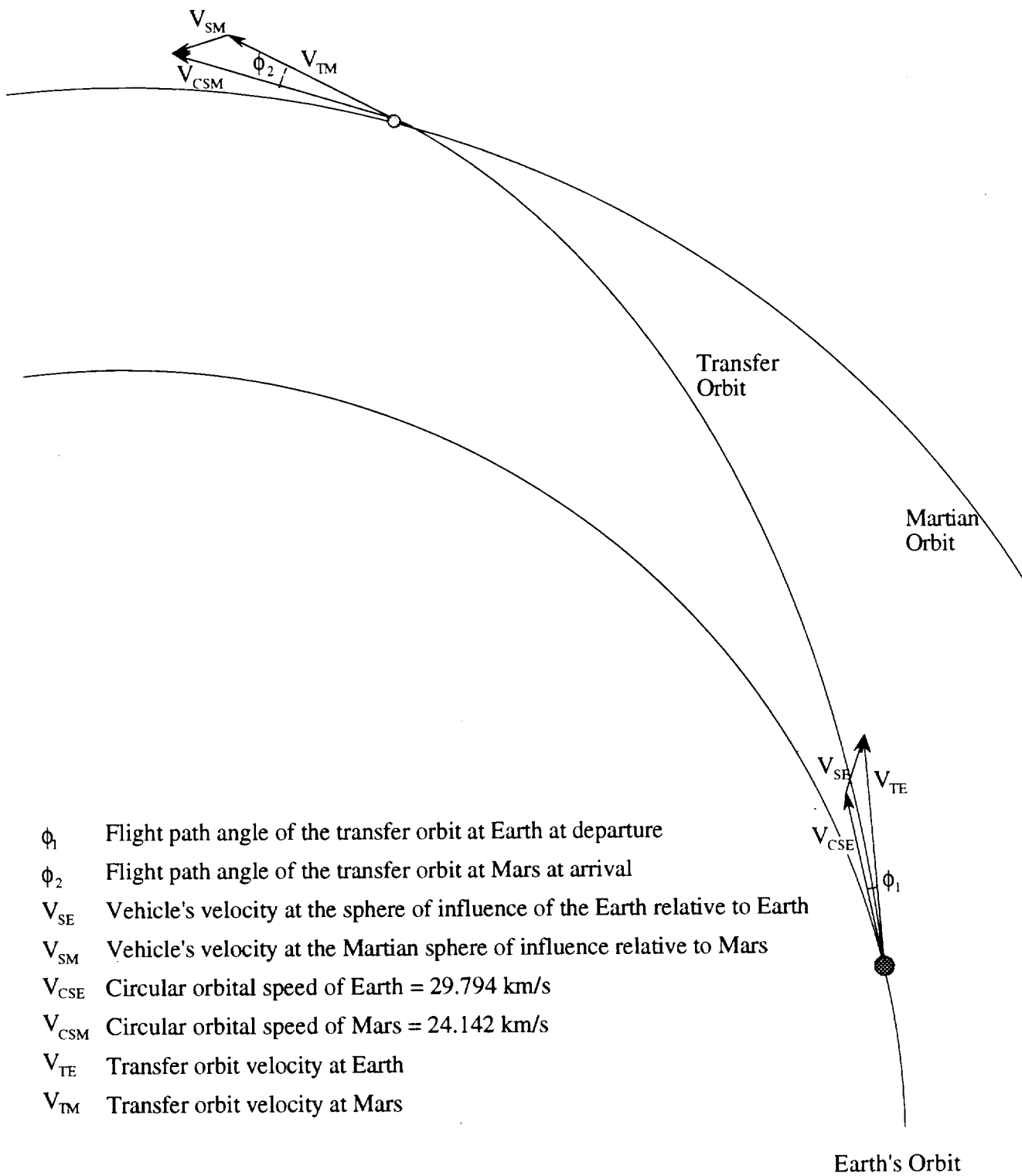


Fig. 2.9 Description of vector addition for heliocentric transfer trajectory [5].

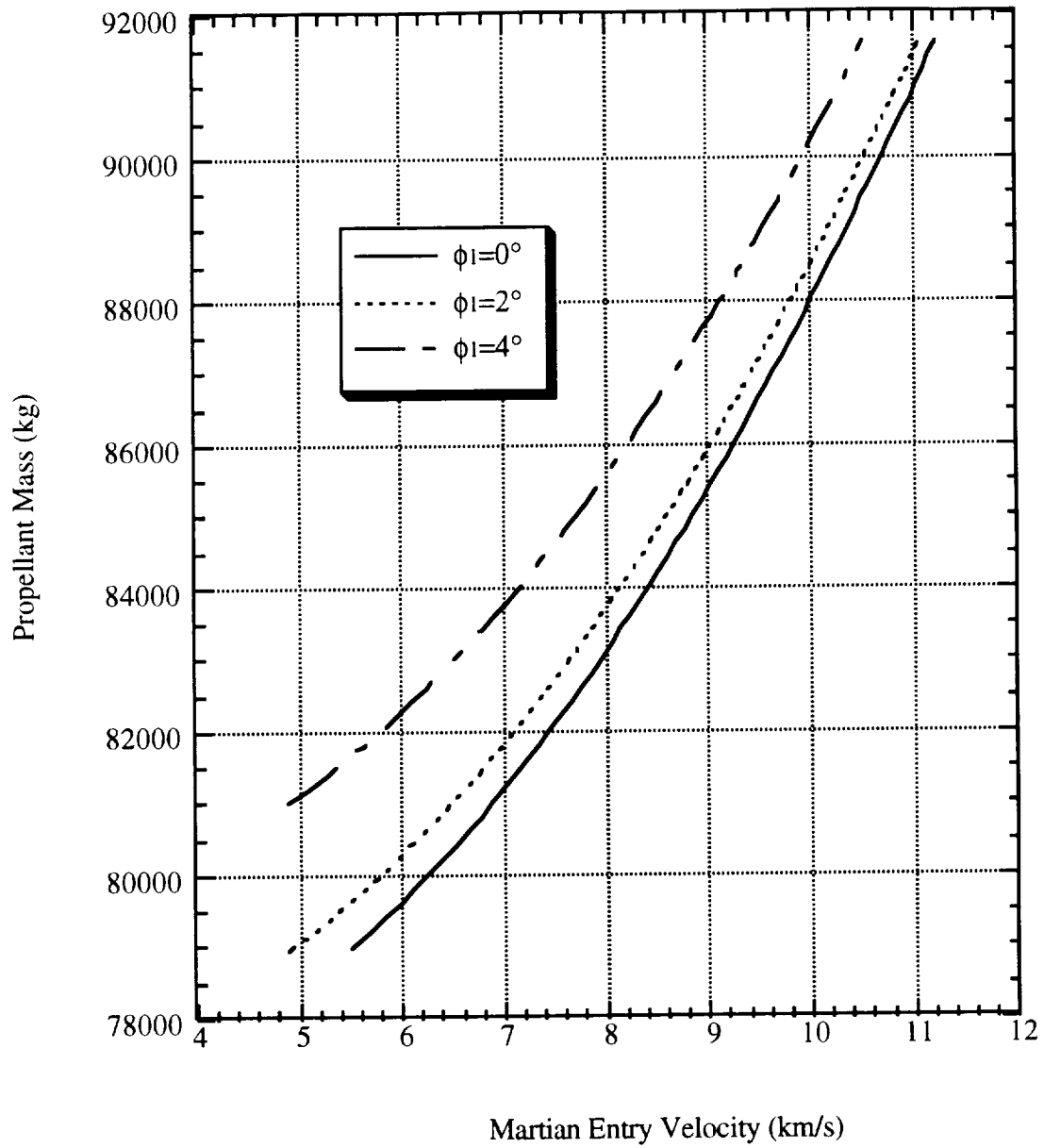


Fig. 2.10 Martian atmospheric entry velocity as a result of a given propellant mass and flight path angle.

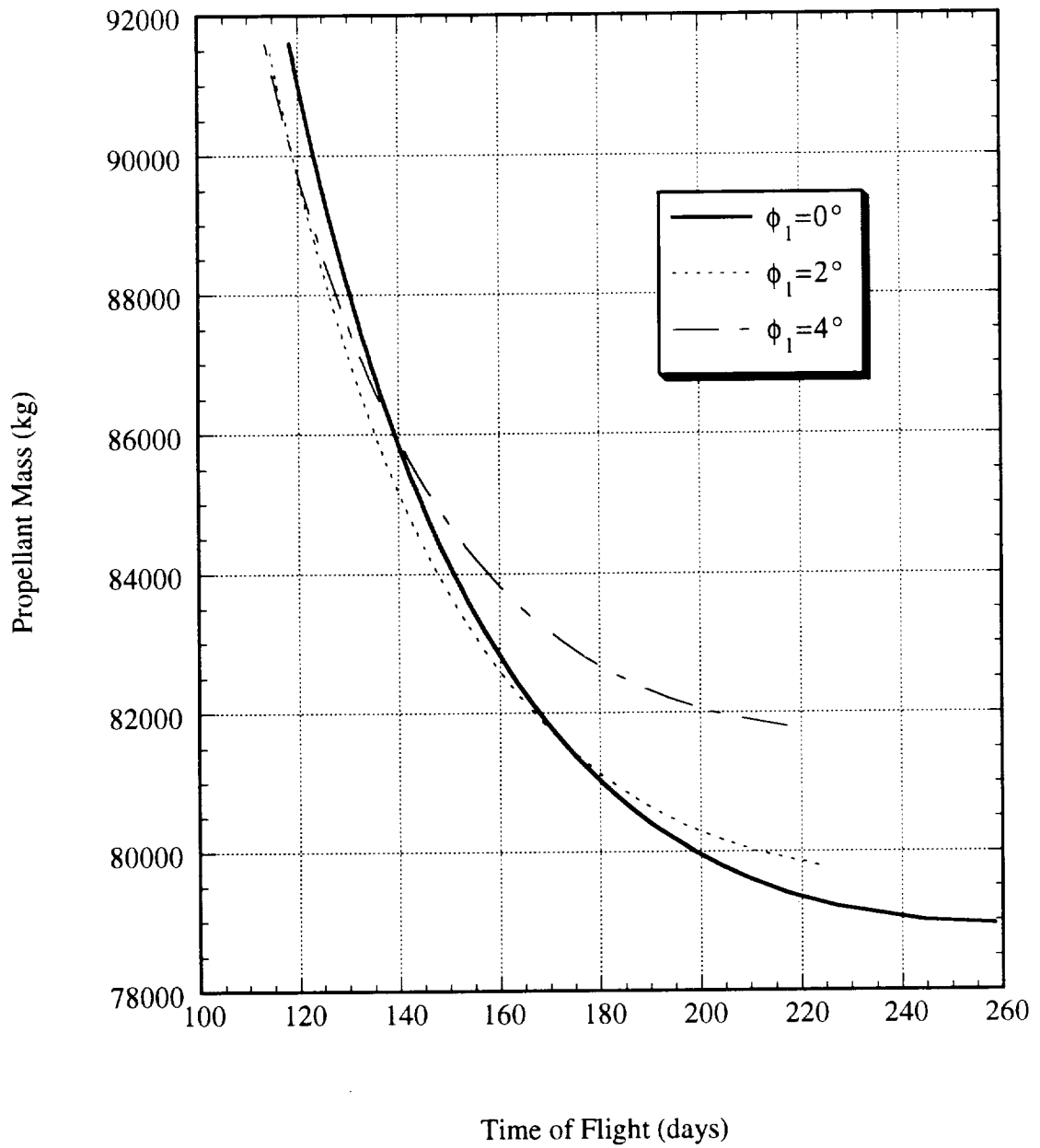


Fig. 2.11 Required propellant for given outbound heliocentric time of flight and flight path angle.

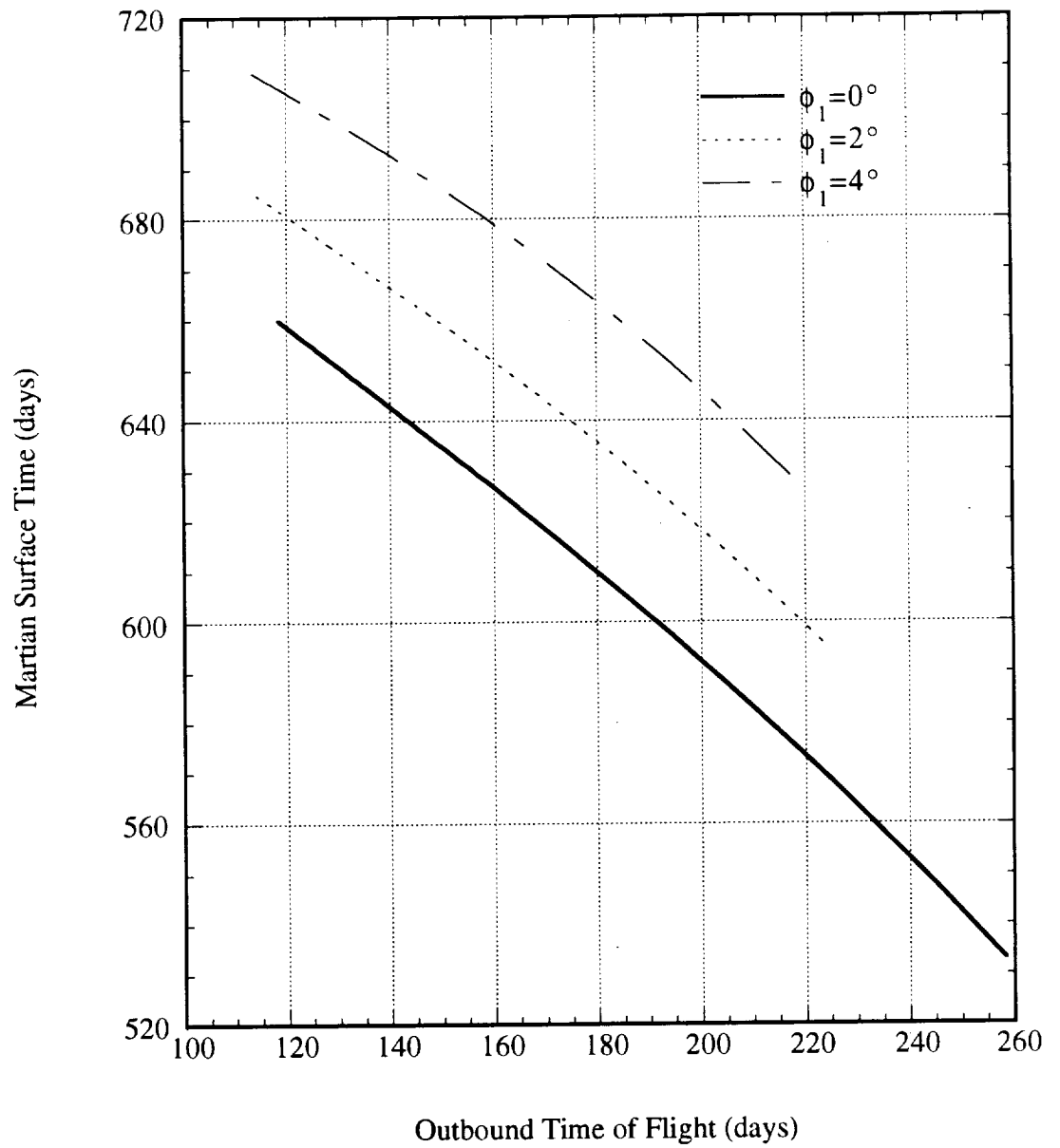


Figure 2.12 Comparison of Time on Mars to possible outbound time of flights.

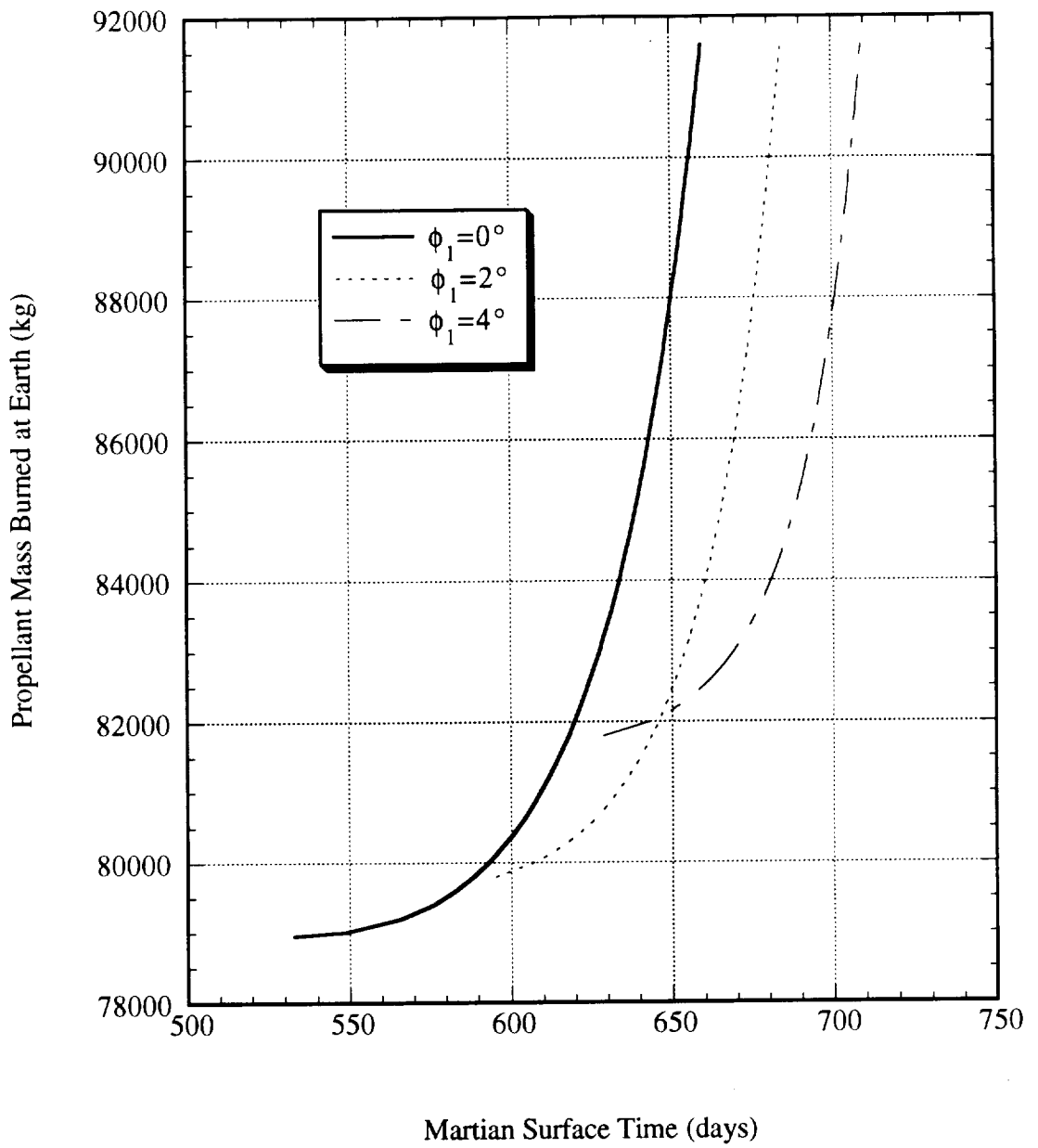


Fig. 2.13 Variation of Martian surface time with Earth propellant burn, and flight path angle.

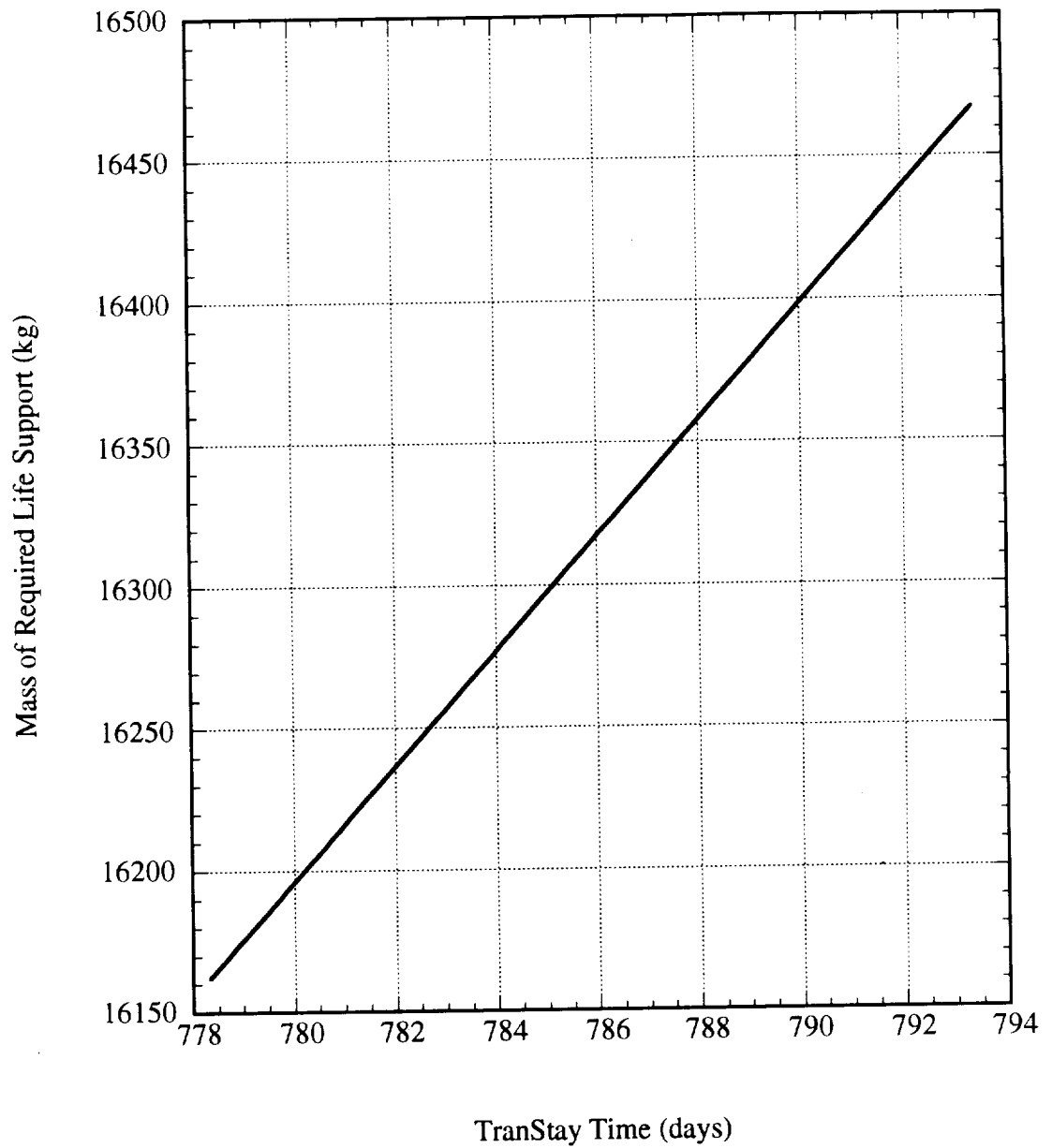


Fig. 2.14 Trend of mass of life support expendables.

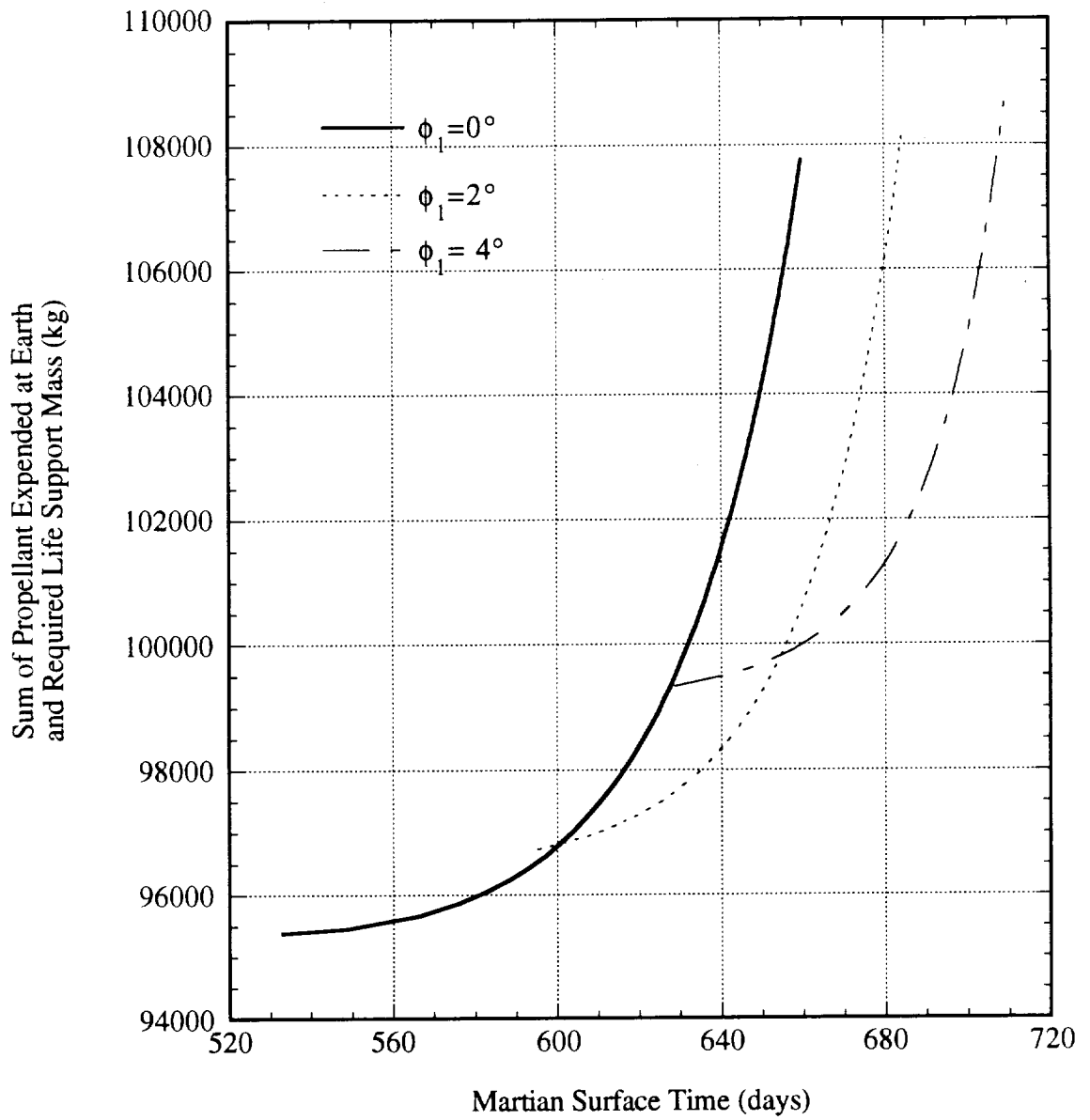


Fig. 2.15 Mass of propellant and life support expendables versus Martian surface time.

### **3.0 DESIGN of TRANS MARS INJECTION TRANSFER VEHICLES**

Tuyen Bui  
Mike Machula  
James Madison  
Kevin Mahn  
John Tran  
Mike Folkers  
Bryan Johnson

# TABLE OF CONTENTS

<b>3.1</b>	<b>INTRODUCTION</b> .....	3.1
<b>3.2</b>	<b>UNMANNED SEGMENT</b> .....	3.1
3.2.1	LAUNCH.....	3.1
3.2.1.1	First Launch Sequence.....	3.2
3.2.1.2	Second Launch Sequence.....	3.5
3.2.1.3	Upper Stage/TMI Booster Vehicle Design.....	3.7
3.2.1.4	Alternative to Upper Stage: Parallel Staging.....	3.26
3.2.2	UNMANNED MARS TRANSFER VEHICLE (UMTV).....	3.27
3.2.2.1	UMTV Propulsion.....	3.27
3.2.2.2	Structural Analysis.....	3.31
3.2.2.3	Unmanned MTV with Masses.....	3.40
3.2.2.4	Propellant lines.....	3.41
3.2.2.5	Docking Port.....	3.42
3.2.3	EARTH RETURN VEHICLE (ERV).....	3.43
3.2.3.1	ERV Propulsion.....	3.44
3.2.3.2	ERV Tank Construction.....	3.45
3.2.3.3	ERV Tank Configuration and Orientation.....	3.47
3.2.3.4	Tank Insulation and Heat Loss.....	3.49
3.2.3.5	ERV Tank Relief Valves and Piping.....	3.50
3.2.3.6	Low Gravity Sloshing.....	3.51
3.2.3.7	Habitat.....	3.51
3.2.3.8	Separation Devices.....	3.52
3.2.3.9	Earth Reentry.....	3.53
<b>3.3</b>	<b>MANNED SEGMENT</b> .....	3.54
3.3.1	LAUNCH.....	3.54
3.3.2	MANNED MTV WITH MASSES.....	3.55
	<b>NOMENCLATURE</b> .....	3.57
	<b>REFERENCES</b> .....	3.60
	<b>FIGURES</b> .....	3.62

## **3.1 INTRODUCTION**

The overall Mars initiative consists of several missions, each of which entails an unmanned and a manned segment . Each segment is comprised of two launches of a heavy lift launch vehicle. Project Minerva uses five different vehicles for each mission: the Antares VII [1], which is capable of delivering 70 tons to low Earth orbit, an upper-stage/TMI booster, an unmanned Mars transfer vehicle (UMTV), a manned Mars transfer vehicle (MTV), and an Earth return vehicle (ERV). The Antares VII is used to put the upper stage/TMI booster, the UMTV, and the MTV into low Earth orbit during each of their respective segments. The upper stage/TMI booster propels the UMTV and MTV to Mars on each the different segments. In LEO, the TMI booster and the transfer vehicle rendezvous and dock.

The unmanned Mars transfer vehicle houses the ERV, hydrogen feedstock, an unmanned rover and a hooper. It is equipped with two RL10s for additional  $\Delta V$ s and landing. It also has an aerobrake for slowing the vehicle down at Mars. The manned Mars transfer vehicle delivers the crew, the habitat , and the manned rover. At the end of their stay on Mars, the crew boards the Earth return vehicle for the voyage home. The ERV is propelled by modified RL10s which run on liquid oxygen and liquid methane. Each one of these vehicles is considered in detail in this section.

## **3.2 UNMANNED SEGMENT**

### **3.2.1 LAUNCH** (Tuyen Bui)

The first set of launches of the eight year exploration initiative involves delivering two unmanned payloads into low Earth orbit (LEO). One launch inserts a 70,000 kg unmanned Mars Transfer Vehicle (UMTV) into LEO (see Fig. 3.1). The other launch inserts an upper stage which contains the trans-Mars injection (TMI) propellant into LEO. In LEO, the two

vehicles are docked and the configuration is then injected into a Mars transfer orbit. The launch from the Earth's surface to LEO for both vehicles was analyzed using Marshall Space Flight Center's OPGUID trajectory program [1]. This program was used to maximize the amount of payload that could be inserted into LEO. OPGUID uses the vehicle's propulsion characteristics to optimize the ascent trajectory. OPGUID analysis was performed using NASA's Kennedy Space Center as the launch site. Its location is 28.5° north latitude and -80.5° longitude [1].

### 3.2.1.1 FIRST LAUNCH SEQUENCE

The first launch carries the necessary TMI propellant to LEO. A two-stage rocket is used to maximize the payload which is the TMI propellant. The first stage is the Antares VII with a reduced quantity of propellant while the upper stage is equipped with two Japanese Mitsubishi LE-7 booster engines (see Fig. 3.2). During the first stage, the Antares VII fires all of its seven engines. After the Antares VII consumes all of its propellant, the upper stage separates from it and the fairing and nose cone jettison from the upper stage rocket. The upper stage then fires its two LE-7 boosters, putting it into a 150 x 300 km orbit (see Fig. 3.3). Part of the upper stage (which is also the TMI booster) propellant is used to get into LEO. OPGUID was used to optimize the trajectory for the first launch. The program operates on a number of parameters including the propulsive characteristics of the Antares VII engine (DMRE) and the LE-7 engine (see Tables 3.1 and 3.2 ). The OPGUID optimization output is presented below.

T + 0 : 00 (min : sec)

At liftoff the Antares VII produces 17,225 kN of thrust with a specific impulse of 334 sec. It has a total liftoff mass of 1,394,000 kg ( 3,073,000 lb). This includes a structural mass of 110,200 kg (242,905 lb), a propellant mass of 1,182,209 kg

(2,606,300 lb), and a maximum payload of 105,000 kg (251,000 lb) which is the propellant for the TMI burn to Mars. Figure 3.4 indicates the relationship between payload mass and Antares VII propellant mass. The upper stage propellant mass is fixed at 115,200 kg, 124,840 kg, and 291,760 kg in order to maximize payload mass. Figure 3.4 shows that loading the Antares VII (first stage) with 1,050,000 kg of propellant will maximize the payload.

T + 0 : 90

At this time, the Antares -upper stage vehicle reaches an altitude of 18 km (57,524 ft ). The nozzle skirt of Antares VII is extended to increase the performance. At this altitude, the Antares produces 18,585 KN of thrust with a specific impulse of 360 sec.

T + 2 : 16

At this time the Antares-upper stage vehicle reaches an altitude of 40 km (132,537 ft). The oxidizer to fuel ratio changes from 12 : 1 to 6 : 1 so as to decrease the mass flow rate and likewise decrease the thrust. The performance characteristics change from a thrust and specific impulse of 19,545 KN and 379 sec, respectively, to 12,960 KN and 466 sec respectively.

T + 4 : 14

At this time, the Antares-upper stage vehicle reaches an altitude of 109 km (358,920 ft). At this height atmospheric effects can be neglected, the payload fairing are jettisoned, and the upper stage separates (see Fig. 3.5). When the upper stage separates from the Antares, the LE-7 engines start their burn at a thrust of 2,365 KN and at a specific impulse of 450 sec.

T + 8 : 20

Since atmospheric effects are negligible during the upper stage flight, thrust and specific impulse are not affected. It takes four minutes and seven seconds for the upper stage to reach LEO burnout. The total burn time of eight minutes and twenty seconds

(including both stages) is required to complete orbital insertion into 150 x 300 km elliptic orbit of 28.5 degree inclination. The total  $\Delta V$  required to reach LEO is 9.03 km/s . See Table 3.3 for mission requirement.

Table 3.1 DMRE Parameters.

	Area Ratio 40 : 1	Area Ratio 150 : 1
Vacuum Thrust		
O : F = 12 : 1	2,670 KN ( 600,000 lbf )	2,790 KN (628,000 lbf )
O : F = 6 : 1		1,850 KN (417,000 lbf )
Vacuum $I_{sp}$		
O : F = 12 : 1	362 sec	379 sec
O : F = 6 : 1		467 sec
Sea Level $I_{sp}$		
O : F = 12 : 1	334 sec	

Table 3.2 Mitsubishi LE-7 Engine Parameters.

Area Ratio	60 : 1
Exit Area	2.62 m <sup>2</sup>
Mixture Ratio	6 : 1
Vacuum Thrust	1180 KN (265,300 lbf )
Vacuum $I_{sp}$	450 sec

Table 3.3 Optimized Baseline Performance.

Total Liftoff Mass	1,394,255 kg (3,073,800 lb )
Total Propellant Mass	1,182,200 kg (2,606,330 lb )
Initial Thrust to Weight (F/W)	1.26
Payload Mass to LEO	102,000 kg ( 224,870 lb )
Total $\Delta V$	9.03 km/sec
<b>Antares VII ( First Stage )</b>	
Total Mass	1,138,900 kg
Propellant Mass	1,050,000 kg
Structural Mass	88,900 kg
Burn Time	254 sec
$\Delta V$	5.63 km/sec
<b>TMI Booster ( Upper Stage )</b>	
Total Mass	255,355 kg
Propellant Mass	132,235 kg
Structural Mass	21,120 kg
Burn Time	247 sec
$\Delta V$	3.4 km/sec

### 3.2.1.2 SECOND LAUNCH SEQUENCE

The second launch carries the 70 metric ton unmanned Mars transfer vehicle (UMTV) to LEO by using the Antares VII (see Fig. 3.6). The Antares VII is sufficient for the mission since it is designed to carry a maximum payload of approximately 70 metric ton into a 150 x 300 km elliptical orbit (see Fig.3.3). However, a modification to the Antares' fairing is necessary to accommodate the UMTV dimension payload. OPGUID is used to optimize the

trajectory. See Table 3.1 for the propulsive characteristics of the Antares VII engines (DMRE). Below is the OPGUID output optimization (see Table 3.4 and Fig. 3.7).

T + 0 : 00 (min : sec)

At an O : F ratio of 12 : 1 and area ratio of 40 : 1 the Antares VII has a gross liftoff mass of 1,379,400 kg (3,041,050 lb). This includes a propellant mass of 1,211,130 kg (2,670,100 lb), structural mass of 85,100 kg (187,610 lb) and a payload of 70,000 kg (154,320 lb). It has a liftoff force of 17,240 KN and a specific impulse of 334 sec. At take off, the thrust to weight ratio is 1.27.

T + 0 : 76

When the Antares VII reaches an altitude of 11.6 km (38,140 ft), the engine nozzles are extended to increase its thrust. At this point the Antares' engines produces 18,430 KN of thrust and has a specific impulse of 357 sec.

T + 1 : 50

At this time, the Antares VII has reached an altitude of 27 km. The O:F ratio changes from 12 : 1 to 6 : 1 and the thrust is reduced from 19,460 KN to 12,870 KN. The specific impulse increases from 377 sec to 463 sec.

T + 3 : 20

At an altitude of 75 km, the atmospheric drag effect on the fairing is less than the payload fairing mass (7,000 kg) so, the payload fairing is jettisoned.

T + 6 : 00

A total burn time of six minutes results in orbital insertion into a 150 x 300 km elliptical orbit of 28.5° inclination. The total  $\Delta V$  required for this launch is 9.17 km/sec.

Table 3.4 Optimized Baseline Parameters.

Total Liftoff Mass	1,379,400 kg (3,041,050 lb)
Propellant Mass	1,211,130 kg (2,670,100 lb)
Structural Mass	86,100 kg (189,818 lb)
Payload Mass	70,000 kg (165,550 lb)
Burn Time	360 sec
$\Delta V$	9.17 km/sec

When the UMTV reaches LEO, it adjusts to the same circular orbit as the upper stage/TMI booster and docks on to the upper stage/TMI booster (see Figs.3.8 and 3.9 ).

### 3.2.1.3 UPPER STAGE/TMI BOOSTER VEHICLE DESIGN (Bryan Johnson)

The main purpose of the upper stage is to deliver the required amount of propellant for the trans-Mars injection (TMI) burn into low Earth orbit (LEO). However, several other objectives must be satisfied in the upper stage design, including the following:

- The upper stage must be adaptable to the Antares VII launch vehicle, therefore, it must not exceed 30 meters in height and 8.5 meters in diameter to fit within the dimensions of the Antares VII payload fairing.
- A 375 kg docking mechanism needs to be attached to the top of the upper stage.
- The TMI burn requires a  $\Delta V$  of 3.65 km/s. For an engine with a specific impulse of 450 sec at least 105,000 kg of LH<sub>2</sub>/LOX propellant must be delivered to LEO.
- The acceleration loads should not exceed 4 g.
- An interstage adapter is required to support the upper stage when atop the Antares VII.
- At least two main engines are required for redundancy.

Many of the concepts for the upper stage design originated from an upper stage study that was conducted by the Boeing Company in 1989 [2].

## **ENGINE MODULE**

The engine module contains three types of propulsive systems: a main engine system, an orbital maneuvering engine system, and an attitude control system. The main engines provide thrust for the upper stage and TMI burns, and the orbital maneuvering engines perform the transfer to a 300 km circular orbit. The attitude control thrusters perform course corrections, propellant settling, stage separation, collision avoidance maneuvers, and stability for tether control.

The engine module contains all of these engine systems and the supporting hardware such as: avionics,  $N_2O_4$  and MMH propellant tanks, a helium tank for pressurization, an avionics mounting frame, and a thrust frame. The main engines are gimballed for pitch/yaw control. All engines are expendable after completing the TMI burn, thus no engine return system is necessary.

### **Main Engine Specifications**

The two main engines for the upper stage/TMI booster are Mitsubishi LE-7's. This engine type is similar to the SSME design and is used as a first stage engine on the Japanese H - II launch vehicle. The LE-7 burns liquid oxygen and liquid hydrogen at an oxidizer to fuel ratio of 6:1 and operates in a staged combustion cycle with a thrust of 1180 kN, a nozzle-to-throat area ratio of 60:1, and a vacuum specific impulse of 449 sec. It has been designed, built, and tested, and is scheduled for first flight in 1993, after which it will become available in the United States. Although this engine is not a true upper stage engine, an auxiliary turbine and power unit can be used to provide restart capability. The two engines will operate at

constant conditions, i.e. constant thrust, since the upper stage and TMI burns occur in a vacuum environment. The dry mass of the LE-7 is 1560 kg, it is 350 cm long, and has an exit diameter of 182.8 cm [3].

Other engines were considered in this research, such as the Space Shuttle Main Engine (SSME) and Pratt and Whitney's RL10. The SSME has a specific impulse of 455 seconds, vacuum thrust of 2091 kN, and a mass of approximately 3100 kg; however, one SSME does not provide sufficient thrust to deliver the necessary payload, and two SSME's exceeded 4 g. Pratt and Whitney's RL10-A4, with a specific impulse of 449 seconds was also considered, but at least 12 engines would be required if utilized in a parallel configuration. Two LE-7 engines were selected primarily because of thrust-to-weight requirements using OPGUID program described in Section 3.2.1.

### **Orbital Maneuvering System**

Two Space Shuttle Orbital Maneuvering Engines (OMS), manufactured by Aerojet, have been selected to provide the  $\Delta V$  necessary for circularizing the initial parking orbit to a 300 km circular orbit. These engines use nitrogen tetroxide ( $N_2O_4$ ) as the oxidizer and monomethyl hydrazine (MMH) as the fuel in an oxidizer to fuel mixture ratio of 1.65:1. The pump-fed engines produce 26.7 kN of thrust with a vacuum specific impulse of 316 seconds. The nozzle area ratio is 55:1. The engines each have a mass of 118 kg, a length of 195.6 cm, a maximum diameter of 116.8 cm, and an exit diameter of 109 cm [3]. The OMS propulsion system was selected for its reliability, and the capability to restart at least 5000 times.

The orbital maneuvering system is used for LEO orbit circularization and rendezvous maneuvers. The Antares VII inserts the upper stage into a 150 km by 300 km elliptical parking orbit. At the apogee of the 150 km x 300 km orbit, a burn is made to circularize the orbit to

300 km where the upper stage rendezvouses with the Mars transfer vehicle. Using the equation for the velocity at apogee of an object in elliptical orbit [4]:

$$v_a = \sqrt{2\mu_E \left[ \frac{1}{r_a} - \frac{1}{(r_p + r_a)} \right]} \quad (3.1)$$

$r_p$  = perigee radius = 150 km +  $R_E$

$r_a$  = apogee radius = 300 km +  $R_E$

$R_E$  = radius of Earth = 6378 km

$\mu_E$  = gravitational parameter of Earth =  $3.986 \times 10^5 \text{ km}^3/\text{s}^2$

$v_a$  = velocity of spacecraft at apogee

The spacecraft velocity at apogee in LEO is 7.682 km/s. To increase the perigee height of the 150 km by 300 km orbit to a 300 km circular orbit, the following equation was used to determine the  $\Delta V$  required [4]:

$$\Delta v_a = \frac{\Delta h_p \cdot \mu_E}{4a^2 \cdot v_a} \quad (3.2)$$

$\Delta h_p$  = increase in perigee height = 150 km

$v_a$  = 7.682 km/s

$a$  = length of semi-major axis =  $R_E + 0.5 (r_a + r_p)$

The  $\Delta V$  required for the OMS engines is 44.6 m/s. From the rocket equation, the amount of propellant can be determined.

$$\Delta V = g_E \cdot I_{sp} \cdot \ln \left( \frac{m_o}{m_o - m_p} \right) \quad (3.3)$$

$\Delta V$  = velocity increment for a given burn = 44.63 m/s

$g_E$  = gravity at Earth's surface =  $9.81 \times 10^{-3} \text{ km/s}^2$

$I_{sp}$  = specific impulse = 316 seconds

$m_o$  = initial spacecraft mass = 117,000 kg

$m_p$  = propellant mass

This results in a requirement of 1672 kg of propellant for the OMS burn.

## **Reaction Control System**

Marquardt R-1E thrusters, which are currently used on the Space Shuttle Reaction Control System (RCS) and Antares boosters for vernier control, have been selected to provide attitude control for the upper stage. Like the OMS engines, the R-1E's use MMH and  $N_2O_4$  as propellants. The sixteen reaction control thrusters provide roll, pitch, yaw, and axial control. By having this many degrees of freedom, the ability to make orbital corrections, rendezvous, and tether control will be facilitated. Many types of thrusters exist with similar performance, but the R-1E thrusters have proven reliability on man-rated vehicles and can use propellant from the same tanks as the OMS engines.

The sixteen thrusters are located in clusters of four at four locations around the avionics support frame. Two of the sets are angled for yaw and roll control, the other two sets are angled for pitch and axial control (see Fig. 3.10). The R-1E has an expansion ratio of 100:1 and produces 111 Newtons of thrust at a steady state specific impulse of 300 seconds. Each thruster is 27.9 cm long and has a mass of 1.4 kg [5]. The propellant usage for the vehicle's attitude control in the 300 km circular orbit is estimated to be 1 kg/day. To account for thirty days between the upper stage launch and the Mars transfer vehicle launch from Earth, 30 kg is required. An additional 250 kg is allotted for attitude maintenance, tether control, and orbital correction maneuvers during the Mars transfer orbit. With 20 kg reserve, this results in a total of 300 kg for RCS propellant.

### **$N_2O_4$ , MMH, and Helium Tanks**

The OMS engines and R-1E thrusters use common propellant tanks in a similar arrangement to the Antares launch vehicles. A total of 2000 kg is required for the OMS and RCS engines: 1245 kg of  $N_2O_4$  oxidizer and 755 kg of MMH fuel. By using the mixture ratio

1.65:1 of the OMS engines, the inside diameter of both tanks is 1.2 meters. All tanks are spherical and manufactured from Aluminum 7075-T6 sheet stock.

The propellants are pressure fed to the engines through the use of a single high-pressure helium tank. To provide a constant pressure of 1.24 MPa to the propellant tanks, 6.4 kg of helium is required. This corresponds to a 0.662 m inside diameter for the helium tank, assuming a temperature of 300 K at a pressure of 20.7 MPa [1]. Table 3.5 contains the specifications of the OMS, RCS, and helium tanks.

Table 3.5 OMS, RCS, and helium tank specifications.

Tank	Diameter (cm)	Thickness (cm)	Empty mass (kg)	Full mass (kg)	Pressure (MPa)
MMH	120.0	0.82	10.4	765.4	1.24
N <sub>2</sub> O <sub>4</sub>	120.0	0.82	10.4	1255.4	1.24
Helium	66.2	7.53	29.7	37.2	20.70

### Engine Module Structure

The engine module structure is divided into two separate units that are connected to one another: a thrust frame and an avionics frame. The thrust frame is responsible for transferring the thrust from the LE-7's and the OMS engines through the avionics frame to the longeron body structure located above. The RCS thrusters, avionics equipment, and the MMH, N<sub>2</sub>O<sub>4</sub>, and the helium tanks are all mounted to the avionics frame (see Fig. 3.10).

The thrust frame configuration is based on the design used on the Antares launch vehicles [1]. The thrust frame consists of a four-member tensile square, which is attached to four compressively loaded struts that connect directly to the gimbaling joint of the LE-7 (see Fig. 3.11). The OMS engine thrust frame is connected to the corners of both LE-7 engine

thrust frames, and to additional struts which are attached to the avionics frame. All frame members are made of titanium tubing. Table 3.6 summarizes the mass of the engine module.

Table 3.6 Engine module component masses.

Component	Mass (kg)
Thrust frame	500
Avionics frame	75
Two OMS engines	236
Two LE-7 engines	3120
Sixteen R-1E thrusters	22.4
MMH propellant tank	765.4
N <sub>2</sub> O <sub>4</sub> propellant tank	1255.4
Helium pressurization tank	37.2
Avionics	490
Miscellaneous hardware	75
<b>TOTAL ENGINE MODULE MASS</b>	<b>6576.4</b>

## STRUCTURAL DESIGN

The upper stage/TMI booster has two main propellant tanks: one liquid oxygen tank and one liquid hydrogen tank. The propellant tanks are lightweight and self-supporting. By having a lightweight structure, the amount of propellant can be increased. The size restrictions prevent the upper stage diameter from exceeding ten meters if using the Antares VII, however, the length can be increased without drastically affecting the launch performance.

The hydrogen tank contains 33,943 kg of liquid hydrogen at a pressure of approximately 2 atm in a volume of 485 cubic meters. The tank has a cylindrical center section

of 7.93 meters length and 7 meters diameter with hemispherical ends of 3.5 meters in diameter. The oxidizer tank contains 203,657 kg of liquid oxygen at a pressure of 7 atm in a volume of 146 cubic meters. The tank shape is spherical (3.26 meters radius) since this provides the best weight to volume ratio possible. The tanks are constructed using aluminum alloy 2219 (see Fig. 3.12). This alloy is the same as that used on the Antares propellant tanks, the Space Shuttle External Tank and a number of other cryogenic-type tanks.

Two options exist for the body structure: cylindrical shells or longerons. Cylindrical shells offer a shorter stage length but they require greater mass, cost, and are more difficult for ground handling. If a cylindrical shell were used to directly cover the tanks several fasteners and molded skins would be required. A longeron truss frame has been selected to surround the propellant tanks (see Fig. 3.12). Since the tanks expand and contract, no portion of the tanks will be integrated with the upper stage outer shell structure and it would also be difficult to connect to the octagonal pattern of the longerons [2].

### **Propellant Tank Orientation**

The location of the oxygen and hydrogen tanks is determined by the location of the center of mass when the upper stage is placed on top of the booster launch vehicle. Two options exist: LOX aft and LOX forward. The moment,  $M$ , is calculated by taking the propellant mass and multiplying by its moment arm and gravitational acceleration. The moment arm is the height of the tank's center of gravity above the launch vehicle interface plane.

$$\text{LOX aft: } M = (203,657 \text{ kg} \times 8.71 \text{ m}) + (33,943 \text{ kg} \times 20.0 \text{ m}) = 2.41 \times 10^7 \text{ N}\cdot\text{m}$$

$$\text{LOX forward: } M = (33,943 \text{ kg} \times 12.9 \text{ m}) + (203,657 \text{ kg} \times 24.2 \text{ m}) = 5.27 \times 10^7 \text{ N}\cdot\text{m}$$

With the LOX tank located in the forward position, the reaction required at the attachment plane is double the load than with the LOX tank in the aft position. Also the g load

requires the forward tank to transmit the weight through more structure than the LOX aft location. This would increase the weight and cost of the structure due to the higher stresses and loads. In summary, the LOX aft location is preferred.

### Propellant Tank Structural Analysis

To determine the wall thicknesses of the hydrogen and oxygen tanks, a stress analysis must be performed. The tanks are independent of the vehicle weight such that neither tank supports any load other than the propellant weight from within. The design load limits are given in Table 3.7 along with the required analytical factors of safety (1.6 for yield and 2.0 for ultimate). The walls are designed to withstand an 6.5 g axial load and a 3 g lateral load based on loads experienced for similar launch vehicles [5] at lift-off.

Table 3.7 Upper stage loading limits (g's) at lift-off.

Direction	Limit (experimental)	Yield (analytical)	Ultimate (analytical)
Axial	6.5	10.4	13.0
Lateral	3.0	4.8	6.0

The first element to be analyzed is the cylindrical section of the hydrogen tank. This section is 7.93 meters in length, and 7.0 meters in diameter. The loads must support the entire propellant mass. The tank loading is equivalent to the liquid hydrogen mass of 33,943 kg multiplied times  $9.81 \text{ m/s}^2$ . The appropriate loading conditions are listed in Table 3.8.

From the data in Table 3.8 the equivalent axial load,  $P_{eq}$ , is determined for the combined lateral and bending conditions on the cylinder.

Table 3.8 Applied loads on cylindrical section of H<sub>2</sub> tank.

Type of load	Force (N)	Distance (m)	Load (g)	Limit load
Axial	332,979	-	6.5	2.16x10 <sup>6</sup> N
Lateral	332,979	-	3.0	9.99x10 <sup>5</sup> N
Bending	332,979	3.97	3.0	3.96x10 <sup>6</sup> N·m

$$P_{eq} = P_{axial} + \frac{2 \cdot M}{R} \quad (3.4)$$

$$P_{axial} = 2.16 \times 10^6 \text{ N}$$

$$M = \text{Bending moment} = 3.96 \times 10^6 \text{ N}\cdot\text{m}$$

$$R = \text{Radius of cylinder} = 3.5 \text{ m}$$

The equivalent applied load is 4.43x10<sup>6</sup> N. The wall thickness must be checked for yield and ultimate loads, thus the corresponding factors of safety are multiplied times P<sub>eq</sub>.

$$P_{applied} = 7.09 \times 10^6 \text{ N (yield)}$$

$$P_{applied} = 8.86 \times 10^6 \text{ N (ultimate)}$$

These values incorporate a margin of safety, thus the allowable loads can be set equal to the applied loads. The cylinder can now be sized for strength using the following equation.

$$\sigma = \frac{P}{A} \quad (3.5)$$

$$P = \text{Applied load}$$

$$A = \text{Cross-sectional area} = 2\pi R t$$

$$\sigma = \text{Allowable stress}$$

Aluminum 2219-T81 sheet was selected because it is a material with good reliability and strength at low temperatures, and it is easily weldable. The allowable stresses are set equal to the tensile strength of the material to determine the minimum required wall thickness.

$$\sigma = F_{ty} = \text{Yield tensile strength of Alum 2219-T81} = 421 \times 10^6 \text{ N/m}^2 \text{ [6]}$$

By substituting this yield strength with  $P = 7.09 \times 10^6$  Newtons and a tank cylinder radius of 3.5 meters into equation 3.5, the required wall thickness is 0.765 mm. The ultimate loading criteria is evaluated by using the applied load of  $8.86 \times 10^6$  N and the following material property.

$$\sigma = F_{tu} = \text{Ultimate tensile strength of Alum 2219-T81} = 572 \times 10^6 \text{ N/m}^2$$

This results in a thickness of 0.704 mm. Since the yield criteria governs, the wall thickness of the cylindrical section of the hydrogen tank will be 0.765 mm. This section has a surface area of 174.5 square meters, and the mass of this section is determined to be 378 kg using the following equation.

$$m = \rho \cdot 2\pi R \cdot t \cdot L \quad (3.6)$$

$$\rho = \text{Density of Alum 2219} = 2.83 \times 10^3 \text{ kg/m}^3$$

$$R = 3.5 \text{ m}$$

$$t = 8.52 \times 10^{-4} \text{ m}$$

$$L = 7.93 \text{ m}$$

The hemispherical ends of the hydrogen tank will need to withstand the axial load presented by the total mass of the liquid hydrogen propellant (33,943 kg). The axial load of 6.5 g results in a limit load of  $2.16 \times 10^6$  Newtons resulting in the following applied loads.

$$P_{\text{applied}} = 3.46 \times 10^6 \text{ N (yield)}$$

$$P_{\text{applied}} = 4.33 \times 10^6 \text{ N (ultimate)}$$

These loads are distributed throughout each hemisphere so equation 3.5 is used to find the minimum wall thickness.

$$t_{\text{required}} = 0.344 \text{ mm (yield)}$$

$$t_{\text{required}} = 0.374 \text{ mm (ultimate)}$$

The forward hemispherical end of the hydrogen tank will need to withstand an internal pressure of 2 atm in addition to supporting the weight of the hydrogen tank. The hoop stress,  $\sigma_h$ , will be used to give the wall thickness.

$$\sigma_h = \frac{p \cdot R}{2 \cdot t} \quad (3.7)$$

$$\sigma_h = \sigma_{\text{allow}} = F_{ty} = 421 \times 10^6 \text{ N/m}^2$$

$$p = \text{internal pressure} = 2 \text{ atm} = 2.03 \times 10^5 \text{ N/m}^2$$

$$R = 3.5 \text{ m}$$

$$t_{\text{required}} = 0.842 \text{ mm (yield)}$$

The aft hemispherical end of the hydrogen tank will have a thickness of 0.374 millimeters and the forward end of the tank will be 0.842 millimeters thick. The mass of the end domes are determined from the volume of a sphere using the following equation.

$$m = \frac{4\pi}{3} \cdot \rho \cdot (R_o^3 - R^3) \quad (3.8)$$

$$R_o = \text{Outer radius of tank wall} = R + t$$

The aft hemispherical end dome is approximately 82 kg and the forward hemispherical end dome of the hydrogen tank is 184 kg.

Two internal rings with stiffeners are located at the upper and lower junctions of the hydrogen tank as shown in Fig. 3.13. These rings will provide for the reaction of the tank support strut fittings and they will also serve as anti-slosh baffles. Additional anti-slosh baffles will be located two meters apart in the cylindrical section of the tank. The combined mass of two skins and seven stiffener rings made of Aluminum 2219 is 387 kilograms.

The spherical oxygen tank is analyzed similar to the hemispherical end domes of the hydrogen tank. After applying equations 3.5, 3.7, and 3.8, the tank thickness required is 2.41 millimeters and the corresponding mass is 912 kilograms. One internal ring is located at the

center of the oxygen tank. This stiffening ring has a mass of 115 kilograms and is the same shape as the rings in the hydrogen tank.

### Tank Insulation

The liquid oxygen is stored at about 80 K and the liquid hydrogen is stored at 20 K. The aluminum walls are insufficient for proper thermal insulation, thus the tanks are covered with polyurethane foam. This type of insulation has a thermal conductivity,  $\kappa$ , of 0.035 W/m·K and a density of 46 kg/m<sup>3</sup>. The heat loss thru the cylindrical wall of the hydrogen tank was determined from the following equation [7].

$$q_r = \frac{(T_1 - T_3)}{\frac{\ln\left[\frac{r_2}{r_1}\right]}{2\pi\kappa_A L} + \frac{\ln\left[\frac{r_3}{r_2}\right]}{2\pi\kappa_B L}} \quad (3.9)$$

$q_r$  = Radial heat loss thru wall in Watts

$T_1$  = Temperature of liquid hydrogen = 20 K

$T_3$  = Temperature of ambient = 298 K

$\kappa_A$  = Thermal conductivity of Alum 2219 = 80 W/m·K

$\kappa_B$  = Thermal conductivity of polyurethane foam = 0.035 W/m·K

$L$  = cylinder length = 7.93 m

$r_1$  = Inner radius of cylinder = 3.5 m

$r_2$  = Outer radius of cylinder = 3.500852 m

$r_3$  = Outer radius of cylinder with foam = 3.510852 m

The hemispheres are analyzed by using the following equation:

$$q_{sph} = \frac{(T_1 - T_3)}{\frac{1}{2\pi\kappa_A} \left( \frac{1}{r_1} - \frac{1}{r_2} \right) + \frac{1}{2\pi\kappa_B} \left( \frac{1}{r_2} - \frac{1}{r_3} \right)} \quad (3.10)$$

The cylindrical tank wall and the upper and lower end domes of the hydrogen tank has 10 mm of insulation and the oxygen tank will have 5 mm of insulation. The total mass of insulation on the hydrogen tank is 151 kg and the oxygen tank will have 31 kg of insulation. The hydrogen and oxygen tanks will lose 291 kW and 100 kW, respectively. By dividing the heat of vaporization (452 kJ/kg for LH2 and 213 kJ/kg for LOX) from the heat loss, the rate of propellant boil-off can be determined. The hydrogen and oxygen will lose 0.64 kg/s and 0.47 kg/s, respectively. It takes 255 seconds until the upper stage reaches 97 km where the ambient temperature will be only a few degree K resulting in insignificant amounts of propellant losses. Assuming that the propellant tanks are filled immediately before lift-off, approximately 164 kg of hydrogen will be boiled off and 120 kg of oxygen will be lost during the 255 sec ascent.

### **Propellant Tank Support Struts**

The propellant tanks are connected to the longeron truss frame via support struts (see Fig. 3.14). These struts are required to hold the propellant tanks in a fixed location, thus the struts must have sufficient strength to resist the loads. To determine the size of the struts required on the hydrogen tank, an analysis is performed with the struts designed to support the mass of the entire tank. The hydrogen tank has a structural mass of 1182 kilograms with a propellant mass of 33,943 kilograms. The analysis will be conducted by assuming that the end of the struts that are attached to the longeron frame are fixed and the other end of the struts are subjected to axial tension and compression, and bending loads. The applied loads on the hydrogen tank support struts are shown in Table 3.9. Note that the g loads on the struts are perpendicular to the g loads on the payload. The struts are 0.85 meters in length. The two loads applied on the tank connection end of the struts are combined to simulate a worst case condition by summing the squares of the axial and normal loads. From Eq. 3.5 the required thickness can be determined using the following information.

Table 3.9 Applied loads on tank support struts of H<sub>2</sub> tank.

Type of load	Force (N)	Distance (m)	Load (g)	Limit load
Normal	344,575	-	3.0	1.03x10 <sup>6</sup> N
Axial	344,575	-	6.5	2.24x10 <sup>6</sup> N
Bending	344,575	0.85	6.5	1.90x10 <sup>6</sup> N·m

$$P_{\text{applied}} = 1.6 \times (2.47 \times 10^6 \text{ N}) = 3.95 \times 10^6 \text{ N (yield)}$$

$$P_{\text{applied}} = 2.0 \times (2.47 \times 10^6 \text{ N}) = 4.93 \times 10^6 \text{ N (ultimate)}$$

$$F_{\text{ty}} = \text{yield tensile strength of Alum 7075-T6} = 455 \times 10^6 \text{ N/m}^2 [6]$$

$$F_{\text{tu}} = \text{ultimate tensile strength of Alum 7075-T6} = 531 \times 10^6 \text{ N/m}^2 [6]$$

$$A = \text{cross-sectional area} = t^2$$

$$t_{\text{required}} = 0.093 \text{ m (yield)}$$

$$t_{\text{required}} = 0.096 \text{ m (ultimate)}$$

Aluminum 7075-T6 bar stock was selected because of its high strength. The struts must also withstand bending stress.

$$\sigma = \frac{M \cdot c}{I} \quad (3.11)$$

$$M = \text{bending moment} = 1.90 \times 10^6 \text{ N}\cdot\text{m (limit)}$$

$$M = 3.05 \times 10^6 \text{ N}\cdot\text{m (yield)}$$

$$M = 3.81 \times 10^6 \text{ N}\cdot\text{m (ultimate)}$$

$$c = t = \text{wall thickness}$$

$$I = \text{moment of inertia} = t^4/12$$

$$\sigma = F_{\text{ty}} \text{ or } F_{\text{tu}}$$

$$t_{\text{required}} = 0.431 \text{ m (yield)}$$

$$t_{\text{required}} = 0.441 \text{ m (ultimate)}$$

All hydrogen tank support struts must have a total of at least 0.441 m in cross-sectional area. Thirty-two tank support struts will be attached to the hydrogen tank, equally spaced around the perimeter and in pairs. Sixteen supports will attach to the upper ring and sixteen to the lower

ring. These members will be made of Alum 7075-T6 bar stock of at least 13.8 mm thickness. The total mass of the bars is 14.5 kg.

The sixteen support struts for the oxygen tank is analyzed the same way as the hydrogen tank struts. Each strut is 4.97 cm thick and 0.85 m long, and the total mass of the struts for the oxygen tank is 94 kg.

### Longeron Truss Frame Body Structure

A longeron truss frame surrounds the propellant tanks in an octagonal pattern. There are four segments: docking port interface, hydrogen tank support, oxygen tank support, and an interstage adapter (see Fig. 3.14). All segments are designed to transmit the loads through the frame members to the launch vehicle interface attachment. The support struts for the propellant tanks attach to eight fittings that are bolted to the longerons. The buckling criteria is applied to the column members of each segment due to compressive loading.

$$P_{cr} = \frac{\pi^2 \cdot E \cdot I}{L^2} \quad (3.12)$$

$E$  = modulus of elasticity of Alum 7075-T6 =  $71 \times 10^9$  N/m<sup>2</sup> [5]

$I$  = moment of inertia =  $t^4/12$

$L$  = length of member = 2 m

$P_{cr} = P_{allow} = \sigma_{allow} \times t^2$

$\sigma_{allow} = 455 \times 10^6$  N/m<sup>2</sup> (yield)

$t_{required} = 0.177$  m

The strength of the columns must support the weight of the entire fully loaded upper stage at 6.5 g's. The strength is verified with the use of Eq. 3.5 and the following information.

$$\sigma = \frac{P}{A} \quad (3.5)$$

$P = P_{applied} = 1.59 \times 10^7$  N (limit)

$P = 2.55 \times 10^7$  N (yield)

$$P = 3.18 \times 10^7 \text{ N (ultimate)}$$

$$A = t^2$$

$$\sigma = \sigma_{\text{allow}} = F_{ty} \text{ or } F_{tu}$$

$$t_{\text{required}} = 0.237 \text{ m (yield)}$$

$$t_{\text{required}} = 0.245 \text{ m (ultimate)}$$

The required thickness is 0.245 m for eight members that are contained in a single plane. The eighty-eight Aluminum 7075-T6 vertical column members are 3.06 cm thick and 2 meters long for a total mass of 462 kg.

The horizontal and diagonal members are subjected to the vibrational modes induced during lift-off. These 184 members are designed for rigidity with an estimated mass of 1544 kg.

### **Propellant Feed Lines**

The upper stage has one liquid hydrogen line and one liquid oxygen line manufactured out of Inconel 625 or Inconel 718. Both feed lines must split to provide a feed line to two engines, and the feed lines will also need to accommodate gimbal motion. The hydrogen feed line could be routed straight through the center of the oxygen tank or it could run along the outside of the oxygen tank. To eliminate pressure differences on the walls, easy mounting, and to improve accessibility, the hydrogen feed line is located outside the oxygen tank (see Fig. 3.14). The hydrogen and oxygen will be drawn from the bottom of the tanks and the fuel and oxidizer lines are insulated with foam to eliminate additional thermal losses as the fluids are pumped to the main engines. The estimated mass is 300 kg.

## Structural Design Summary

Table 3.10 shows a summary of the structural mass distribution of the upper stage. Miscellaneous items include tank fittings, frame connections, valves, regulators, and sensors for an estimate of 300 kg.

Table 3.10 Structural component masses.

<b>Component</b>	<b>Mass (kg)</b>
Liquid hydrogen tank	
Cylindrical wall	378
Aft hemispherical end dome	82
Forward hemispherical end dome	184
Internal stiffening rings	387
Insulation	151
Liquid oxygen tank	
Spherical walls	912
Internal stiffening ring	115
Insulation	31
Hydrogen tank support struts	15
Oxygen tank support struts	94
Vertical longeron members	462
Horizontal and diagonal longeron members	1544
Propellant lines	300
Miscellaneous	300
<b>TOTAL STRUCTURAL MASS</b>	<b>4955</b>

## LAUNCH VEHICLE INTERFACE

### Interstage Adapter

The interstage adapter is a longeron truss frame that supports the upper stage when atop the Antares VII. The top of the interstage adapter frame is attached to the avionics frame and the bottom of the interstage adapter frame is bolted to the Antares VII. During flight, the interstage adapter will separate from the upper stage when the Antares VII has completed its burn. The estimated mass is 600 kg.

### Nose Cone Fairing

The base nose cone fairing of the Antares VII will need to be stretched 5 meters in length to accommodate the upper stage. Three portions of the fairing will add to the mass: acoustic shielding, rails, and the graphite/epoxy structure. The modified fairing will be increased by 849 kg over the Antares VII fairing [1] as listed in Table 3.11.

Table 3.11 Fairing mass and size comparison.

Fairing type	Fairing length (m)	Payload diameter (m)	Fairing mass (kg)
Base Antares VII	26.24	9.14	8500
Stretch fairing for upper stage	31.24	9.14	9349

## PAYLOAD FAIRING (John Tran)

Since the original Antares payload fairings are inadequate to cover both the transfer vehicle and the booster, an expanded fairing was designed. The new payload fairing (Fig. 3.6)

incorporates the design of both the Antares I GEO and the Antares II [1], which both consist of an upper cone and a support fairing.

There are three dimensional options for the upper cone: parabolic, a parabolic with a circular dome, or conical cone with a circular dome. Using methods of analysis that are similar to the original payload fairing calculations [1], the conical cone option is the best. The dimension of the the upper cone will be 12 m in height and 10 m in width.

The support fairing is similar to the Antares I GEO support fairing [1]. However, because the transfer vehicle will be connected to the Antares VII via a docking port, the fairing is not required to carry much weight. This means it is used mostly for aerodynamic purposes. The payload fairing is designed to cover both the aerobrake and the transfer vehicle. With these criteria in mind, the support fairing must be 21 m in height, 15 m in diameter at its base, and 10 m in diameter at its forward end. The three components of the fairing have a combined mass of 7000 kg.

#### **3.2.1.4 ALTERNATIVE TO UPPER STAGE: PARALLEL STAGING** (Tuyen Bui)

One option to adding an upper stage is to parallel stage the Antares VII. The purpose of parallel staging is to reduce the structural mass by jettisoning empty modular units. During the first portion of the burn all seven Antares engines will operate, drawing fuel from four of the seven propellant tanks. After the four propellant tanks are used up, they are jettisoned, leaving three modular units. All three remaining engines will burn drawing fuel from two of the three tanks. When these two tanks are used up, they are ejected. The third stage consists of a single Antares booster that propels itself into LEO with 82,900 kg of propellant remaining. However, this method of staging will not deliver enough propellant for the TMI burn, which requires 105,000 kg, hence, it is second choice.

### 3.2.2 UNMANNED MARS TRANSFER VEHICLE (UMTV)

In the first segment, an unmanned transfer vehicle (UMTV) is sent to Mars (see Fig. 3.1). Once the UMTV is in LEO it will be docked with, a TMI booster. The UMTV payload consists of: .

- 1) Unmanned Rover
- 2) Propellant Manufacturing Unit
- 3) H<sub>2</sub> needed to produce CH<sub>4</sub>
- 4) Science Equipment
- 5) Retrorockets
- 6) Propellant for landing and additional  $\Delta V$ 's
- 7) Aerobrake
- 8) Earth Return Vehicle (ERV)

#### 3.2.2.1 UMTV PROPULSION (Mike Machula)

Once the initial TMI booster burn is complete, the booster is jettisoned. The additional  $\Delta V$  needed for orbital correction, descent and landing is supplied by Pratt and Whitney RL10 engines. This engine was chosen because of its low mass, high thrust and availability. In addition, the rocket engines required to complete a long duration mission, such as the Minerva project, must have high reliability. These engine requirements are satisfied by the Pratt and Whitney RL10 due to its simple cycle and conservative design. As for the reliability of the engine, "the RL10 has accumulated over 20 hours of operation in space; 174 engines have produced 282 in-space firings without a single engine failure, and it has demonstrated the highest reliability of any operational liquid rocket engine" [8].

Currently, the LOX/LH<sub>2</sub> RL10-A4 weighs 167.8 kg and can produce a thrust of 73.4 kN with a specific impulse of 449 sec [9]. Unfortunately, the RL10-A4 has no throttling

capability and therefore does not meet the needs of the Minerva project., which requires throttling capabilities and a greater thrust for landing. However, the near future promises to produce a modified RL10 that matches the Minerva project, needs. “A 157 kN class RL10 has been evaluated for a number of different applications and is currently being worked on for the NLS upper stage and the single engine Centaur” [9]. In addition, work on 3 to 1 throttling capabilities is being undertaken for McDonald Douglas’ SSTO [9]. Even if these new modifications do not materialize, a modified RL10 engine could be developed specifically for Project Minerva , for very little compared to the research and development costs of a new engine. Figure 3.15 presents the upgraded engine performance of the LOX/LH2 RL10. For the Minerva project, this engine will have a thrust of 155.68 KN, and a specific impulse of 449 seconds. It burns H<sub>2</sub> and O<sub>2</sub> at a mixture of 6:1. The length of this engine is 3.45 m (with skirt extended) and has a exit diameter of 1.78 m (see Fig 3.16).

The initial deceleration of the UMTV in the Martian atmosphere is effected by aerobrake maneuvers. The aerobrake slows the vehicle to a velocity of approximately 500 m/s and then is jettisoned. After that the RL10’s provide the final deceleration required for a soft landing. The amount of propellant required for these maneuvers is determined with the use of the rocket equation:

$$M_p = M_o \left[ 1 - e^{\frac{-\Delta V}{I_{sp}g}} \right] \quad (3.13)$$

With  $M_o = 70$  tons,  $I_{sp} = 449$  sec and  $\Delta V = 500$  m/s, 8.4 tons of propellant are required to decelerate the vehicle. An additional 1.6 tons of propellant is brought along for hovering maneuvers and as a safety factor. The UMTV thus carries 10 tons of propellant for landing maneuvers.

The number of engines required for descent was determined by the thrust to weight ratio needed to hover and maneuver immediately above the Martian surface. For safe

maneuvers, the thrust to weight ratio should be in the range of 1.2 to 1.4. The UMTV has a mass of approximately 63 tons when hovering maneuvers commence. This is after approximately 7 tons of propellant have been used for deceleration purposes. The 63 tons has a weight on Mars of approximately 235 kN. Therefore two modified RL10-A4 engines to produce a thrust to weight ratio of 1.33 at full throttle.

### **UMTV THRUST STRUCTURE**

The thrust created by the RL10 engine is transferred to the rest of the vehicle with the use of a thrust structure. The UMTV employs a modified Boeing thrust structure that has been adapted to meet its two engine needs (Fig. 3.17). The thrust structure consists of eight 9.1 m long cross-beams that attach to the aft section of the body. These cross beams, along with additional supports, distribute the engine load equally along each of the eight cross beams. The engine support beams are of conventional stiffened web and chord construction manufactured from aluminium 7075. The mass of the thrust structure is 83.5 kg.

### **UMTV THRUST VECTOR CONTROL**

In addition to providing a propulsive force, the rockets can also provide attitude control, that is, control of the vehicle's pitch, yaw and roll moments [10]. Normally, the two rockets' correct thrust vector is in the direction of the vehicle's axis and passes through the vehicle's center of gravity. Therefore, by deflection of the thrust vector, attitude control can be obtained. For the RL10 engine, the thrust vector is rotated by gimbaling (essentially a universal joint) the engine which permits the whole engine to be pivoted in two planes, as demonstrated in Fig. 3.18. During operation, the engine gimbaling capability will permit locating the thrust chamber center line  $\pm 4^\circ$  from the engine center-line [9]. Accounting for engine gimbaling, the engine requires a diameter 2.26 m.

Due to gimbaling, the engines require flexible propellant lines to allow propellant to flow from the tanks to the moveable engines. Figure 3.19 presents the propellant line configuration needed to overcome this problem. As the figure demonstrates, two perpendicular propellant line sections are connected to the main propellant distribution unit and the engine with flexible joints. This configuration permits the engine to be gimbaled without propellant line damage. As the engine moves from the null position to a gimbaled position, the propellant line joints permit the propellant lines to move both vertically and horizontally.

Thrust vector control (TVC) is accomplished by activating a pair of thrust actuators which are attached to a moment arm on the engine and to the thrust frame. These actuators deflect the rocket's thrust vector as shown on the right hand side of Fig. 3.20. In order to produce a circular gimbal pattern as shown in Fig 3.18, the actuators are placed in two planes 90° apart, and are operated either separately or simultaneously.

The TVC system employs on-demand, electrically driven Electrohydrostatic Actuators (EHA). Figure 3.21 shows an EHA developed jointly by Allied Signal and Boeing. The EHA is a three-channel system. Each channel utilizes an electric motor to drive a reversible hydraulic pump which supplies a piston actuator, resulting in nozzle directional movement. Each EHA has the approximate dimensions: length = 2 ft, width = 1 ft and mass = 65 kg [11].

The EHA has many desirable characteristics ideal for the Minerva project. Because the EHA is an on-demand system using only electrical power when needed, it is able to use the minimum power required. The EHA uses self-contained hydraulics which eliminate the need for long distribution lines and a centralized hydraulic system, thus providing significant mass savings over conventional systems. In addition, the EHA ensures the high reliability needed to accomplish the Minerva project.

The EHA system is a single fault tolerant and uses three channels for redundancy purposes. During normal operation the loads are distributed equally among all three channels.

If a fault is detected, the system is re-configured so the remaining two channels continue to operate. The faulted channel is then taken off line by opening a hydraulic bypass valve so that no loads can be developed by the faulted channel. In the event that two channels fail, the EHA still provides nearly the maximum operational capability. With only a single channel operating there is sufficient power to provide 87% of the required nozzle operating needs [12]. The EHA was chosen for the Minerva project because of its high tolerance to system failures, self-contained hydraulic system and its low mass.

For the Project Minerva, the EHA is powered by a 220 V dc battery which eliminates the need to carry along a separate consumable fuel power system. A Nickel-Cadmium rechargeable battery will be used for energy storage. The battery, located in the ERV module will power both the UMTV's and the ERV's TVC system. After descent of the UMTV the batteries are recharged with the DIP's power system so that they can then be used for the ERV. This configuration eliminates the need to carry a battery for each stage. The battery is sized to meet the power supply needs of the ERV since it has two more engines than the UMTV and therefore requires more power. The battery mass is estimated to be 400 kg.

### **3.2.2.2 STRUCTURAL ANALYSIS**

#### **Hydrogen Tank Design** (James Madison)

The hydrogen tank geometry is based on an ellipsoidal tank designed by the Boeing Company's Defense and Space Group [2]. The tank geometry was decided on for a number of reasons. First, hydrogen must be kept at 20 K. Thus, it is vital to keep the surface to volume ratio as small as possible in order to minimize heat transfer. Also, it is important to keep the height at a minimum. The tank must hold  $106 \text{ m}^3$  of hydrogen. Based on this, the tank is 8 m in diameter and 3.2 m in height.

The internal tank forces must be calculated to determine the tank wall thickness. The internal forces were calculated using the Affine transformation outlined in reference [13]. A sphere was used as the initial geometry (S). One of the axes was then compressed by a factor of b/a. This gave the required ellipsoidal geometry ( $\tilde{S}$ ). The formulas used to calculate the longitudinal and hoop forces are as follows [13]:

$$\tilde{N}_\phi = \tilde{n}_x \text{COS}^2\alpha + \tilde{n}_y \text{SIN}^2\alpha \quad (3.14)$$

$$\tilde{N}_\vartheta = \tilde{n}_x \text{SIN}^2\alpha + \tilde{n}_y \text{COS}^2\alpha \quad (3.15)$$

where

$$\tilde{n}_x = \frac{n_1^2}{n_3} n_x \quad (3.16)$$

$$\tilde{n}_y = \frac{n_2^2}{n_3} n_y \quad (3.17)$$

and where  $n_1$ ,  $n_2$ , and  $n_3$  are factors by which the x, y, and z axis are compressed respectively. For a sphere under a pressure loading where a is the tank radius along the x axis and g is the applied load:

$$N_\phi = \frac{-a^2 g}{a + \sqrt{a^2 - y^2}} \quad (3.18)$$

$$N_\vartheta = \frac{-a^2 g}{a + \sqrt{a^2 - y^2}} + g\sqrt{a^2 - y^2} \quad (3.19)$$

in the untransformed state. Transforming this to the ellipsoidal geometry one arrives at:

$$\tilde{N}_\phi = \frac{a}{b} \left[ N_\phi - \frac{\text{TAN}^2\alpha (N_\vartheta \text{COS}^2\alpha - N_\phi) + N_\vartheta \text{SIN}^2\alpha - N_\phi \text{TAN}^2\alpha}{\text{COS}^2\alpha - \text{TAN}^2\alpha} \right] \quad (3.20)$$

$$\tilde{N}_\vartheta = \frac{a}{b} \left[ N_\phi \text{TAN}^2\alpha - \frac{\text{SIN}^2\alpha \text{TAN}^2\alpha (N_\vartheta \text{COS}^2\alpha - N_\phi) + N_\vartheta \text{COS}^2\alpha - N_\phi}{\text{COS}^2\alpha - \text{TAN}^2\alpha} \right] \quad (3.21)$$

Using aluminum 2219 as the tank material and a pressure of 2 bars, the tank thickness needs to be 8.8 mm. This is an approximation, however, since this model yields a singularity point at  $\alpha = 90$  degrees. Once the thickness is known, the mass of the tank was found to be 2970 kg.

The tanks are insulated using organically bonded, fine fiber, glass insulation blankets. A more detailed analysis of this insulation type is presented in more detail in Section 3.2.3.4. Using a spherical tank approximation with a volume of 106 m<sup>3</sup> of hydrogen, the optimum insulation thickness is 0.3 meters for which the heat loss on the Martian surface is about 3.2 kW. This quantity of insulation ( $\rho = 12 \text{ kg/m}^3$ ) has a mass of 390 kg.

### **Payload Bay** (Kevin Mahn)

The payload bay houses the science equipment, the hopper and the unmanned rover (see Fig. 3.22). The propellant manufacturing unit is stored under the payload bay. The science equipment and other accessories (piping, etc.) are stored in the remaining area around the rover. The liquid hydrogen for producing propellant is stored above the payload bay to enable the unmanned rover to enter and exit the bay.

The payload bay walls are designed to withstand an 8 g axial force and a 3 g lateral force (see Table 3.12). The walls are also designed for an ultimate load of 2 times the applied load and an yield load of 1.6 times the applied load. These values are chosen as guidelines which include a margin for structural safety. Two types of wall structure were considered. The first was monocoque skin panel (panel structure without attached stiffening members). The

second was semimonocoque structures, skin panels with stiffeners (called stringers and frame members).

Table 3.12 Loads.

Type of Load	Force (N)	Distance top to g payload bay (m)		Load
Axial	70,000 x 9.81=686,700	-	8	5.50x10 <sup>6</sup> N
Lateral	686,700	-	3	2.06x10 <sup>6</sup> N
Bending Moment	686,700	13	3	26.8x10 <sup>6</sup> N·m

### Monocoque Panels

The payload bay is 3 m high and has a diameter of 9.1 m (refer to Fig 3.22). From the data in Table 3.13, an equivalent load,  $P_{eq}$ , was found.

$$P_{eq} = P_{axial} + \frac{2M}{R} = 5.50 \times 10^6 + \frac{2(26.8 \times 10^6)}{4.55} = 17.3 \times 10^6 \text{ N} \quad (3.22) \quad [13]$$

where:  $P_{eq}$  = the equivalent load produced by the axial force and bending moment  
 $P_{axial}$  = the vertical load on the structure  
 $M$  = bending moment  
 $R$  = radius of payload bay

This is the equivalent applied load. To find the ultimate and yield loads,  $P_{eq}$  must be multiplied by the factor mentioned above for safety.

$$P_{ult} = 34.5 \times 10^6 \text{ N}$$

$$P_{yld} = 27.6 \times 10^6 \text{ N}$$

The wall thickness can be calculated using the above forces. Because these include a margin of safety (MS), any additional safety margin consideration is unnecessary. Using the equations below, the thickness of the wall,  $t$ , required can be found [13].

$$MS = \frac{\text{Allowable load}}{\text{Applied load}} - 1 = \frac{P_{cr}}{P_{ult}} - 1 = 0 \quad (3.23)$$

$$P_{cr} = A_{cyl} \sigma_{cr} \quad (3.24)$$

$$A_{cyl} = 2\pi R t \quad (3.25)$$

$$\sigma_{cr} = 0.6\gamma \frac{Et}{R} \quad (3.26)$$

$$\gamma = 1.0 - 0.901(1.0 - e^{-\phi}) \quad (3.27)$$

$$\phi = \frac{1}{16} \sqrt{\frac{R}{t}} \quad (3.28)$$

where:

MS = margin of safety  
 $P_{cr}$  = critical buckling load  
 $P_{ult}$  = ultimate tensile load  
 $A_{cyl}$  = cross-sectional area of a cylinder  
 $\sigma_{cr}$  = critical buckling stress  
 $E$  = modulus of elasticity  
 $t$  = thickness of the wall  
 $\gamma$  = reduction factor [13]  
 $R$  = radius of payload bay  
 $\phi$  = geometric parameter for cylinders [13]

With the thickness determined and the materials specified, the masses can be calculated. Aluminum was considered because it is inexpensive, easily machineable, and readily available. Also, graphite/epoxy was considered because of its low density and high tensile strength. Table 3.13 shows the characteristics of the material, thickness of wall needed to support load, mass corresponding to that thickness, and the resultant moment of inertia.

Table 3.13 Aluminum alloys and masses.

Aluminum Alloy	Density (kg/m <sup>3</sup> )	E (N/m <sup>2</sup> )	Thickness (m)	Mass (kg)	I = πR <sup>3</sup> t (m <sup>4</sup> )
2014 - T6	2.80x10 <sup>3</sup>	72x10 <sup>9</sup>	0.0173	<b>4151</b>	5.12
2024 - T36	2.77x10 <sup>3</sup>	72x10 <sup>9</sup>	0.0173	<b>4106</b>	5.12
6061 - T6	2.71x10 <sup>3</sup>	67x10 <sup>9</sup>	0.0178	<b>4137</b>	5.27
7075 - T6	2.80x10 <sup>3</sup>	71x10 <sup>9</sup>	0.0174	<b>4178</b>	5.15
<b>Graphite/Epoxy</b>					
HTS	1.49x10 <sup>3</sup>	151x10 <sup>9</sup>	0.0127	<b>1625</b>	3.76
HM	1.61x10 <sup>3</sup>	186x10 <sup>9</sup>	0.0117	<b>1612</b>	3.45
UHM	1.69x10 <sup>3</sup>	289x10 <sup>9</sup>	0.00976	<b>1415</b>	2.89

The table shows that a structure made from graphite/epoxy weighs less than one made from aluminum alloy. These results must be compared to the results from using semimonocoque panels, which are evaluated next.

### Semimonocoque Panels

Twelve longitudinal members (stringers) and 4 circumferential rings (frames) are considered for this method. The frames are spaced one meter apart. Since there are 12 stringers around the circumference of the payload bay, each is spaced 30° apart (refer to Fig 3.23). The P<sub>ult</sub> is the same as above. The margin of safety is also set equal to zero.

$$\sigma_{cr} = \frac{K\pi^2 E}{12(1-\nu^2)} \left(\frac{t}{b}\right)^2 \quad (3.29)$$

$$I = \pi R^3 t \quad (3.30)$$

where:

MS = margin of safety  
P<sub>cr</sub> = critical buckling load  
P<sub>ult</sub> = ultimate tensile load

$A_{cyl}$  = cross-sectional area of a cylinder  
 $\sigma_{cr}$  = critical buckling stress  
 $E$  = modulus of elasticity  
 $t$  = thickness of the wall  
 $R$  = radius of payload bay  
 $b$  = spacing =  $\text{rad}(30^\circ) \times 3.55 = 1.86$  m  
 $\nu = 0.30 - .034$   
 $K = 65$   
 $I$  = moment of inertia

Using equations 3.23 - 3.25 and 3.29- 3.30, the thickness of the panels,  $t$ , moment of inertia of the panels ( $I_{pan}$ ), and moment of inertia of the stringer can be calculated ( $I_{str}$ ). From  $I_{str}$ , the cross-sectional area of the stringers can be calculated. To do this,  $I_{str}$  as a function of area must be found.

$$I_{str} = \sum (I_{cm} + Ad^2) \quad (3.31)$$

where:

$I_{cm}$  = moment of inertia about the center of mass of each stringer  
 $A$  = stringer cross-sectional area  
 $d$  = distance from neutral axis (from Fig 3.23)

$I_{cm}$  can be ignored since the  $Ad^2$  term is much greater. Table 3.14 summarize the calculation to find  $I_{str}$ .

Table 3.14 Moment of inertia based on stringer area.

Stringer	d (m)	d <sup>2</sup> (m <sup>2</sup> )	$\Sigma A$	$\Sigma Ad^2$
1,7	0	0	2A	0
2,6,8,12	2.275	5.176	4A	20.70A
3,5,9,11	3.940	15.52	4A	62.09A
4,10	4.550	20.70	2A	41.41A
			<b>Total</b>	<b>= 124.2A</b>

Now the area of the stringer can be found. This is summarized in Table 3.15 for each aluminum alloy and graphite/epoxy.

Table 3.15 Stringer cross-sectional areas.

Alloy	t (m)	$I_{pan}$ (m <sup>4</sup> )	$I_{tot}$ * (m <sup>4</sup> )	$I_{str}$ ** (m <sup>4</sup> )	$I_{str}$	Area (m <sup>2</sup> )
2014-T6	0.0117	3.47	5.12	1.65	124.2A	0.0133
2024-T36	0.0117	3.47	5.12	1.65	124.2A	0.0133
6061-T6	0.0121	3.58	5.27	1.69	124.2A	0.0136
7075-T6	0.0117	3.47	5.15	1.68	124.2A	0.0135
Graphite/ Epoxy						
HTS	0.00909	2.69	3.76	1.07	124.2A	0.00864
HM	0.00848	2.51	3.45	.945	124.2A	0.00761
UHM	0.00732	2.17	2.89	.714	124.2A	0.00575

\*  $I_{tot}$  is from Table 3.14

\*\*  $I_{str} = I_{tot} - I_{pan}$

Now the total mass can be found, which is summarized in Table 3.16.

Table 3.17, a comparison of panel types, indicates that mass is not a function of material (aluminum or graphite/epoxy) or of payload bay design. Thus other factors, such as panel style, must be considered when deciding on payload bay design. Because of the connection points, the payload bay must be designed for point forces. The monocoque panel design is therefore not feasible because this design is good only for distributed loads. Because of the way the ERV will be attached, the payload bay will be subjected to some point loads. For this reason, semimonocoque is the better design. Other properties must be considered when choosing the material to construct the payload bay. Upon entry to Mars, the vehicle will experience heating. For this reason a material with a low coefficient of thermal expansion and low thermal conductivity needs to be chosen. The aluminum alloy that best fits these requirements is aluminum 2024-T36 and the best graphite/epoxy is UHM.

Table 3.16 Total mass of semimonocoque panels.

Alloy	t (m)	Area (m <sup>2</sup> )	Volume (m <sup>3</sup> )	Mass (kg)	Tot Mass (kg)
2014-T6					
•Skin	0.0117	0.334	1.00	2800	<b>4140</b>
•Stringer*	-	0.159	0.477	1336	
2024-T36					
•Skin	0.0121	0.334	1.00	2770	<b>4090</b>
•Stringer*	-	0.159	0.477	1321	
6061-T6					
•Skin	0.0135	0.346	1.04	2812	<b>4140</b>
•Stringer*	-	0.163	0.489	1325	
7075-T6					
•Skin	0.0117	0.334	1.00	2800	<b>4160</b>
•Stringer*	-	0.162	0.486	1361	
<b>Graphite/Epoxy</b>					
HTS					
•Skin	0.00909	0.260	0.780	1162	<b>1630</b>
•Stringer*	-	0.104	0.311	463.3	
HM					
•Skin	0.00848	0.242	0.727	1171	<b>1610</b>
•Stringer*	-	0.0913	0.274	441.2	
UHM					
•Skin	0.00732	0.209	0.628	1061	<b>1410</b>
•Stringer*	-	0.0690	0.207	349.9	

\* Data for all 12 Stringers

We can use this same design to support the rest of the vehicle that needs to be supported (Fig 3.1). These areas include the propellant manufacturing unit bay, the hydrogen tank, and the engines and tanks of the ERV. The total mass of the UHM-graphite/epoxy to support these areas is 7.3 metric tons. If aluminum 2024-T36 is used, the mass will be 21 metric tons.

Table 3.17 Comparison of panel types

Aluminum Alloy	Type of Panel	
	Monocoque	Semimonocoque
2014-T6	4150 kg	4140 kg
2024-T36	4110 kg	4090 kg
6061-T6	4140 kg	4140 kg
7075-T6	4180 kg	4160 kg
<b>Graphite/Epoxy</b>		
HTS	1630 kg	1630 kg
HM	1610 kg	1610 kg
UHM	1420 kg	1410 kg

**3.2.2.3 MASSES**  
(Kevin Mahn)

Table 3.18 Mass breakdown for the UMTV.

Structure	10 metric tons
Retro-Rockets	0.7
Propellant	10
ERV (4 engines+Hab+Structure)	18
Thruster	0.5
Power	7.6
Propellant unit	2
Hydrogen	6
Hydrogen tank	3
Unmanned rover	1
Science	0.5
UMTV Aerobrake	9
Piping and Wiring	1
<b>TOTAL</b>	<b>69.3 metric tons</b>

This is a list of the estimated masses in metric tons for the UMTV. The structure mass of 10 tons includes the floors of the payload bay and propellant manufacturing unit and the engine thrust structure. The ERV is limited in weight by the amount of CH<sub>4</sub> that is available for the return trip (98 metric tons of propellant).

#### **3.2.2.4 PROPELLANT LINES** (Mike Folkers and Mike Machula)

The unmanned vehicle contains very little piping. The main piping are the propellant connections between the tanks, propellant manufacturing unit and the engines. Listed below in Table 3.19 are the mass flows for the propellant manufacturing unit. As can be seen, these are very small values. It is therefore evident that the piping to and from the propellant manufacturing unit will also be small. To account for surges and adverse pressure gradients the piping to the tanks and to the propellant manufacturing unit is nominally 1/4 in. diameter. The piping from the tanks to the rover fill station is yet to be determined. This information is all shown schematically in Figure 3.24.

The propellant lines of the vehicles run outside the propellant tanks and along the inside walls of the vehicle. This line configuration is more massive than that of propellant lines that run directly through the propellant tanks to the engines. However, running the propellant lines outside of the tanks provides additional safety and ease of tank construction that outweigh "minimal mass" savings. There is one main propellant line per fuel and oxidizer tank. Figure 3.25 presents a schematic of the propellant line configuration. Each of these propellant lines feed into a main distribution unit and then the propellant is dispensed to the rocket engines. The main fuel lines from the tanks to the UMTV descent engines and the Earth return vehicle has a 6 in. inner diameter. They are constructed from Inconel 718. The lines are insulated with polyurethane foam so that the propellant will be maintained at cryogenic temperatures as it is pumped into the engines.

Table 3.19 Propellant Manufacturing Unit Mass Flow Rates.

Gas	Weight (lb/ft <sup>3</sup> )	Flow (kg/day)	Flow (kg/s)	Flow (ft <sup>3</sup> /s)
CO <sub>2</sub>	0.1234	201	0.002326	0.041570
H <sub>2</sub>	0.0056	18	0.000208	0.082031
CH <sub>4</sub>	0.0424	73	0.000845	0.043939
H <sub>2</sub> O	62.4300	169	0.001956	0.000069

### 3.2.2.5 DOCKING PORT (John Tran)

The UMTV and the upper stage carrying the propellant make a rendezvous at an altitude of 300 km (Fig. 3.8). They connect, via a docking port, (Fig. 3.9) and make final checks before initiating the transfer. The docking port design must follow the 1973 International Space Docking Agreement. This agreement set the following criteria ( Table 3.20).

Table 3.20 Docking allowances.

Closing velocity	0.05-.03 m/sec
Lateral velocity	0.1 m/sec
Lateral misalignment	0.3 m
Angular misalignment	7 deg
Roll misalignment	7 deg
Angular velocity	1 deg/sec

From this criteria and research on previous docking ports, the Apollo-Soyuz International Docking System was chosen [14,15,16]. This system is considered to be the safest docking structure available [17].

The docking port (Fig. 3.26) is 4 m in diameter with a 3 m diameter aperture in the center. This configuration allows the tether for manned mission to be connected through the docking port of the TMI Booster. There are alignment forks and a beacon on each port to help align the ports for connection. A truss system is used for the docking port so as to minimize mass. Stress analyses and Euler's critical buckling load was calculated to find the optimum material to construct the docking ports. Aluminum 7075-T6 was found to satisfy the criteria better than other materials [1]. The port is constructed of 29 aluminum tubular elements, each having an outer diameter of 6.4 cm and an inner diameter of 5.6 cm. The port is mounted and supported by 6 graphite/epoxy Mounting struts with an external diameter of 25 cm and an internal diameter of 22.5 cm (Fig. 3.26). Both structures were designed to withstand a 8 g force. The docking ports are mounted 2 m above the TMI booster, and 0.5 m above the UMTV and the MTV aerobrake. The total mass for each docking port is 375 kg.

In order to keep all axial forces in one direction, the UMTV docking port is mounted over the aerobrake. Since engine holes interfere with the aerobrake structure, the mounting struts are not uniform. Fortunately, the structure was designed to withstand a 8 g load, there should be no major problems to the structure. The docking port is mounted on the aerobrake with 'hard spots' titanium plugs (Fig. 3.27 and 3.28). The mounting struts and support beams of the aerobrake are connected with explosive bolts. This allows separation of the docking port before reaching Mars.

### **3.2.3 EARTH RETURN VEHICLE (ERV)**

The Earth return vehicle (ERV) is designed to use methane and oxygen as propellants, which are both manufactured on the Martian surface. The vehicle is equipped with a habitat to transport the crew back to Earth, and has an Apollo-like capsule for reentry at Earth.

### 3.2.3.1 ERV Propulsion (Mike Machula)

The RL-10A4 rocket designed by Pratt and Whitney, although designed to burn hydrogen and oxygen can be easily modified to use methane fuel. The RL10 has been successfully tested with various hydrocarbon fuels [8]. With the modifications proposed to the RL10, the methane fueled RL10 will have the same thrust of 155.68 kN; however, the specific impulse drops from 449 sec to 376 sec (see Fig. 3.29) [9]. In addition, the oxidizer to fuel mixture ratio decreases from 6:1 to 3.5:1. The engine has a mass of 363 kg, a length of 5.33 m (fully extended) and an exit diameter of 2.80 m.

Other methane rockets were also considered. Aerojet did a preliminary design study which resulted in a rocket with a specific impulse of 364.3 seconds; thrust of 2969 kN and a weight of 2589 kg [18]. Rocketdyne has recently proposed a methane rocket (RS44) with a specific impulse of approximately 400 seconds. The problem with the RS44, as well as the Aerojet engine is that they are still in the design phase. The main advantage of the RL10 is its near term availability.

The mission requires a total  $\Delta V$  of 6.6 km/s (with a safety factor) in order to return to Earth from the Martian surface. Reentry at earth will be similar to the Apollo missions. Using RL10 methane rocket engines, a total of 98.29 tons of propellant will be required to complete the mission. This amount of propellant was calculated using equation (3.13) with  $M_0 = 117$  tons,  $I_{sp} = 376$  sec and  $\Delta V = 6.6$  km/s.

In order to lift off the Martian surface with this propellant and the 19 ton ERV (including the DIPs), the ERV is outfitted with four RL10's which give a total thrust of 623 kN. These four engines at full thrust produce a thrust to weight ratio of 1.43 at take-off. The engines contribute 1.45 tons to the mass of the ERV.

## **THRUST STRUCTURE**

The thrust created by the RL10-A4 engine is transferred to the rest of the vehicle with the use of a thrust structure similar to the one used on the UMTV. The modified Boeing thrust structure is adapted to meet the four engine needs of the ERV (Fig. 3.17). The mass of the thrust structure is 100 kg.

## **THRUST VECTOR CONTROL**

The ERV uses the same thrust vector control mechanisms as the unmanned Mars transfer vehicle (UMTV). Accounting for engine gimbaling, the methane fueled engine requires a space 3.55 m in diameter. The same battery that powered the UMTV thrust vector control (TVC) supplies the power for the ERV's TVC.

### **3.2.3.2 ERV TANK CONSTRUCTION** (James Madison)

The propellant tanks on the ERV must meet a number of stringent requirements. First, the tanks must be designed and oriented in such a way as to minimize height and still fit into a cylinder 9.1 m in diameter. Second, the tanks must be as light as possible. Third, the tanks must maintain their elastic properties at cryogenic temperatures. Fourth, the tanks must be insulated as much as possible to hold cryogenic oxygen and methane for the year and a half spent on the Martian surface. Finally, the tanks must be able to withstand an 8 g acceleration while fully loaded.

The tanks are constructed using the aluminum alloy 2219. This alloy is the same as that used on the Antares propellant tanks [1], the Space Shuttle External Tank and a number of other cryogenic type tanks. The first consideration in choosing this alloy is its tensile properties, given in Table 3.21.

Table 3.21 Tensile properties of aluminum alloys at 77 K [19].

Alloy & Temper	Tensile Strength (MPa)	Yield Strength (MPa)
5083-O	434	158
5083-H321	455	274
6061-T651	402	337
<b>2219-T851</b>	<b>568</b>	<b>440</b>
7005-T5351	578	465
A356-T61	356	262

Even though aluminum 7005 has a slightly higher yield strength, when one considers the manufacturability of the materials one finds that aluminum 2219 is the superior alloy at cryogenic temperatures. Aluminum 2219 is readily weldable by both the gas metal arc and the gas tungsten arc processes [19]. Aluminum 2219 has a joint efficiency of over 90%, where joint efficiency is defined as the tensile strength of the weld divided by the tensile strength of the parent alloy. Aluminum in general is easily cast and is very machinable. These properties are particularly important when the piping and relief valve construction is considered. Although the 2219 alloy is not the lightest, it is comparable to other alloys. Aluminum 2219 has a density of 2.83 g/cm<sup>3</sup> whereas other alloys have densities ranging from 2.65 to 2.83 g/cm<sup>3</sup>. Tank, tank system, insulation and valve masses are considered in sections 3.2.3.3-3.2.3.6. A summary of masses is presented in Table 3.22.

Table 3.22 ERV Tank Masses.

COMPONENTS	MASSES (kg)
Methane Tank	200
Oxygen Tanks	255
Insulation	180
Piping / Valves	150
<b>Total =</b>	<b>785</b>

### 3.2.3.3 ERV TANK CONFIGURATION AND ORIENTATION (James Madison)

The stringent volume constraints necessitate a slightly unorthodox tank configuration. The methane tank must hold 22 m<sup>3</sup> and the oxygen tank must hold 78 m<sup>3</sup>. A number of configurations were considered, most of which suffer from a variety of problems. These include problems but not limited to: small volume to surface area ratio, higher number of connections, high heat loss, and poor structural integrity. The configuration shown in Fig. 3.1 was chosen because of its simple geometry and proven reliability. This configuration only uses two tanks, minimizing heat loss and the number of piping connections, and thus the number of possible failure points.

The tank thickness plays a vital role in the pressure the tanks can withstand and the number of g the tanks can withstand before buckling. The tanks are designed to handle a gauge pressure of 2 bars. Since the geometry, critical yield stress of aluminum 2219 and gauge pressures are known, the required tank thickness is calculated using the following equation where  $\sigma_h$  is the stress and P, R and t are the internal pressure, radius and thickness respectively.

$$\sigma_h = \frac{P \times R}{t} \quad (3.32)$$

The tank thickness, based on pressure requirements alone, must be 1.1 mm.

The buckling analysis is performed using the methods outlined in reference 13.

The critical buckling load is defined as:

$$P_{cr} = \sigma_{cr} \times P \quad (3.33)$$

where

$$\sigma_{cr} = \frac{.6Et}{R} \left[ 1 - .901 \left( 1 - e^{-\frac{1}{16} \sqrt{\frac{R}{t}}} \right) \right] \quad (3.34)$$

and P is the applied load. The critical load using this model and a thickness of 1.1 mm is 59,850 N. The actual equivalent load is then calculated. The tanks are expected to experience a maximum 8 g axial load and a 3 g lateral load [13]. Given this information and the tank mass one can calculate the equivalent load using equation 3.22:

$$P_{eq} = P_{axial} + \frac{2M}{R} \quad (3.22)$$

where M is the equivalent moment experienced by the tank. The equivalent load is calculated to be 23,630 N. Thus, the actual loads are far less than the critical loads. The margin of safety (MS), as defined by equation 3.23, is 1.53. This exceeds even the most stringent margins of safety which are typically no more than 1.4. Thus, the tank thickness can be set at 1.1 mm since this thickness meets both pressure and axial load requirements.

### 3.2.3.4 TANK INSULATION AND HEAT LOSS (James Madison)

Since the volumes and tank configurations have been specified, one is faced with the problem of insulating the tanks. The average Martian surface temperature is 250 K, the oxygen must be stored at about 80 K, and the methane must be stored at about 100 K. The tank walls have 10 cm of insulation.

There are a number of possibilities for insulation type. One stipulation that must be made is that the insulation must not contain more than 20% aluminum powder [19] because in the event of oxygen tank leakage, the possibility exists that the vapor may be ignited. For this reason the insulation must not sustain combustion once ignited. It has been found that insulations with less than 20% aluminum powder do not sustain combustion [19]. The insulation must also be as light as possible to reduce structural mass. All of these considerations along with thermal conductivity lead to the choice of organically bonded, fine fiber, glass insulation blankets [20]. This type of insulation has a thermal conductivity of  $k = 0.035 \text{ W/mK}$ , and a density of  $12 \text{ kg/m}^3$ . It is known that fiber glass insulation is fire retardant. This is also a very light insulator.

Heat loss from the tanks is of vital importance. Because refrigeration requires energy, heat loss must be calculated so that refrigeration capacity, and energy allotment on the Martian surface can be estimated. The thermal conductivity of aluminum 2219 is  $80 \text{ W/mK}$ . The tank thickness is 1.1 mm. The heat loss was calculated using the following two formulae [20] where  $q$ ,  $r$ ,  $T$  and  $L$  are the heat loss in Watts, tank radius, Temperature, and tank length respectively. The subscripts  $r$  and  $sph$  refer to the radial heat loss of the cylindrical section and the spherical heat loss of the end caps. The results are shown in Table 3.23.

$$q_r = \frac{(T_1 - T_2)}{\frac{\ln \left[ \frac{r_2}{r_1} \right]}{\Sigma \frac{1}{2\pi\kappa L}}} \quad (3.35)$$

$$q_{sph} = \frac{4\pi\kappa(T_1 - T_2)}{\frac{1}{r_1} - \frac{1}{r_2}} \quad (3.36)$$

Table 3.23 Heat Losses..

<b>Tank</b>	<b>Losses (Watts)</b>
Methane	3,570
Oxygen	5,050
<b>Total</b>	<b>8,620</b>

Thus approximately 8.6 kW of heat must be transported away from the tanks via the refrigerator. The refrigerator must, however, be able to transport more heat if the occasion arises, for instance a warm day. In order to account for temperature variation a 20% allowance is included in the refrigeration capacity range. The thermostatically controlled refrigeration unit will thus be able to remove up to 10.3 kW of heat.

### 3.2.3.5 ERV TANK RELIEF VALVES AND PIPING (James Madison)

The ERV tanks are equipped with relief valves [21]. This precaution is necessary in case of refrigeration failure. If the refrigeration units do fail for some reason, the tanks must be able to release the pressure of the boiling fluids to avoid explosion. Thus, the worst case scenario is that the refrigeration does fail, and the boil off gases are harmlessly released into the Martian atmosphere.

The relief valves are made of aluminum 2219. This material is chosen because of all the reasons mentioned in Section 3.2.3.2 and taking thermal expansion into account. Because the tank temperature will vary due to discontinuous refrigeration cycles, the whole system must expand and contract evenly. Even small differences in thermal expansion can cause seal breakage or structural cracking over a large number of thermal cycles. As mentioned in Section 3.2.3.2, aluminum is easily machinable, weldable and castable, making relief valve construction easier. The relief valves are connected to pipes leading to the ship's exterior. The oxygen and methane are piped to the opposite sides of the ship so as to eliminate the risk of mixing and possible ignition of the gases.

#### **3.2.3.6 LOW GRAVITY SLOSHING** (James Madison)

Sloshing as a phenomenon is an important factor in the Earth's gravity field which is caused by any type of lateral movement, usually uneven thrust or flight maneuvers. Sloshing can cause inertial unbalance which ultimately leads to dynamic unbalance and can cause control problems [1].

Sloshing in low gravity fields is a completely different problem. The Bond number, which is the ratio of the gravitational forces to the propellant surface tension forces, determines whether sloshing requires further consideration [22]. The Martian gravitational field is 0.38 that of Earth's. It has been determined that sloshing under low gravity is small compared with the structural capability of the tank [22], thus sloshing loads have been neglected in the ERV tank design.

#### **3.2.3.7 HABITAT** (Kevin Mahn)

The ERV's habitat is a scaled-down model of the manned mission habitat (discussed in detail in Section 5.0). There are four staterooms, a bathroom, an airlock, a lounge, a control

center, and the Earth return module, ERM, as shown in Figs. 3.30 and 3.31. The ERM is contained in the center of the habitat. The ERM can be used as a shelter against any harmful radiation. The habitat is 3 m high, however, 0.5 m is used for plumbing and wiring. The floor plan areas are summarized in Table 3.24.

Table 3.24 Floor plan areas of ERV habitat.

State room	3.5 m <sup>2</sup>
Bathroom	3.5 m <sup>2</sup>
Airlock	3.5 m <sup>2</sup>
Lounge/Control center	16.5 m <sup>2</sup>
<b>Total</b>	<b>37.5</b>

The state rooms are the astronauts' living quarters. In each there is a sleeping harness, foldout desk, chair, and storage area. The bathroom houses a sink, shower, toilet, and laundry facilities. The airlock contain space suits and enables the crew to enter and exit the vehicle for EVA's. The lounge contains a "kitchen," entertainment items, exercise equipment, and medical supplies. The control center is where the communications and guidance are housed. More on the design approach to the rooms, food, and life support is discussed in Section 5.0.

### 3.2.3.8 SEPARATION DEVICES (Mike Machula)

In order to allow the ERV to lift off at the end of the mission and yet remain attached to the TMI at all other times prior, a separation device must be employed. Since the ERV structure terminates in a series of point attachments, explosive nuts at the separation plane are used [2]. Each of the eight hard point locations (Fig. 3.17) installs a pyrotechnic separation nut in the ERV module and another in the UMTV (Fig. 3.32). A threaded stud between the two nuts keeps the vehicles together. For redundancy purposes two nuts are used for each

stud. Ignition of either nut will release ERV from the UMTV. Many nuts are available “off the shelf” and qualified for use in space, and have proven reliable in previous space flights [2]. Attachment bolts are located at each of the eight hard points on the thrust structure (Fig. 3.32).

Figure 3.33 shows how the ERV is held in place by the explosive nuts and studs. Before the RL10’s are ignited, the explosive nuts separate the ERV from the UMTV (shown in the top part of the figure). The methane rockets are then ignited and transfer their thrust to the ERV through the thrust structure. The detached ERV is then able to lift off, leaving the UMTV descent stage on the surface of Mars.

### **3.2.3.9 EARTH REENTRY** (Mike Machula)

Many different options for returning the astronauts and the payload safely to the Earth were evaluated. One option employs the same type of aerobrake that was used for the Mars entry. This system will work; however, the disadvantage is the large mass of the system. Another option was to use a light-weight ablative heat shield for reentry. The shield is made of a brazed stainless steel honeycomb and filled with an ablative type carbon-carbon composite. To return this vehicle to Earth, the ERV sections that are not shielded must be kept inside the wake angle. This system also suffers from mass problems.

The solution to the problem is to not re-enter the entire vehicle but only re-enter a small Earth reentry module (ERM). This reentry vehicle is similar to that of the Apollo missions. Only the four astronauts and the payload are returned to Earth, while the rest of the ERV is destroyed upon reentry. Figure 3.34 shows the ERM developed by Boeing for their space transfer vehicle that we propose to use for the Minerva project. This module has room for the four astronauts and has a mass of 6.1 tons.

Figure 3.35 illustrates the ERM reentry sequence. When the time comes for reentry, the ERM carrying the crew and scientific payload, separates from the ERV. Explosive bolts separate the two units while compressed springs push them apart. Two small solid rockets on the ERV fire, further separating the two modules, sending the ERV downrange of the ERM's deorbit trajectory. The ERV proceeds to burn up in the atmosphere while the ERM reenters. After reentry maneuvers, the ERM deploys a parachute to slow the descent rate to a safe landing speed. The ERM then splashes down in the ocean and awaits recovery.

### **3.3 MANNED SEGMENT**

(Kevin Mahn)

#### **3.3.1 LAUNCH**

The manned segment launches approximately 2 years after the unmanned segment. This segment, like the unmanned segment, requires two Antares VII launches. The first launch utilizes a two-stage scenario to maximize the amount of propellant delivered into LEO aboard the TMI booster, as in the case of the unmanned vehicle. During the first stage, Antares VII fires all its engines. After all the propellant is consumed, the upper stage separates, fires, and continues to LEO. Once in LEO, the upper stage/TMI booster adjust to a circular orbit (refer to Figs. 3.2, 3.3, 3.5).

The second launch puts the manned Mars transfer vehicle (MTV) into LEO (see Fig. 3.36). Antares VII is used as designed, except for a modified payload fairing (same design as unmanned mission refer to Figs. 3.6, 3.7). Once in LEO, the MTV circularizes to the same orbit as the upper stage/TMI booster. Both launches will again take place at the Kennedy Space Center.